Vortex "Bogusing" using Advanced Microwave Sounding Unit Data, Applied to Hurricane Floyd

by

Rémi Montroty

Department of Atmospheric and Oceanic Sciences McGill University Montreal

A thesis submitted to the Faculty of Graduate Studies and Research In partial fulfillment of the requirements for the degree of Master of Science

© Rémi Montroty, February 2004



Library and Archives Canada

Published Heritage Branch

395 Wellington Street Ottawa ON K1A 0N4 Canada Bibliothèque et Archives Canada

Direction du Patrimoine de l'édition

395, rue Wellington Ottawa ON K1A 0N4 Canada

> Your file Votre référence ISBN: 0-612-98703-5 Our file Notre référence ISBN: 0-612-98703-5

NOTICE:

The author has granted a non-exclusive license allowing Library and Archives Canada to reproduce, publish, archive, preserve, conserve, communicate to the public by telecommunication or on the Internet, loan, distribute and sell theses worldwide, for commercial or non-commercial purposes, in microform, paper, electronic and/or any other formats.

The author retains copyright ownership and moral rights in this thesis. Neither the thesis nor substantial extracts from it may be printed or otherwise reproduced without the author's permission.

AVIS:

L'auteur a accordé une licence non exclusive permettant à la Bibliothèque et Archives Canada de reproduire, publier, archiver, sauvegarder, conserver, transmettre au public par télécommunication ou par l'Internet, prêter, distribuer et vendre des thèses partout dans le monde, à des fins commerciales ou autres, sur support microforme, papier, électronique et/ou autres formats.

L'auteur conserve la propriété du droit d'auteur et des droits moraux qui protège cette thèse. Ni la thèse ni des extraits substantiels de celle-ci ne doivent être imprimés ou autrement reproduits sans son autorisation.

In compliance with the Canadian Privacy Act some supporting forms may have been removed from this thesis.

While these forms may be included in the document page count, their removal does not represent any loss of content from the thesis.

Conformément à la loi canadienne sur la protection de la vie privée, quelques formulaires secondaires ont été enlevés de cette thèse.

Bien que ces formulaires aient inclus dans la pagination, il n'y aura aucun contenu manquant.



Abstract

A case study of hurricane Floyd (1999) is performed using the Penn State/NCAR MM5 model. Hurricane Floyd was the third most costly hurricane to have hit the United States. The estimated property damage is 4.5 billion dollars. 56 lives were lost and massive floods occurred over North Carolina, Virginia and South Carolina.

To predict accurately the track and evolution of the hurricane, a vortex bogusing technique has been devised. A more realistic initial vortex was specified and introduced into the large-scale analysis for model initialization. The technique used follows closely that described by Zhu et al. (2002) where Advanced Microwave Sounding Unit (AMSU) data are employed to retrieve the temperature of the hurricane vortex. An algorithm is then applied to compute the sea level pressure, geopotential heights, winds and moisture content. Three experiments initialized with three different data sets were performed, using respectively the original Canadian Meteorological Centre (CMC) analysis, the bogus-vortex modified CMC analysis with the original CMC sea surface temperature (SST) field, and a bogus-vortex modified CMC analysis with a spatially-constant SST of 28°C.

The retrieved bogus vortex possessed realistic structures in temperature, geopotential height, winds and moisture content, similar to those observed by a satellite. A 15°K warm core in the vertical structure is present in agreement with observations in other hurricanes. Unrealistic cold anomalies in the lower levels due to scattering in regions of strong precipitation were corrected. The overall magnitude and structure of the retrieved winds are consistent with those obtained in reconnaissance flights.

The bogus vortex simulation captures adequately the evolution, magnitude and intensity of the hurricane, despite some initial spin up problems. The vortex bogusing run showed notable improvement over the original, non-bogused analysis run, which intensifies the hurricane in an unrealistic manner. However, the results are found to be very sensitive to a 1 or 2 degree colder SST anomaly. In that cold SST experiment, the track deviates more to the north and the intensity and evolution of the hurricane are not well simulated.

Résumé

Le modèle MM5 de l'université Penn State/NCAR est utilisé pour une étude de cas de l'ouragan Floyd (1999). Floyd se situe en troisième position des ouragans ayant causé le plus de dégâts après avoir frappé la côte des Etats-Unis. Il aura couté 4.5 milliards de dollars, fait plus de 56 victimes et provoqué d'énormes inondations en Caroline du Nord, Virginie et Caroline du Sud.

Une technique a été mise au point pour améliorer la précision des prédictions d'ouragans à l'aide de simulation numériques, spécialement la prédiction de la trajectoire et de l'évolution de l'intensité. Cette technique consiste à définir le vortex initial d'une manière plus réaliste et à l'introduire dans les analyses à plus large échelle pour ensuite initialiser les modèles méso-échelle. Cette technique se nomme la spécification vorticale. Dans cette étude, nous suivons la technique de spéficication vorticale définie par Zhu et al. (2002) dans laquelle les données de l'Unité Avancée de Sondage Micro-ondes (UASM) sont utilisées pour obtenir les températures atmosphériques. Un algorithme est ensuite appliqué pour calculer la pression au niveau de la mer, les hauteurs géopotentielles, les vents et l'humidité. Le modèle MM5 est alors initialisé avec trois types de données différentes : les analyses originales du Centre Météorologique Canadien (CMC) pour le premier, les analyses du CMC modifiées par l'insertion du vortex spécifié comprenant la température à la surface de la mer (TSM) des analyses CMC pour le deuxième et la même chose à l'exception d'un champ constant de 28 degrés pour la TSM pour le troisième dans le but d'une étude de sensitivité.

Le vortex spécifié obtenu possède des structures et valeurs réalistes pour les températures, les hauteurs géopotentielles, les vents et l'humidité, tels qu'observés dans les images satellitaires. Une structure verticale de température à noyau chaud de 15 degrés Celsius est obtenue et est en accord avec les structures typiquement observées dans de multiples cas d'ouragans. Des anomalies de température irréalistement froides sont cependant obtenues dans les bas niveaux de l'atmosphère. Deux corrections sont proposées pour les supprimer car elles sont causées par la diffraction du signal micro-onde dans les zônes à haute précipitation de l'ouragan. Les vents obtenus par notre algorithme ont globalement la même magnitude et la même structure que ceux observés durant les vols de reconnaissance dans l'ouragan.

La simulation initialisée avec le vortex spécifié simule de manière satisfaisante l'évolution, la magnitude et l'intensité de l'ouragan, malgré quelques problèmes durant la période d'ajustement initial dûs à la problématique inconsistence des champs obtenus vis-à-vis de la paramétrisation physique et dynamique du modèle. La spécification vorticale améliore considérablement la simulation de l'ouragan comparée à la simulation initialisée avec les analyses CMC originales, qui s'intensifie de manière irréaliste possiblement à cause de champs d'humidité trop humides. Les résultats sont enfin très sensibles à une différence négative de 1 ou 2 degrés dans la TSM: la trajectoire dévie vers le nord tandis que l'intensité et son évolution ne sont pas simulées de manière appropriée.

Contents

ABSTRACT	
RÉSUMÉ	III
CONTENTS	V
LIST OF FIGURES	VI
LIST OF TABLES	VIII
ACKNOWLEDGEMENTS	
CHAPTER 1 INTRODUCTION	
1.1 ESTIMATING AND FORECASTING THE INTENSITY OF HURRICAL 1.2. NUMERICAL WEATHER PREDICTION OF HURRICANES	
1.2 NUMERICAL WEATHER PREDICTION OF HURRICANES	
1.4 OBJECTIVES OF THE STUDY AND OUTLINE	
CHAPTER 2 HURRICANE FLOYD	
2.1 SYNOPTIC HISTORY	
2.2 NATIONAL HURRICANE CENTER BEST ANALYSIS	
2.4 IMPACT OF SEA SURFACE TEMPERATURE ON THE HURRICANI	
	•
3.1 AMSU BACKGROUND	
3.1.1 Passive Remote Sensing	
3.1.2 AMSU Instrument	
3.1.3 AMSO Data	
3.2.1 Temperature retrieval	
3.2.2 Geopotential height diagnosis	
3.2.3 Gradient Balance Inversion and wind diagnosis	
3.2.4 Humidity specification	
CHAPTER 4 RESULTS	
4.1 Retrieval	37
4.1.1 Temperature retrieval	
4.1.2 Geopotential height diagnosis	
4.1.3 Wind retrieval	
4.1.4 Relative Humidity Specification	
4.2 Bogusing	
4.3 NUMERICAL SIMULATIONS	
4.3.1 Model Design	
CHAPTER 5 SUMMARY, FUTURE WORK AND CONCLUSION	
5.1 SUMMARY	
5.2 FUTURE WORK	
5.3 CONCLUSION	
APPENDIX A: THE SAFFIR-SIMPSON SCALE	62
APPENDIX B: TEMPERATURE RETRIEVAL COEFFICIENTS.	65
DEFEDENCES	79

List of Figures

Figure 2-1: Best track analysis from the NHC, 12 hours intervals positions	13
Figure 2-2: Best Analysis Minimum Central Sea Level Pressure; 6-hourly intervals	15
Figure 2-3: Best Analysis Maximum winds, 1-minute average; 6-hourly intervals	15
Figure 2-4: Total accumulated precipitation from the passage of hurricane Floyd over the Unit	ed
States, taken from September 13 to September 17, 1999. (courtesy of the Climate Predict	ion
Center)	16
Figure 2-5: GOES-8 Infrared Image on September 11, 0015 UTC	
Figure 2-6: GOES-8 Water Vapour Image on September 11, 0015 UTC	17
Figure 2-7: AOML Analysed Surface Winds on September 11, 0130 UTC	
Figure 2-8: 7-day average AVHRR-derived Western Atlantic SST (ending on September 9, 19	99,
at 2256 UTC), correlated with hurricane Floyd intensity evolution as noted by the Saffir-	
Simpson scale wind ranges (copyright Ray Sterner & Steve Babin, John Hopkins Univers	sity
Applied Physics Laboratory)	
Figure 3-1: Polar Orbiting Coverage for AMSU	24
Figure 3-2: MSU vs AMSU-A footprints (from Kidder et al., 2000)	
Figure 3-3: AMSU-A Constraints: Limb warming and data-void gaps	
Figure 3-4: Cloud Liquid Water passes, on September 10 12Z (left, descending)	29
Figure 3-5: AMSU-A Channels 3-14 theoretical weighting functions at nadir over land	31
Figure 3-6: Diagnosed RMS error for temperature retrievals compared to rawinsonde observati	ions.
	32
Figure 3-7: Slope m of CLW vs temperature deviation regression, for each pressure level (from	n
Demuth (2001))	
Figure 4-1: Low-CLW coefficients retrieved PTA at 1000 hPa	39
Figure 4-2: Correlation of the cold anomalies (color lines in K) with the high CLW (in mm) are	eas
(black lines)	
Figure 4-3: Dual coefficients retrieved PTA at 1000 hPa	39
Figure 4-4: PTA in Fig. 4-1 corrected by Demuth's CLW correction	39
Figure 4-5: Vertical cross-sections of the PTA for	
Figure 4-6: Temperatures from CMC analyses (left panels) and temperatures modified by the b	ogus
vortex (right panels) at the surface (a,b), 5km (c,d) and 10km (e,f) at 0000 UTC September	er 11.
Figure 4-7: Same as in Figure 4-6, except for relative humidity	42
Figure 4-8: Same as Figure 4-6, except for horizontal winds in m/s	44
Figure 4-9: Holland scheme derived sea level pressure (hPa) at 0000 UTC, September 11	45
Figure 4-10: MM5 simulated tracks compared to the NHC Best Analysis Track, with SST contractions of th	ours
superimposed	53
Figure 4-11: Evolution of the distance of each simulated track from the Best Analysis Track	
Figure 4-12: Evolution of the maximum surface winds for the different runs	
Figure 4-13: Same as in Fig. 4-12 except for minimum Sea Level Pressure	54
Figure 4-14: Evolution of the area-averaged environmental wind shear speed over a 600km x	
600km area	55

Figure 4-15: Same as in Fig. 4-14 except for wind shear direction	. 55
Figure 4-16: Evolution of Equivalent Potential Temperature (θe)	. 58

List of Tables

Table 3-1: Satellite Microwave Radiometers (from Janssen, 1993)	
Table 3-2: AMSU-A Specifications	26
Table 3-3: Channel weighting coefficients for a temperature retrieval at 850 hPa	

Acknowledgements

I would like to thank my supervisor, Dr. Peter Yau, whose guidance and teachings helped make this Master thesis a reality. I am especially grateful for the constant availability and endured patience throughout the project as well as the diligence with which he corrected the earlier drafts when the time was pressing.

Thanks go to Tong Zhu and Da-Lin Zhang for providing us with the algorithm and to Ralph Ferraro and Huang Meng from NESDIS for the AMSU data. Thanks also go to faculty members who helped me in various ways through discussions and suggestions.

I also wish to thank all the people in our group: Badrinath Nagarajan for his renewed, cheerful and invaluable help and his enthusiasm for the higher purposes of scientific research that kept me focused on the big picture, Yongsheng Chen for his friendship and for saving my research life with this MM5 simulation (truly!), Shih-Li Jou for his constant generous friendship and always willing help as well as his beneficiary example for taking a new direction where his aspirations lied (good luck!), Irena Paunova for her gracious smile which made life in 811 a bit less sky-less, Jason Milbrandt for having helped me on numerous occasions and for his thoughtful remarks on somewhat demoralized days, Charmaine Franklin for many relaxing conversations and moral support, Lily Ioannidou for her help with science and recipes and Xingbao Wang for his help on technical computational issues.

Other thanks go to Brian Rose for being an amazing companion in room 811, livening up those long days with many insightful and interesting conversations and for proofreading much of what the final thesis looks like, Brian Papa for more proofreading of the introduction, Rick Danielson for his always friendly help and manners, Ornella Cavaliere for her incredible generosity and support in the administrative as well as personal matters, Karin Braidwood for her help as the Graduate Program Coordinator and Lucy-Ann Joseph for her cheerful and helpful presence. I also wish to send my appreciation to Marco Perez, Edwin Campos and Urs German for their help with IDL.

To my fellow Masters students, a big warm goodbye and good luck with the rest: Nathalie Voisin, Gregor Probst, Shih-Li Jou, Andrew Teakles, Brian Rose, Marco Perez, Mike Waite, Desjanelles Matthews and everyone else!

Final personal thoughts go to my parents and friends whose presence and support made the harshness of some events smoother and magnified the fun of others! Gael, Denis, Clarisse, Lydia, Liz, Pascal, Selma et les autres: je vous aime tous! Un grand merci et beaucoup d'amour à mes parents!

Chapter 1 INTRODUCTION

1.1 Estimating and forecasting the intensity of hurricanes

Intense tropical cyclones are called hurricanes (typhoons) when they occur east (west) of the International Date Line. These powerful cyclones are giants of the atmosphere and are comprised of low-pressure cores surrounded by converging winds. These winds advect warm moist oceanic air that subsequently rises vertically in the eyewall and then condenses. The liberated energy through latent heat release in the mid to upper levels can enhance further intensification. Therefore, hurricanes act as thermodynamic engines by extracting huge quantities of energy from the warm waters of the tropical oceans and transport it both vertically and meridionally. Vertically, the hurricane's secondary circulation creates a Carnot cycle that enables its development and intensification (Emanuel, 1986). Meridionally, on a larger scale, hurricanes usually undergo a Coriolis-induced propagation shift towards mid-latitudes after they reach the mature stage, which allows for a poleward heat transport. Understanding the complex mechanisms behind the multiscale interactions and the detailed thermodynamical and kinematical structures in a hurricane is not straightforward. Forecasting of hurricanes is also a very difficult task. In order to make accurate forecasts, one needs to properly assess the intensity of the hurricane, its mesoscale features as well as the large-scale environment in which it is embedded.

Given that hurricanes develop over the tropical oceans, a major issue that confronts researchers and forecasters is the lack of reliable, frequent and high-resolution data. In situ observations can be made by reconnaissance aircrafts: they provide the only source of accurate temperature and humidity soundings and wind speed measurements. Several observational studies have yielded much insight into the structure of hurricanes: Shea and Gray (1973) presented the results of numerous reconnaissance flights, which resolved many of their inner-core features. Specifically, their findings included the warm core structure, the radius of maximum winds, the radial variations of tangential winds, as well as the symmetries and asymmetries in these features. In a landmark paper, Frank (1977) presented a composite study of 10 hurricanes through rawinsonde measurements and revealed many aspects of the energetics and thermodynamic profiles

in various regions of the hurricane. The airborne radar also allows for accurate depiction of the structures of the eyewall, the distribution of radar reflectivity and other volumetric features. In particular, Marks *et al.* (1992) used an airborne Doppler-radar to map the full 3D winds inside the hurricane core for the first time. However, *in situ* observations are costly and lack sufficient temporal resolution to give detailed information on the evolution of the storm. Although very useful products come from air reconnaissance flights (such as maximum surface winds estimates, minimum sea level pressure, soundings, radar imagery, etc...), there is still a need for less discretized and more global data and tools.

Since their introduction in the 1960's, satellites have proved to be an invaluable tool in monitoring, intensity-estimation and forecast of hurricanes. Satellites come in two different types: polar-orbiting satellites (POS) and geostationary satellites (GEOS). The former satellites constantly change orbit as they fly 850km above the surface of the Earth while the latter satellites revolve at the same speed as the Earth at an altitude of about 36,000km. Starting in May 1960 with the TIROS-1 (Television InfraRed Observation Satellite), the National Oceanic and Atmospheric Administration (NOAA) launched a series of polar-orbiting weather satellites known as the TIROS series. They were closely followed by the TIROS-N series in the 1970's. After 1979, the TIROS-N series became the NOAA-# series, where # represents the number that replaced the pre-launch designating letter (e.g. NOAA-11 was referred to as NOAA-H prior to its successful launch in orbit, see NESDIS 2003). The TIROS Operational Vertical Sounder (TOVS) instruments became the Advanced TOVS (ATOVS) starting with NOAA-K (NOAA 15). Most sensors flying onboard of POS and GEOS are passive sensors however, in the visible, infrared or microwave part of the electromagnetic spectrum. Active sensors such as radar would encounter too many problems related to antenna size, absorption, scattering and backscattering.

Dvorak (1975) proposed an intensity estimation technique from satellite infrared imagery. The technique uses time-dependent visible (VIS) analysis to monitor several features of the storm at any given time: such as its central features – namely, the characteristics of the innermost curved cloud line as well as the characteristics of the Central Dense Overcast (CDO) - and the outer banding features – the size and curvature of the bands forming around the central features. From the previously observed features and the apparent rapidity of their evolution, an intensity-related 'T' number is assigned to the storm. Tropical analysts can further assess the evolution based on the current intensity and organization of the observed convection – still somewhat subjectively.

Furthermore, the limitation implied by the use of VIS imagery (i.e. unavailable at night time) was then overcome by an enhanced infrared (IR) technique (Dvorak, 1984), which gave forecasters the 24 hour a day tool they needed.

Velden et al. (1998) refined that technique by introducing the Objective Dvorak Technique (ODT): in an attempt to remove the subjective errors and biases of each individual forecaster, they used algorithms based on the Dvorak technique to estimate the intensity of the tropical storm. These techniques are now operational in many tropical centers around the world and can predict quite accurately the minimum sea level pressure (MSLP) as well as the maximum surface sustained wind speeds (UVMAX). These ODT analyses are based on GEOS imagery: GEOS have high temporal resolution capabilities over a fixed area and have achieved extremely high horizontal resolution in recent years. For example, NOAA's GOES series have a 1km resolution in both VIS and IR. Yet, VIS and IR imagery can only yield cloud top temperatures and winds; only microwave imagery can truly assess the vertical structure of the storm.

Microwave observations not only penetrate clouds, but they are also sensitive to various geophysical parameters. Microwave radiation is indeed affected by atmospheric temperature, moisture content, cloud liquid water, cloud ice and rain - each affecting the radiation to varying extent. The history of passive microwave remote sensing started in the mid 1970s. On board the Nimbus 6 satellite which was launched in June 1975, the Scanning Microwave Spectrometer (SCAMS) was amongst the first of the microwave sensors to ever board satellites. Despite a fairly coarse resolution (145km at nadir degrading to 360km at the maximum angle of the cross-track scanning), the SCAMS was able to retrieve a positive warm anomaly in the upper level temperatures of typhoon June (Rosenkrantz et al., 1978). Kidder (1978) showed that the anomaly extended 300km radially with a maximum magnitude as large as 4.1°K typically located around 250hPa. He also showed that the magnitude of the retrieved warm anomaly could be used to estimate the maximum surface winds and further proposed a refined algorithm to retrieve surface wind speeds (Kidder et al., 1980). A new Microwave Sounding Unit (MSU) was then flown onboard the TIROS-N series. This new instrument has a resolution of 110km at nadir and about 200km at maximum scanning angle. Velden and Smith (1983) and Velden (1989) further showed that the reduced noise equivalent temperature (0.2°K in MSU as opposed to 0.5°K in SCAMS) would yield better insight on the retrieved warm upper level anomalies. Using the 250hPa horizontal temperature gradient (between the core and its environment), he used statistical

correlations to estimate the surface intensity by correlating it with the SLP gradient obtained in reconnaissance flights. The maximum warm anomalies retrieved by the MSU were always on the order of 5-6°K. However, Gray (1979) and Frank (1977) had shown that the maximum anomaly - as retrieved by rawinsondes during aircraft reconnaissance flights - can be as high as 10-15°K. Therefore, there was a need for a better microwave instrument that could resolve such magnitudes.

Starting in May 1998 with the launch of NOAA 15 (NOAA-K, first of the NOAA-KLM series, see NOAA KLM User Guide 2000), the new generation of Advanced Microwave Sounding Units (AMSU) came into being. The cross-scanning instrument is comprised of two sounding units: AMSU-A and AMSU-B, respectively dedicated to brightness temperatures and water vapour retrieval. Further geophysical quantities could also be retrieved. Considerably increased vertical resolution (15 sounding channels for AMSU as opposed to 4 for the MSU) and improved temperature retrieval (less than 1.5°K vertical root mean square error (RMSE) when compared to rawinsonde temperature profiles, see Kidder et al. 2000) made it the perfect instrument to study the large-scale features of tropical cyclones. Horizontal resolution was also considerably improved: 48km at nadir for AMSU-A and 16km for AMSU-B, respectively degrading to 150km and 50km at the maximum cross-scanning angle. Kidder et al. (2000) showed that this new AMSU-A could retrieve a 14°K warm anomaly in Hurricane Bonnie (1998) around the 250hPa pressure level. DeMaria et al. (2000) presented an algorithm to retrieve tropical cyclone winds using the AMSU-A data. Demuth (2001) applied that algorithm on several types of tropical cyclones: tropical storms, tropical depressions and hurricanes. It was found that wind estimates were comparable to the Dvorak estimates with the notable advantage of being applicable to all sorts of tropical mesoscale systems. Grody et al. (1999) also showed how water vapor, cloud liquid water, total precipitable water, cloud ice and rainfall rates could be obtained from AMSU A and B.

However, asymmetric radiances along a scan line of the AMSU-B instrument, as well as antenna contamination problems due to radio frequency interference between the 150 and 183 ± 3 GHz for the AMSU-B unit, prevented general use of these techniques until Weng *et al.* (2000) and Grody *et al.* (2000) proposed the respective, appropriate corrections that led to operational products. In September 2000, NOAA 16 (L) was launched followed by NOAA 17 (M) in June 2002: both satellites had similar AMSU units onboard and were set to be on sun-synchronous orbits and at an ascending local solar time of 1400 UTC and 1000 UTC respectively (NOAA 15 is at 0730 UTC local solar time). This chronological order of each satellite's ascending pass thus allows for

better temporal resolution and minimizes the researchers' nightmare of having the tropical cyclone of interest sitting in a data-void gap between two cross-scanning swaths. Very recently, Brueske and Velden (2003) proposed a single-channel technique for estimating MSLP by attempting to correct for undersampling due to AMSU-A's fairly coarse resolution while Spencer and Braswell (2001) refined the estimation of surface winds using AMSU data. They studied 190 storms, which occurred during the 1998 and 1999 seasons, with strengths ranging from tropical depression to hurricane. They managed to obtain a 4.7m/s error standard deviation (ESD) in the observed winds from 82 storm cases with *in situ* reconnaissance measurements and 7.5m/s ESD for 102 storm cases with no *in situ* reconnaissance measurements but with their maximum winds estimated using the Dvorak technique. With so much ongoing work and interest, AMSU is truly a tool of interest for assessing a hurricane's intensity and its large-scale features (finer inner core features are still not resolvable with 48km nadir resolution). However, it cannot be used alone for forecasting, numerical models are required to accurately forecast hurricane tracks and intensity.

1.2 Numerical weather prediction of hurricanes

Numerical weather prediction (NWP) relies on numerical models to represent the state and time-evolution of the atmosphere. The goal of NWP is to improve models in order to reduce forecasting errors and thus increase forecast accuracy. Improvements may come from new theories being implemented, new ways of representing physical and dynamical processes and their interactions, increased computer power to achieve higher resolution and better initial conditions from better observations and assimilation methods.

In order to predict a future state of the atmosphere, models usually solve a set of equations that describe the evolution of atmospheric variables which define the current atmospheric state (temperature, humidity, wind speed, pressure, etc...). Numerical models differ depending on the set of equations used to produce the forecasts and on the assumptions leading to those equations. The equations are called the governing equations and vary from one model to the other, not to mention their implementation. As a result, various models exist and they all have their strengths and weaknesses. NWP in the tropics also suffers from the lack of observational data over oceans to estimate the current state of the atmosphere. However, the use of global models can give realistic-enough initial conditions to initialize limited-area models (LAM). Theoretical models do not need realistic initial conditions since they usually assume idealized, typical states.

Historically, NWP in the tropics started in the late 1950's with the development of barotropic models such as Charney's model (1963). In that paper, Charney derived the famous balance equation, which is a first order truncation of the vorticity-divergence equations and represents an improvement over the zero-order truncation linear balance equation. Later, Kasahara (1961) was among the pioneers to develop an axisymmetric hurricane model. Subsequent improvements of the axisymmetric hurricane model include improvement in the vertical resolution (up to 13 levels for Yamasaki's model (1968)), in implicit cumulus parameterization (Ooyama, 1969) and in the use of an explicit water vapour scheme (Rosenthal, 1970). Kuo (1965; 1974) proposed a cumulus parameterization scheme, which soon became very popular, in which convection was triggered by moisture convergence. The Kuo scheme is suited for meso-α and upper meso-β scale simulations (according to Orlanski's scale classification (Orlanski 1975)).

Anthes (1972) achieved a major breakthrough with the development of a fully threedimensional model for tropical cyclones. It was the first model to resolve the asymmetries in the vortex. These asymmetries are always present in real tropical storms in the form of spiral rainbands, azimuthally varying winds and asymmetric inflows/outflows. The model had a 30km horizontal resolution (lower meso-β scale). Further improvements led to the Penn State/NCAR MM4 model (Anthes et al. 1987) which was a hydrostatic LAM using two-way nested movable grids (technically speaking, only the innermost grid could be moved) similar to the one developed by Kurihara et al. (1980) at GFDL. The non-hydrostatic version of that model became known as MM5 (see Dudhia 1993 and Grell et al. 1995) and featured many improvements in terms of a multitude of convective, radiative, microphysical and other schemes. Many successful studies were done using MM5: Liu et al. (1997) simulated skillfully the evolution, finer scale features and large scale features of hurricane Andrew in a multiscale study down to a finest resolution of 6km, Chen and Yau (2001) studied vortex Rossby-waves in the context of a similar Andrew simulation, Braun (2002) simulated hurricane Bob using a finer grid mesh of 1.3km thus resolving most convective cells. To-this-date, MM5 is still one of the most widely used models for mesoscale studies in the tropics and its versatility has few equals.

Emanuel (1986) proposed some new insight on the thermodynamical structure of hurricanes and the effects of the thermodynamical profiles of the atmosphere and the upper-ocean on hurricane intensity. Emanuel's (1999) model produced impressive results in capturing the maximum wind evolution of many famous and intense hurricanes. Emanuel's definition of the maximum potential

intensity of hurricanes closely links the maximum attainable wind speed to the efficiency of the air-sea thermodynamic engine at transporting energy from the warm waters into the atmosphere (Emanuel, 1988).

Kurihara et al. (1980) proposed a new model with several new features that became the famous Geophysical Fluid Dynamics Laboratory (GFDL) model. Two-way triply nested grids allowed for interconnectivity of scales at all times of the simulation and allowed for tracking of small vortices. The authors also noted that the absence of moisture and surface friction in the model was a major problem: computational power at the time did not allow for such sophistication. Kurihara et al. (1993) presented a refined version together with a new initialization technique, which they introduced as vortex bogusing. The rationale behind this new technique was that, in order to reduce false spin up problems that all models encounter especially when starting from coarse or unrealistic initial conditions, one could specify the size and intensity of the initial vortex and insert it into the initial condition fields. Bender et al. (1993) showed that the new version of GFDL, together with this accurate specification of structure and intensity, led to significantly reduced track-forecasting error (RTFE) when four vortex-bogused cases were compared to both non-bogused simulations (60% and 51% RTFE at 24h and 48h) and NCEP forecasts (51% and 56% RTFE at 24h and 48h). Bender (1997) also investigated the effect of environmental wind shear on the asymmetries inside a hurricane using the GFDL model, proving that the shear was indeed one of the main forcing terms for the asymmetries. Therefore, a definite improvement came from the insertion of a bogus vortex in the analyses: the next section reviews the historical evolution of that technique.

1.3 History of bogusing techniques

Up until recently, many numerical simulations of vortical flows were initialized with over simplistic, idealized Rankine vortices, as defined by William Rankine in the late nineteenth century. A Rankine vortex features a radially varying specification of the tangential wind speed that would increase linearly from zero at the center to its maximum V0 at some maximum wind radius R0 and then decrease linearly again. Beer and Giannini (1980) used such a vortex to initialize their hurricane model in order to resolve spiral rain bands.

By the early 1990's, computer power having improved significantly over the last decade, finer grid resolution was achievable on larger domains with increased vertical resolution. This

called for an improvement of the vortex specification in mesoscale models. Starting first at the National Meteorological Center, Mathur (1991) presented a way to compensate for the lack of observational data by inserting an idealized vortex into the analysis. Geopotential heights and wind fields were derived to satisfy the gradient wind balance, while the structure and intensity depended on those of the observed storm. Carr and Elsberry (1992) showed that any vortex could be decomposed into an axisymmetric vortex, an environmental steering flow and the asymmetrical circulation which would become the residual once the first two are removed from the total wind field. They proved that track forecasting could be improved notably by specifying an analyzed asymmetrical wind field using their method. They also suggested other mechanisms to introduce various types of analyzed wind fields (symmetrical, environmental or asymmetrical) and blending them with the analyses.

Kurihara et al. (1993) followed that line of thinking and presented a new vortex bogusing scheme, based on the theoretical work of Ross and Kurihara (1992). Appropriate filters were used to filter out the analyzed vortex leaving a smooth large-scale analysis vortex-free. The complete bogus vortex (axisymmetric and asymmetric parts) is then defined as a deviation from the smoothed environmental field and is incorporated back into the environmental flow in a seemingless fashion later on. A crucial issue is stated in Kurihara et al. (1993):

An important and still unresolved issue in such an approach is that of vortex consistency with the properties of the prediction model. Above all, the initial moisture field, which affects the intensity change of the vortex, has been especially difficult to specify in a realistic yet model-consistent manner.

They proposed a solution to that issue by integrating an axisymmetric version of their model to retrieve axisymmetric components of the vortex in accordance with the internal physics and dynamics of the model in order to avoid complex spin up adjustment problems. Similarly, Liu et al. (1997) made a pre-simulation in order to spin up a vortex that was of the intensity of the observed initial-time vortex. After a 48h run, they cropped out the 3D vortex and inserted it back into the original analysis at the best-analysed position. This method proved very successful in capturing

further evolution of the storm but is still somewhat arbitrary and does not seem like a viable operational solution for proper initialization of hurricane forecasts.

Zou and Xiao (2000) proposed yet a new technique to create bogus vortices. Physical and dynamical consistency is achieved by fitting the forecast vortex to a specified surface low dependent on various observed parameters. They call this method the Bogus Data Assimilation (BDA). Following the example of Krishnamurti et al. (1989, 1991, 1995), satellite – as well as radar - data can be added in their initialization technique. For example, satellite-derived variables including water vapour retrieved winds, satellite-derived rain rates, satellite brightness temperatures, ozone, as well as radar radial velocity and reflectivity data, can all be used to improve the initial conditions. An axisymmetric SLP is then formulated according to Fujita's (1952) formulation. The choice is then made to specify only one variable of the bogus vortex and let the other variables be spun up by the forecast model. The technique allowed for the specification of a more compact and more intense vortex in the case of hurricane Felix (1995) and yielded very realistic results. It should however be noted that hurricane Felix did not undergo much intensity change over the 72h period of their simulation and maintained a steady, average category-2 intensity: the MSLP was oscillating between 962 hPa and 972 hPa while the UVMAX was almost constant at 35 m/s. Such a lifecycle and evolution do not seem to impose as much of a challenge as other hurricanes with more rapidly changing lifecycles.

Hurricane Bonnie (1998) had a more interesting lifecycle: it evolved from a 991 hPa, 65 knots, category-1 hurricane on August 22 0000 UTC to a 954 hPa, 100 knots, category-3 hurricane 48 hours later. Zhu *et al.* (2002) managed to capture this MSLP drop pretty accurately, even though the simulation failed to resolve the intensification between 12h and 36h as observed by the Best Analysis. The track and features of Bonnie were fairly well resolved thanks to their new bogusing technique: using AMSU-A data, they were able to retrieve the vertical distribution of temperatures and, by using the Holland (1980) scheme, which requires as input data such as MSLP, UVMAX and radius of maximum winds (RMW) from reconnaissance flights, they could specify a non-circular SLP that meshes with the environmental SLP – as specified from the analysis. This SLP was further integrated upwards hydrostatically using the retrieved temperatures to derive the geopotential heights. The balance equation was then inverted using streamfunctions from analyses at the boundaries to retrieve the vortex streamfunction and, through simple spatial derivative, to compute the winds. A simple humidity scheme was developed in accordance with the retrieved

temperatures. With the exception of the BDA scheme, it was the first bogusing technique that relied on observational data as the main source of data for the bogus vortex, i.e. a technique which did not rely only on idealized features or on model integration to specify the initial vortex. This reduces the subjectivity of the technique and increases the potential for operational implementation of such a technique.

1.4 Objectives of the study and outline

It is therefore the motivation of this study to use the Zhu et al. (2002) technique for vortex bogusing for another hurricane case, with significant intensity evolution and with the constraint of having available AMSU data. We wish to demonstrate the capability of using a bogus vortex to improve hurricane simulations in a mesoscale model. We pick the case of hurricane Floyd, initialized on September 11 0000 UTC using the AMSU-retrieved vortex and try to assess MM5's capacity at resolving the hurricane's features and evolution using this real data initialization. Unlike the work of Zhu et al., we use the Canadian Meteorological Centre (CMC) global analyses as the main input source for our large-scale initial conditions.

The thesis outline is as follows. In Chapter 2, the synoptic history of Floyd is summarized and various analysis products relevant to the rest of the work are presented. A theoretical discussion on the potential effect of the analyzed warm SST anomaly on the hurricane intensity evolution is included.

In Chapter 3, a background on AMSU passive remote sensing, the AMSU instrument and AMSU data is provided. The algorithm of Zhu *et al.* (2002) is then reviewed in detail.

In Chapter 4, the results from the retrieval are presented. The numerical experiments using standard CMC analyses, bogus-vortex modified analyses and a sensitivity experiment for SST are then presented and compared to the Best Analysis.

Finally, in Chapter 5, the results are summarized and conclusions are presented.

Chapter 2 Hurricane FLOYD

2.1 Synoptic History

Hurricane Floyd's lifecycle spanned 10 days from September 7 until September 17, 1999. At peak intensity, it approached the threshold of category 5 on the Saffir-Simpson scale (cf Appendix A). The storm was amongst the costliest hurricanes to ever hit the United States, with total damage estimates around 4.5 billion dollars. The following synoptic history is based closely on the National Hurricane Center (NHC) Best Analysis (Pasch *et al.*, 1999).

Floyd could be tracked first as a tropical wave on September 2, off the west coast of Africa. It moved slowly westward, undergoing little organization until September 7 when a favourable upper-level outflow helped to strengthen the tropical disturbance to Tropical Depression 8. The storm was located at about 1000 miles east of the Lesser Antilles at 1800 UTC. At this point, a notable curved band of deep convection existed around the center as revealed from visible, infrared and microwave observations. Steering currents associated with a deep-layer ridge north of the system bent its course west-northwestward. Further organization led to the formation of Tropical Storm Floyd at 0600 UTC, September 8. However, there is an absence of a clear inner core and Floyd only intensified slowly over the following two days, with its central pressure going below 1000 hPa around 1800 UTC on September 9. Finally achieving hurricane status at 1200 UTC September 10, the storm reached a SLP of 989 hPa with maximum winds of 80 knots. Floyd kept on intensifying and almost became a category-3 hurricane on the Saffir-Simpson scale at 0600 UTC, September 11. Then it became caught in a mid-tropospheric trough, slowed itself down and moved north-westward. By the end of the 11th, the upper-level outflow was disrupted and Floyd weakened, barely maintaining its status as a category-2 hurricane.

Starting on September12, a very strong mid- to upper-tropospheric high developed to the north of Floyd. This synoptic condition forced a westward turn of the storm and a subsequent major intensification similar to other observed cases such as Andrew (Rappaport, 1993), Roxanne (Avila, 1995) and Mitch (Guiney and Lawrence, 1998). Although no definite explanation exists as to why such a westward turn would provoke an intense deepening, one dominant factor might be the sudden weakening in shear occurring with the change of direction. Indeed Corbosiero and Molinari

(2002) showed that, as a common rule, the motion vector of the storm is located 45 degrees counter clockwise of the wind shear vector. Consequently, a westward motion vector could be associated with a southeasterly wind shear. This is a very interesting finding since such a shear could negate the typical northwesterly wind shear induced by the beta effect (Bender, 1997). Another factor might have been the presence of a warm upper oceanic "blob" in the sea surface temperature (SST) east of the Bahamas, directly along on Floyd's track. This will be discussed further in section 2.4.

Over a 24h period from 0600 UTC September 12 to 0600 UTC September 13, the winds increased by 40 knots to 135 knots while the central pressure dropped by roughly 40 hPa to a minimum of 921 hPa at 1200 UTC September 13. Floyd was therefore at the threshold of a category-5 hurricane from 0600 to 1800 UTC on September 13.

Tracking towards the Bahamas but shifting west-northwestward late on September 13, Floyd spared San Salvador and Cat Islands, but its eyewall moved over Eleuthera and Abaco island on September 14. Late that day, Floyd was on the threshold between category 3 and 4 hurricane status.

Florida was spared from a direct impact thanks to the presence of a mid- to upper-tropospheric trough over the eastern part of the United States. Gradually weakening the ridge situated at the westernmost part of the Atlantic, the trough allowed for a right turn of Floyd's track early on September 15. The track then became parallel to the coast, with the eye located 200km from the coastline. Unfortunately, the right turn was not strong enough to deflect Floyd back to the northeast, and Floyd was nearing the North Carolina (NC) coast as a category-2 hurricane late on September 15. Part of the weakening at that stage was due to the entrainment of dry air from the northwest, together with increasing wind shear from the southwest.

Floyd made landfall on at 0630 UTC September 16 near Cape Fear, NC. It was losing its eyewall structure and tremendous rainfall rates followed, as can be seen from the accumulated precipitation depicted in Figure 2-4. Floyd then moved rapidly across NC, reaching Long Island at 0000 UTC September 17. The propagation speed of Floyd was about 30 knots. Further penetration inland into New England resulted in a deceleration.

Merging with a frontal zone over the Atlantic, Floyd underwent extratropical transition around 1200 UTC and it continued to move northeastward towards the coast of New Brunswick later that day. It affected Prince Edward Island and Newfoundland on September 18 and then

moved out to sea where it finally merged with a large extratropical low over the North Atlantic on September 19.

2.2 National Hurricane Center Best Analysis

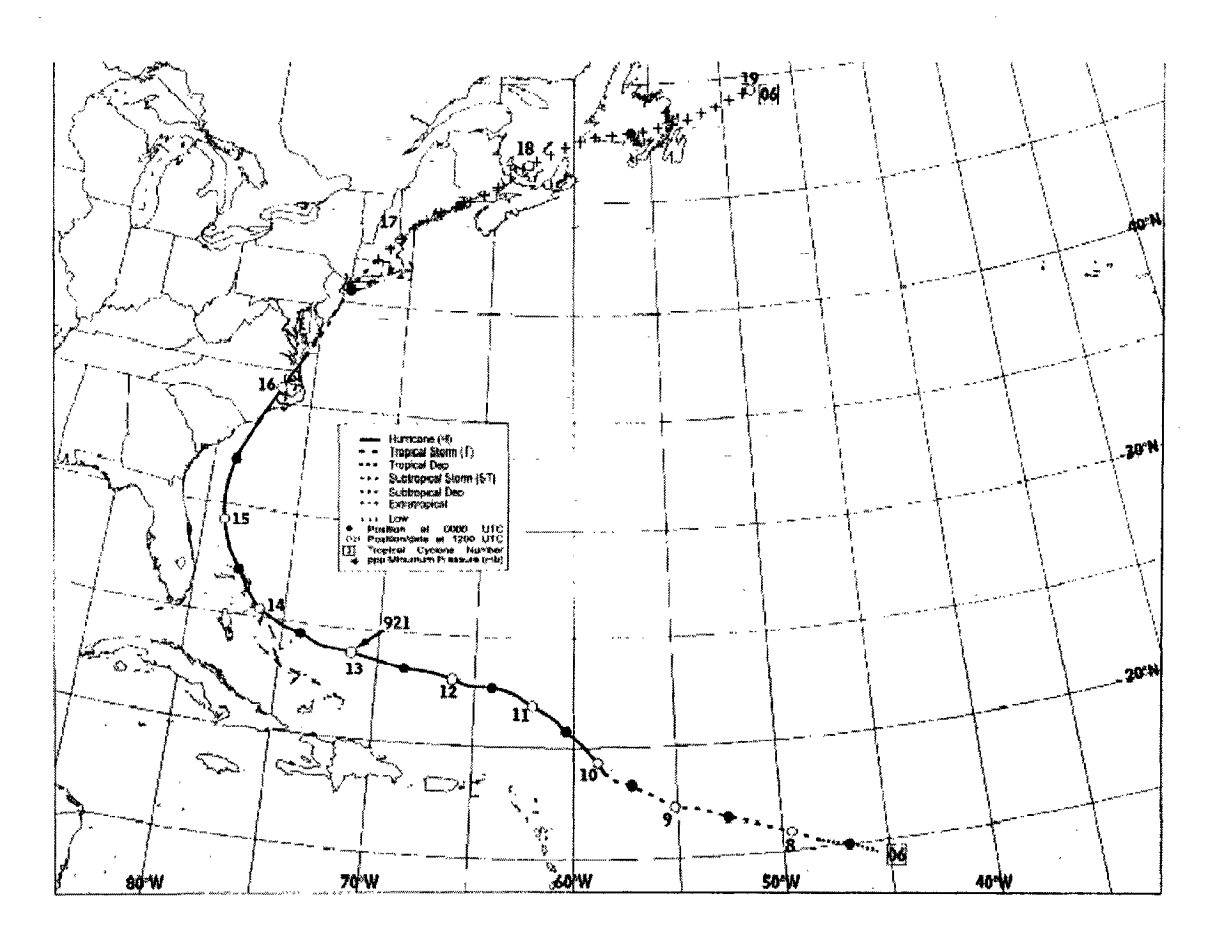


Figure 2-1: Best track analysis from the NHC, 12 hours intervals positions

The NHC Best Analysis is the post-analysis based on information from all relevant meteorological observations for a particular tropical cyclone. It is released at the end of each hurricane season, spanning from June 1 to November 30 of each year for the region comprising the Atlantic, the Caribbean and the Gulf of Mexico. The Best Analysis is a subjectively smoothed representation of a tropical cyclone's location and intensity over its lifetime. The best track analysis includes the cyclone's latitude, longitude, maximum sustained surface winds, and minimum sealevel pressure at 6-hourly intervals. Because the Best track positions and intensities are based on a post-storm assessment of all available data, they may differ from values contained in storm

advisories. In general, they will not reflect the erratic motion of the storm obtained by connecting individual storm positions observed by reconnaissance flights.

The assimilated data in the Best Analysis come from many diverse sources such as:

- Aircraft reconnaissance and dropsonde data from the U.S. Air Force Reserves (the Hurricane Hunters) and National Oceanic and Atmospheric Administration (NOAA),
- Estimates from analyses of surface synoptic data, as well as Dvorak-technique (1975, 1984) estimates from the Tropical Analysis and Forecast Branch (TAFB), the Satellite Analysis Branch (SAB), and the U.S. Air Force Weather Agency (AFGWC) using satellite imagery,
- Ship reports,
- Surface observations from land stations and data buoys,
- Radar imagery from NOAA/WP-3D aircraft research missions,
- Microwave, visible and infrared imagery from satellite data, and
- Analyses from the Physical Oceanography Division of NOAA/ AOML (Atlantic Oceanographic and Meteorological Laboratory).

Caution must still be exercised when dealing with the Best Analysis products: although it is the most comprehensive analysis available, the assimilated data are obtained, for the most part, from spatially discrete observations (dropsonde, buoy, ship reports and flight data). There is still a major lack in terms of area-derived, if not volume-derived, accurate, observational data. Most of the large-scale environmental features are analysed using numerical weather model output, the quality of which is obviously area and model dependent. The Best Analysis nevertheless remains the most accurate depiction of the storm life available.

The Best Analysis for Floyd is summarized below. Figure 2-1 presents the Best Analysis track, at 12-hourly intervals. Figure 2-2 depicts the corresponding sea level pressure (SLP) evolution while Figure 2-3 shows the associated wind magnitudes, as well as the corresponding category of the storm according to the Saffir-Simpson scale.

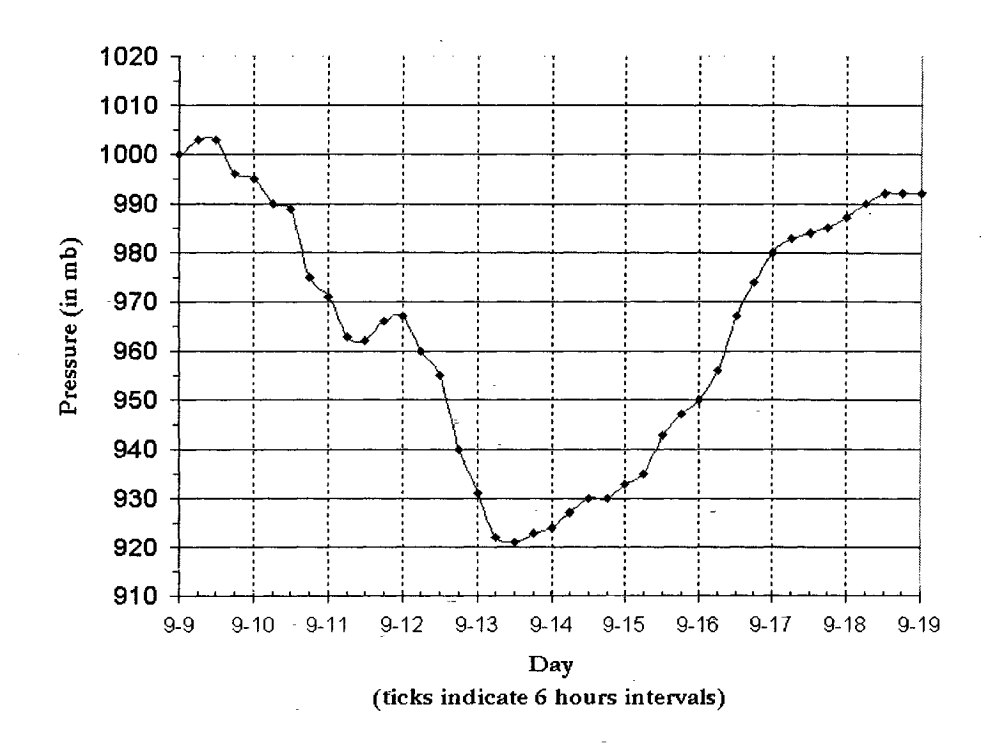


Figure 2-2: Best Analysis Minimum Central Sea Level Pressure; 6-hourly intervals

Saffir/Simpson Scale Category :

Floyd's Best Analysis Maximum Winds

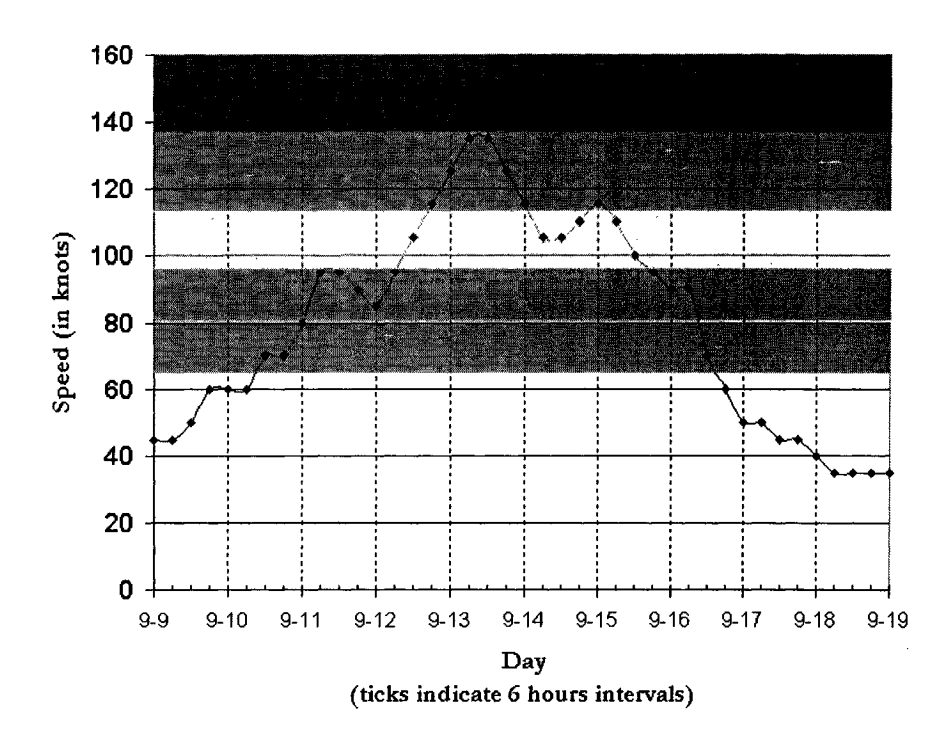


Figure 2-3: Best Analysis Maximum winds, 1-minute average; 6-hourly intervals

2.3 Other satellite and analysis products

The following products are presented here for future reference.

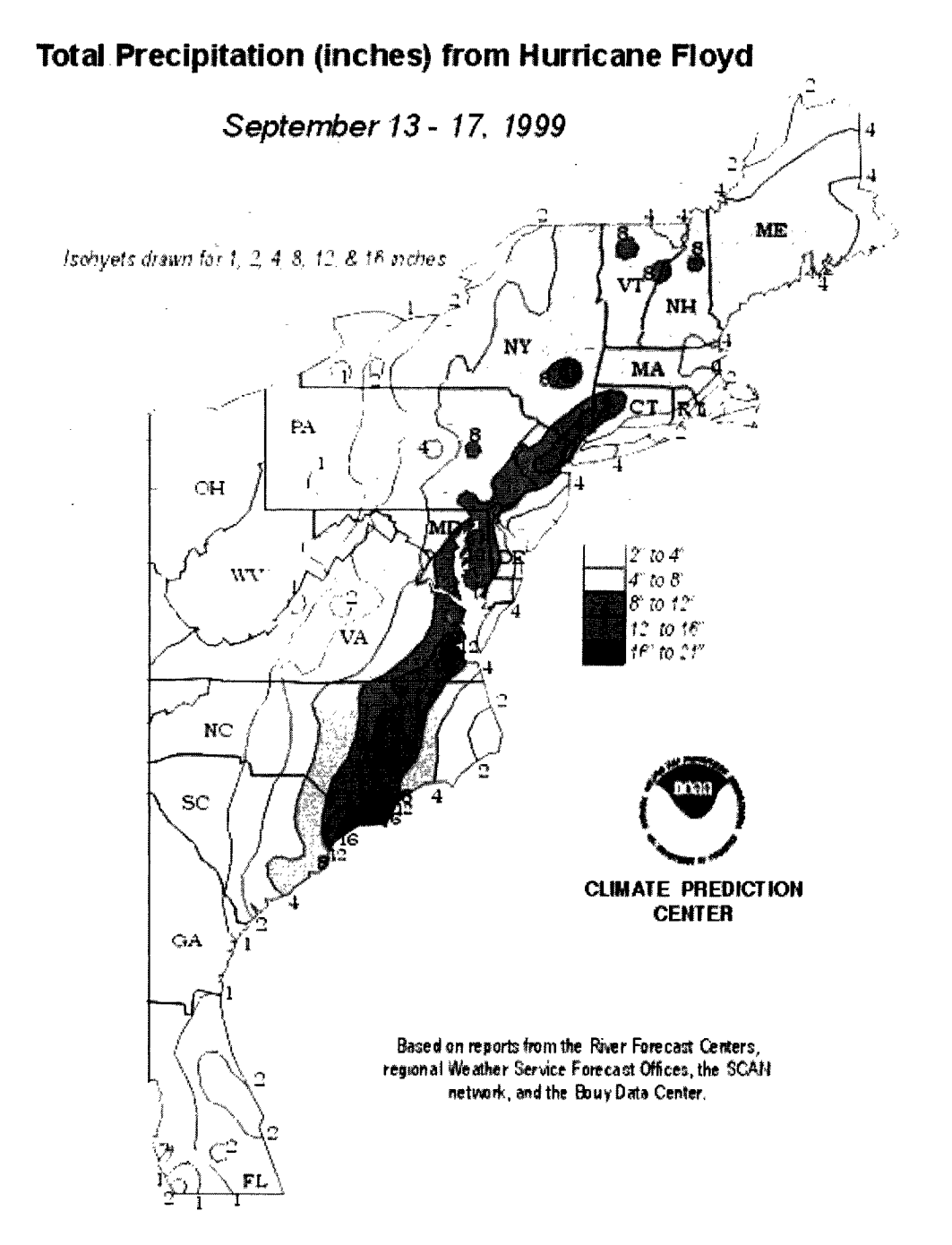


Figure 2-4: Total accumulated precipitation from the passage of hurricane Floyd over the United States, taken from September 13 to September 17, 1999. (courtesy of the Climate Prediction Center)

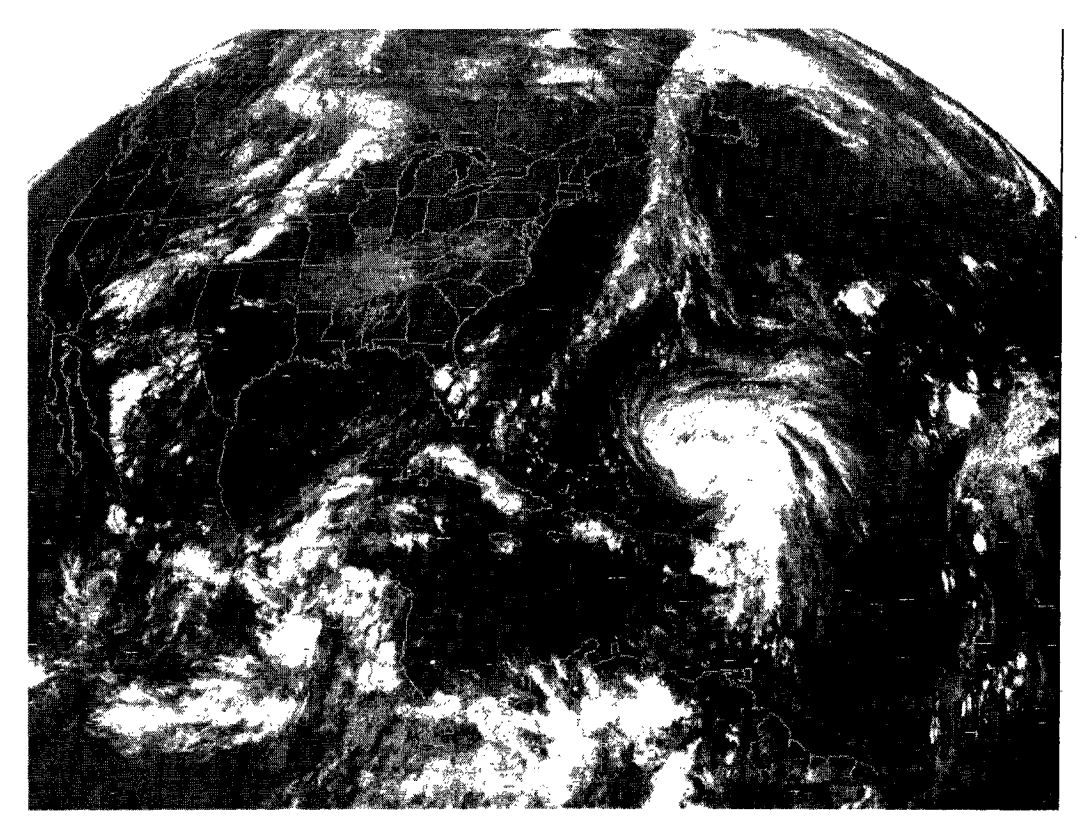


Figure 2-5: GOES-8 Infrared Image on September 11, 0015 UTC

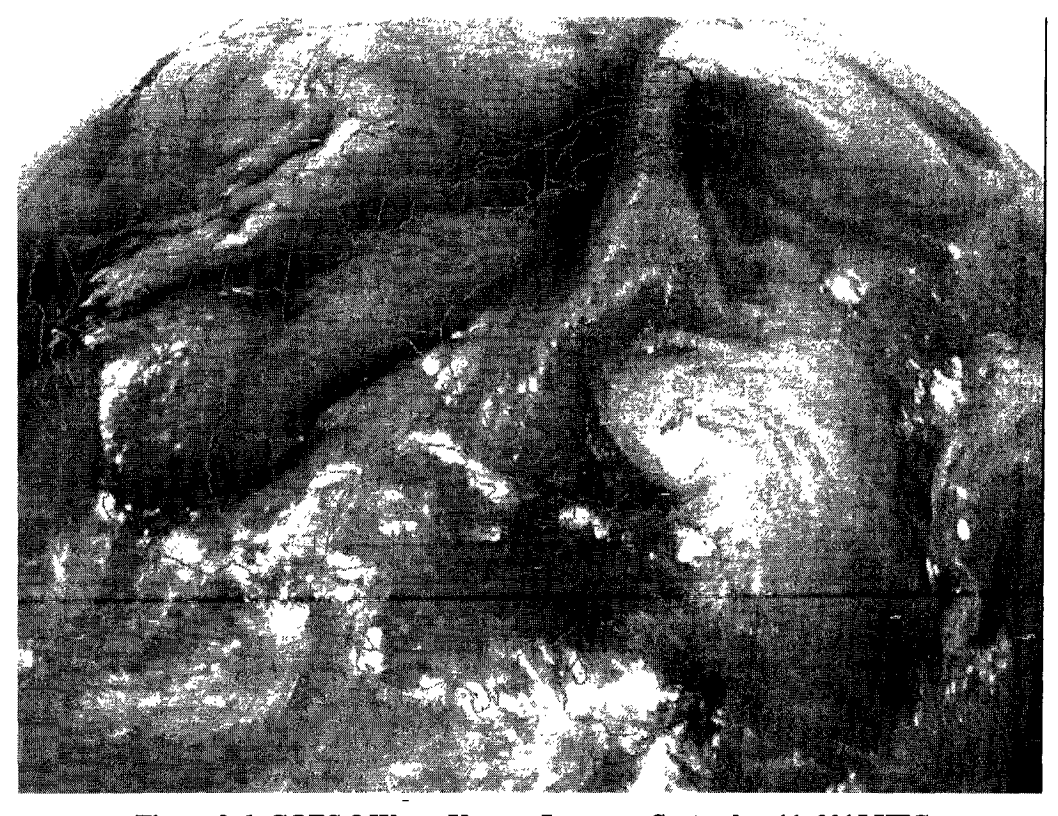


Figure 2-6: GOES-8 Water Vapour Image on September 11, 0015 UTC

Hurricane Floyd 0130 UTC 11 Sept. 1999

Max. 1-min sustained surface winds (kt) for marine exposure

Analysis based on US AFRES C-130 Recon. winds at 700 mb adj. to sfc: 2030 -2335 z. 3 GPS sondes sfc. obs.: 2127-2307 z;

0130 z position extrapolated from 2307 z wind center fix using 3150 @ 10 kt , mslp = 971 mb.

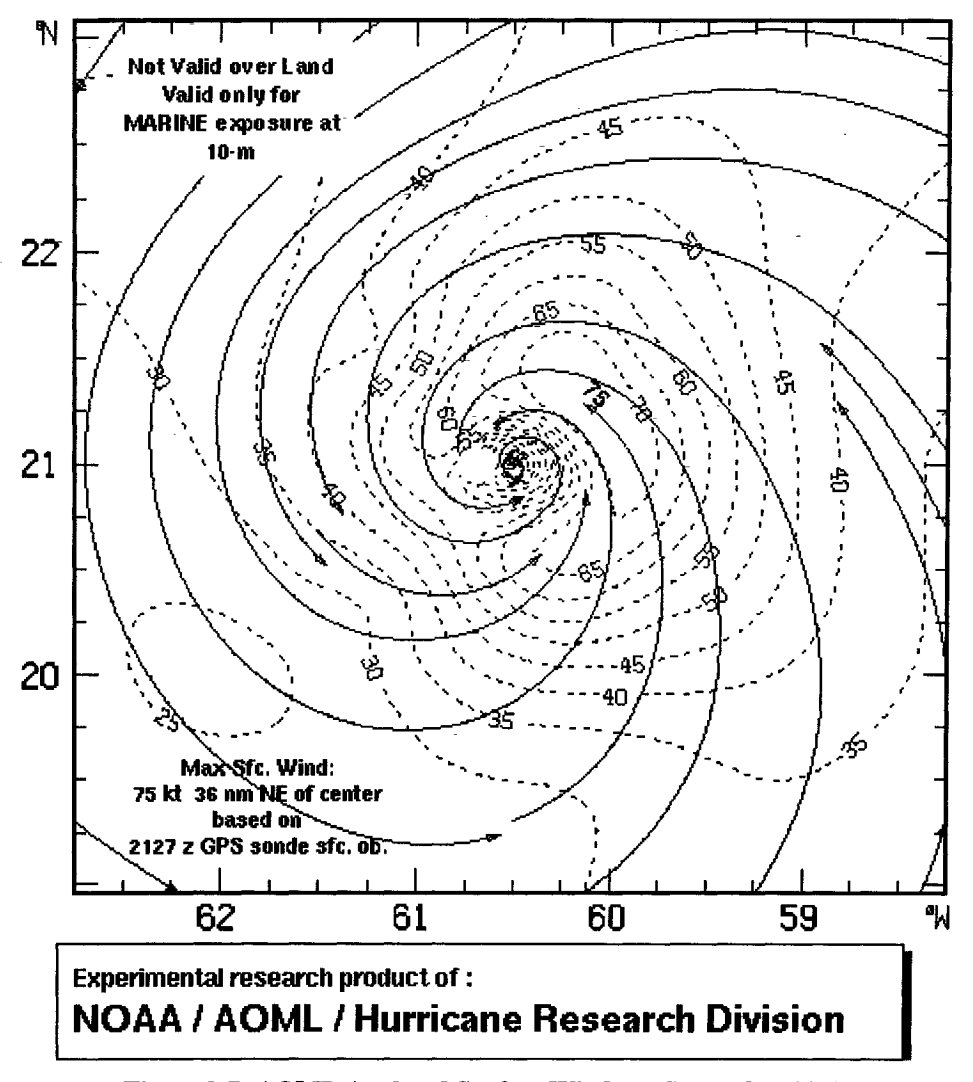


Figure 2-7: AOML Analysed Surface Winds on September 11, 0130 UTC

2.4 Impact of Sea Surface Temperature on the hurricane

As noted in section 2.1, the Physical Oceanography Division of NOAA/ AOML analysed a zone of warm upper ocean to the east of the Bahamas, a few days prior to the passage of hurricane Floyd. The Sea Surface Temperature (SST) product from the Advanced Very High Resolution Radiometer confirmed that analysis (Figure 2-8). There seems to be evidence of very good

correlation between the hurricane intensity and SST anomaly as the storm passed over the zone of warm water.

Let us recall here the theoretical impact of a varying SST on the surface heat fluxes. Changes in SST will affect both the sensible heat flux (SHF) and, to a much lesser extent, the latent heat flux (LHF). This difference is due to the fact that the LHF is not dependent on temperature variations per se, but to the subsequent changes in specific humidity of the overlying air.

A typical SHF can be expressed by a standard bulk atmospheric formulation using the gradient method (e.g. Kraus 1972):

$$SHF = c_{p} \rho_{a} \xi_{s} (\theta_{SST} - \theta_{10}) \times U_{10}$$

where c_p is the specific heat of air, ρ_a is the air density, θ_{SST} is the sea surface potential temperature, θ_{10} is the potential temperature at 10 meters above sea surface and U_{10} is the 10 m wind, and ξ_s is the drag coefficient for sensible heat. For the latter, a linear dependence on wind speed can be approximated by ξ =(0.75+0.067*U) where U is in m/s. A typical value would be $2x10^{-3}$ for surface winds of about 20 m/s (Garratt, 1977). The linear dependence of the SHF on the potential temperature differences suggests that an increase of one degree Kelvin in the temperature difference would result in an increase in SHF of about 50 Wm⁻² for winds reaching 20 m/s. Data obtained from observations of hurricanes seem to confirm the validity of the expression for the drag coefficient for winds up to 50 m/s. At such wind speeds, the expression yields SHF values of 270 Wm⁻² for a 1°K temperature difference. The neglect of the effects of sea spray in the calculation might account for such high values.

In the case of Floyd, we can estimate the values of SHF during the storm passage over the warm SST anomaly. From the dropsonde data available, the maximum surface air temperature is about 29.2°C on September 11 at 1200 UTC. As shown by the 7-day average SST in Figure 2-8, there is an SST excess of one to two degrees Celsius in the region of the blob (from 30-31°C in the surrounding to 32°C in the blob). This results in a temperature difference between the sea surface in the blob and the overlying air of about 2.8°C. Using the observed surface winds of 50 m/s at that time, the computed SHF is about 750 Wm⁻². Again, sea spray effects are not accounted for in this crude estimate of the SHF. Yet, it still falls within the upper range of minimum-maximum SHF observed in a large number of hurricanes (Cione, 2000).

Such strong fluxes could be partly responsible for the major strengthening episode that Floyd underwent upon passing over the blob, where its intensity increased rapidly from a category-2 to a category-4 hurricane (Figure 2-8).

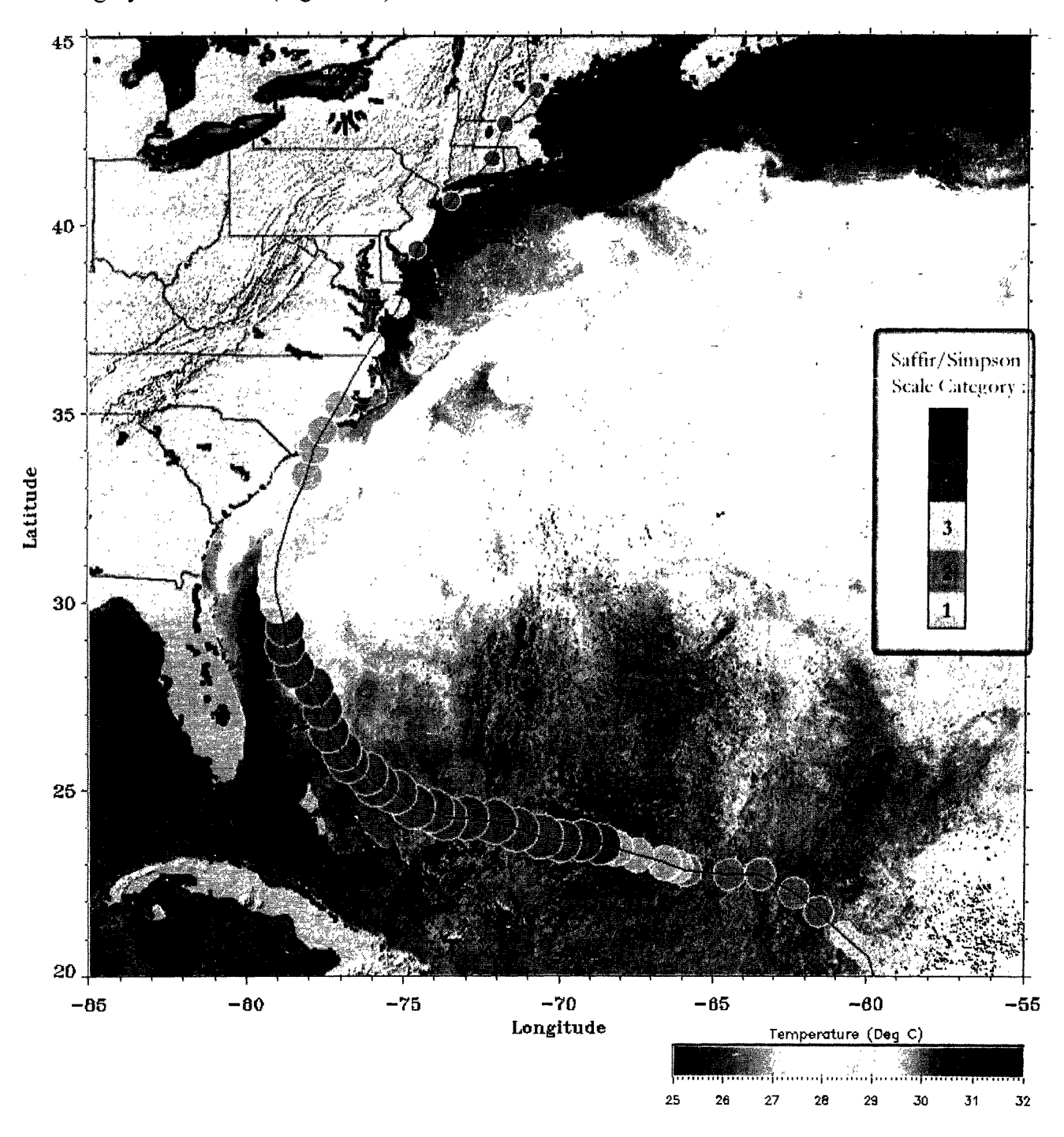


Figure 2-8: 7-day average AVHRR-derived Western Atlantic SST (ending on September 9, 1999, at 2256 UTC), correlated with hurricane Floyd intensity evolution as noted by the Saffir-Simpson scale wind ranges (copyright Ray Sterner & Steve Babin, John Hopkins University Applied Physics Laboratory)

Chapter 3 AMSU: Specifications & Retrieval

3.1 AMSU Background

3.1.1 Passive Remote Sensing

Passive remote sensing is defined as the means through which a sensor (radiometer) receives an intrinsic electromagnetic radiation from the medium (e.g. the atmosphere) to measure the intensity of a particular frequency in that spectrum. Contrary to active remote sensing (e.g. radars), radiometers do not emit any signal and there is no measurement of the back-scattered signal.

Electromagnetic radiation is characterized by its wavelength (λ , in meters) or frequency (ν , in Hertz), which are inversely proportional:

 $\nu = c/$

where c is the speed of light in vacuum (c=2.997*10⁸ m/s).

3.1.1.1 Brief overview

Radiation remote sensing is based on two fundamental properties:

- 1. All bodies with temperatures above absolute zero emit radiation in the electromagnetic spectrum.
- 2. Electromagnetic radiation transports energy that interacts with the atmosphere before being measured by the sensor.

The types of interactions that can take place are absorption, emission and scattering. For a non-scattering medium in thermodynamic equilibrium, the radiative transfer equation becomes the following standard integral equation (Grody in Janssen 1993):

$$I_{\nu}(0) = I_{\nu}(s0)e^{-\tau(s0)} + \int_{0}^{s0} B_{\nu}(T)e^{-\tau(s)}ds$$
(3.1)

where I represents the instantaneous radiant power that flows in the medium, per unit area, per unit frequency interval at a given frequency, s is the path length (0 being the location of the sensor, s0 the distance to which measurements are being made), T is the temperature, Bv (T) is the Planck function and τ is the optical depth defined as:

$$\tau(s) = \int_{0}^{s} \alpha(s') ds'$$

where α is an absorption coefficient.

The Planck function, derived by Max Planck in his theory of the blackbody, is sometimes considered as a surface brightness and is defined as follows:

$$B_{\nu}(T) = \frac{2h\nu^3}{c^2} \frac{1}{e^{\frac{h\nu}{kT}} - 1}$$

where h is Planck's constant and k is Boltzmann's constant and c, v, T are as previously defined.

3.1.1.2 Application to the microwave spectrum

In the case of the microwave, further limits can be introduced. Since $hv \ll kT$, the Planck function can be approximated as defined in the *Rayleigh-Jeans limit*:

$$B_{\nu}(T) \approx \frac{2\nu^2 kT}{c^2} = \frac{2kT}{\lambda^2}$$

The fundamental result is that the Planck function varies *linearly* with temperature. A scaling of intensity can thus be introduced so as to define the **microwave brightness temperature** T_b :

$$T_b(v) \equiv \frac{\lambda^2}{2k} I_v$$

One can then rewrite Eq (3.1) as:

$$T_b(\nu) = T_{b0}e^{-\tau(s0)} + \int_0^{s0} T(s)e^{-\tau(s)}\alpha ds$$
 (3.2)

where
$$T_{b0} = \frac{\lambda^2}{2k} I_{\nu}(s0)$$
.

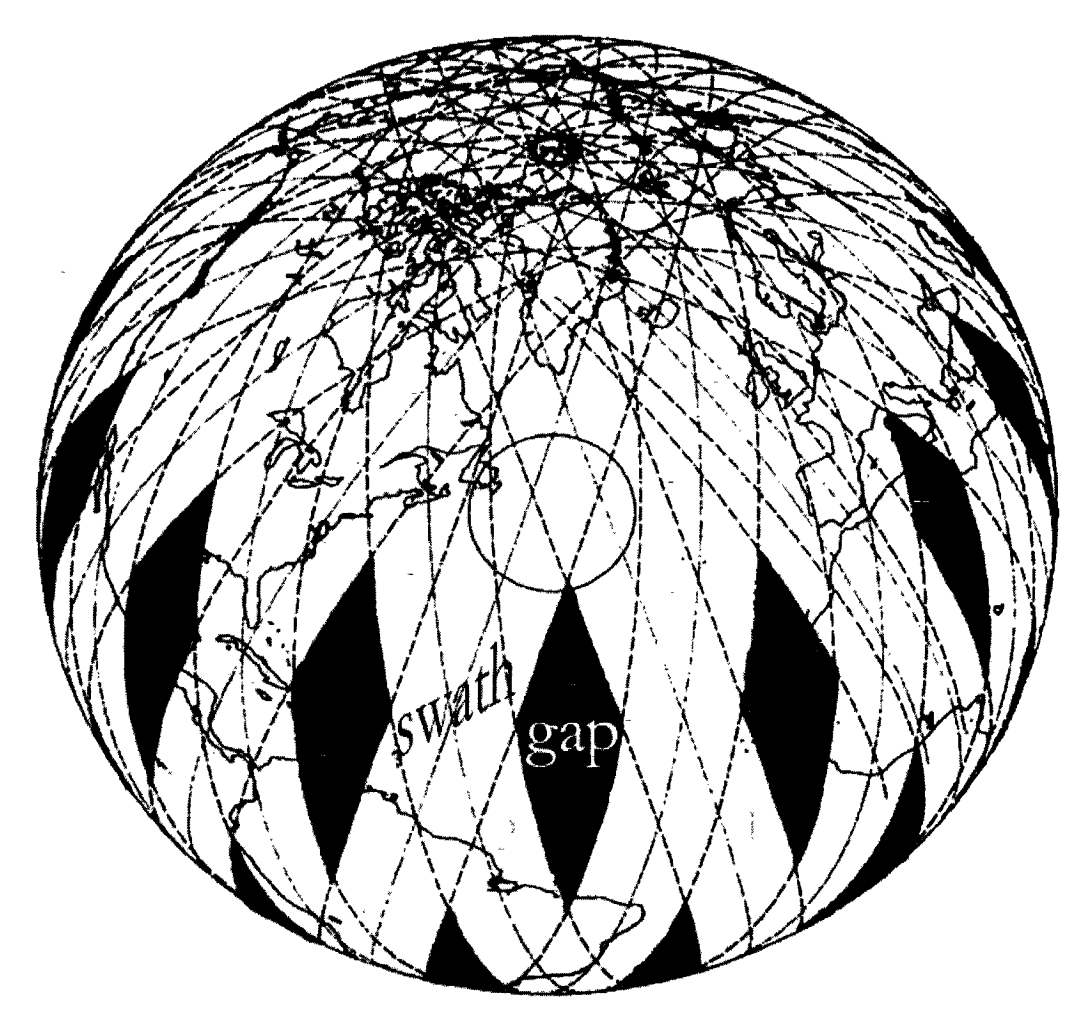
This is the common radiative transfer equation used in microwave remote sensing. It is applicable for unpolarized and non-precipitating atmospheres free from scattering.

3.1.2 AMSU Instrument

Meteorological observational data are very sparse over many regions of the globe. Less populated and less developed areas do not benefit from regular, and quality-controlled observations. There is even less data coverage over the oceans posing considerable problems for data assimilation and numerical weather prediction.

Over the last 30 years, however, the increasing number of satellites, both polar-orbiting and geostationary, has provided the scientific community with many more global, accurate and well-calibrated sensors. Remote sensing is nowadays the most effective way of obtaining data over regions where data coverage is sparse. Historically, the visible and infrared spectra were preferred. However, they both suffer from two very limiting constraints: visible data are only available during the daytime and infrared emissions are strongly absorbed by clouds. Microwave frequencies are much less affected by hydrometeor scattering and are thus more appropriate for vertical soundings.

All microwave sounding units are flown on polar orbiting satellites (POS). As a result, data are acquired in a non-continuous manner. Geo-synchronous orbits would be more valuable for acquiring synoptic and continuous views for any given location of the atmosphere. In fact, they are in use for optical and infrared sensors but there are still complicated technical issues for microwave sounding units over such a large distance, as a much larger antenna is required for useful spatial coverage. Sun-synchronous orbits are common for actual POS. This provides data at time intervals between 12h and 24h for a given location. Mid-latitudes and polar regions are scanned more frequently than tropical regions as depicted in Figure 3-1.



• Swath: 2179 km

• Retrograde orbit: Ascending pass #2 comes 102 minutes after #1, and 25.5 degrees west of its previous equatorial crossing

• Inclination: 99 degrees; Sun-synchronous

Figure 3-1: Polar Orbiting Coverage for AMSU

Launched in 1978 by the National Oceanic and Atmospheric Administration (NOAA), the Microwave Sounding Unit (MSU) was placed onboard the first generation of NOAA POS. It contained 4 channels within the oxygen band (cf Table 3-1) and, despite a fairly low horizontal resolution, the MSUs proved to be extremely stable and allowed for accurate measures of global temperature changes (Grody in Janssen 1993). The limitations inherent to the capacities of the MSU were overcome with the new generation of POS from NOAA.

Satellite	Sensor	Center Frequencies (GHz)	Nadir IFOV (km)	Year
NOAA 6 to	MSU	50.3, 53.74, 54.96, 57.95	110 (X-Scan)	1978-1995
NOAA 14				
NOAA 15	AMSU-A	23.8, 31.4; 50.3, 52.8, 53.481,	48.05 (X-Scan)	1995
&	-	54.4, 54.94, 55.5, 57.29,		
NOAA 16	-	57.073, 56.92, 56.946, 56.958,		
	_	56.964, 89.0		
NOAA 15	AMSU-B	89.0, 157.7, 183.31±1,	16 (X-Scan)	1995
& 16	_	183.31±3, 183.31±7		

Table 3-1: Satellite Microwave Radiometers (from Janssen, 1993).

(IFOV= Instantaneous Field of View, X-Scan= cross-scanning)

The first of the new generation of Advanced Microwave Sounding Units (AMSU) was launched in May 1998 onboard NOAA 15 (NOAA-K prior to launching). Comprised of both AMSU-A and AMSU-B sensors, it marked a definite improvement over the previous MSU sensors. Indeed higher spatial scanning now allows for near meso- scale resolution (an IFOV of 48km allows for roughly 100km resolution, according to Nyquist frequency). Figure 3-2 presents a comparison of the spatial improvement of the AMSU-A footprints (open circles, 30 per scan pass) and AMSU-B (dots, 90 per scan pass) over the MSU ones (grey circles, 11 per scan pass).

Table 3-2 presents a detailed overview of the AMSU-A, which is the only sensor used in this study. As presented, we can see that 15 channels are now used. Those 15 brightness temperatures thus allow for increased vertical resolution when compared to the 4 channels of the MSU. Appropriate weighting of each channel allows for temperature retrieval, as discussed later. AMSU-A is effectively composed of two units: AMSU-A1 and AMSU-A2.

AMSU-A2 contains two window channels at 23.8 GHz and 31.4 GHz. The former frequency is used to retrieve the total precipitable water (TPW) over the oceans whereas the latter serves to monitor the surface emissivity features. AMSU-A1 contains 12 channels in the 50-60GHz

oxygen band to provide brightness temperature soundings and one last channel at 89 GHz used to monitor precipitation (Grody, 1999).

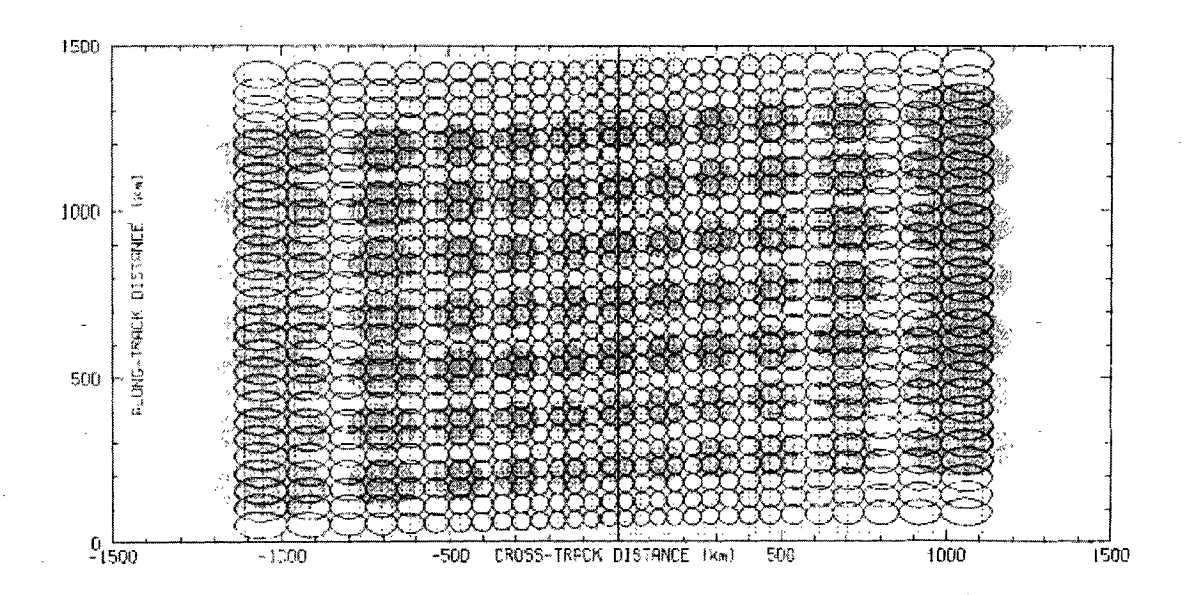


Figure 3-2: MSU vs AMSU-A footprints (from Kidder et al., 2000)

Satellites	NOAA 15+ 15			
Number of Channels				
Frequency Range (GHz)	23.8 – 89.0			
Scan Type	Cross Track			
Beamwidth	3.3°			
Instantaneous Field Of View (Nadir, km)	48.05			
Scan Steps	30			
Swath Width (km)	2179			
AMSU-A1 Frequencies (surface emissivity, Channels 1-2, GHz)	23.8, 31.4			
AMSU-A2 Frequencies (Brightness temperatures, Channels 3-15, GHz)	50.3, 52.8, 53.481, 54.4, 54.94, 55.5, 57.29, 57.073, 56.92, 56.946, 56.958, 56.964, 89.0			

Table 3-2: AMSU-A Specifications

3.1.3 AMSU Data

3.1.3.1 Constraints

Since the AMSU is flown on a POS, tropical data is usually available once a day at a given location (twice at a 12h interval if both ascending and descending passes of the satellites overlap). Moreover, if NCEP analyses are to be used, there is a challenge trying to find a pass close enough to the times of the 6-hourly analysis.

Besides the temporal constraint, the very nature of the polar orbit makes it such that satellite swaths do not overlap over the tropics. As a result, there are gaps in the data. It can happen that the meteorological phenomenon (i.e. the hurricane in our case) is located inside the gap, and in this case, 12 hours or more have to pass before a new measurement is obtained.

Finally, since AMSU is a cross scanning sensor, we encounter the issue of limb correction. As the scan goes from left to right, the beam travels initially through a thicker portion of the atmosphere which becomes minimum at nadir and increases again as it finishes its scan to the right of the swath. On both external sides of the swath, we thus encounter a perturbation, which needs to be corrected during the temperature retrieval. Figure 3-3 presents a typical channel as retrieved by the satellite: one can clearly see the warmer limb anomalies as well as the gaps (within which the hurricane happens to be at that time).

3.1.3.2 Hurricane Floyd case data

The data used in this study came from NOAA/NESDIS/ORA and was kindly provided to us by Ralph Ferraro and Huan Meng. It consists of daily-composites from all the AMSU passes, mapped on a 0.5° uniform latitude-longitude grid. We tried to avoid choosing data during the incipient stage of the hurricane and, as much as possible, to pick a date and time where numerous observations existed: dropsonde data, flight data, NHC best analysis, surface wind analysis, etc...

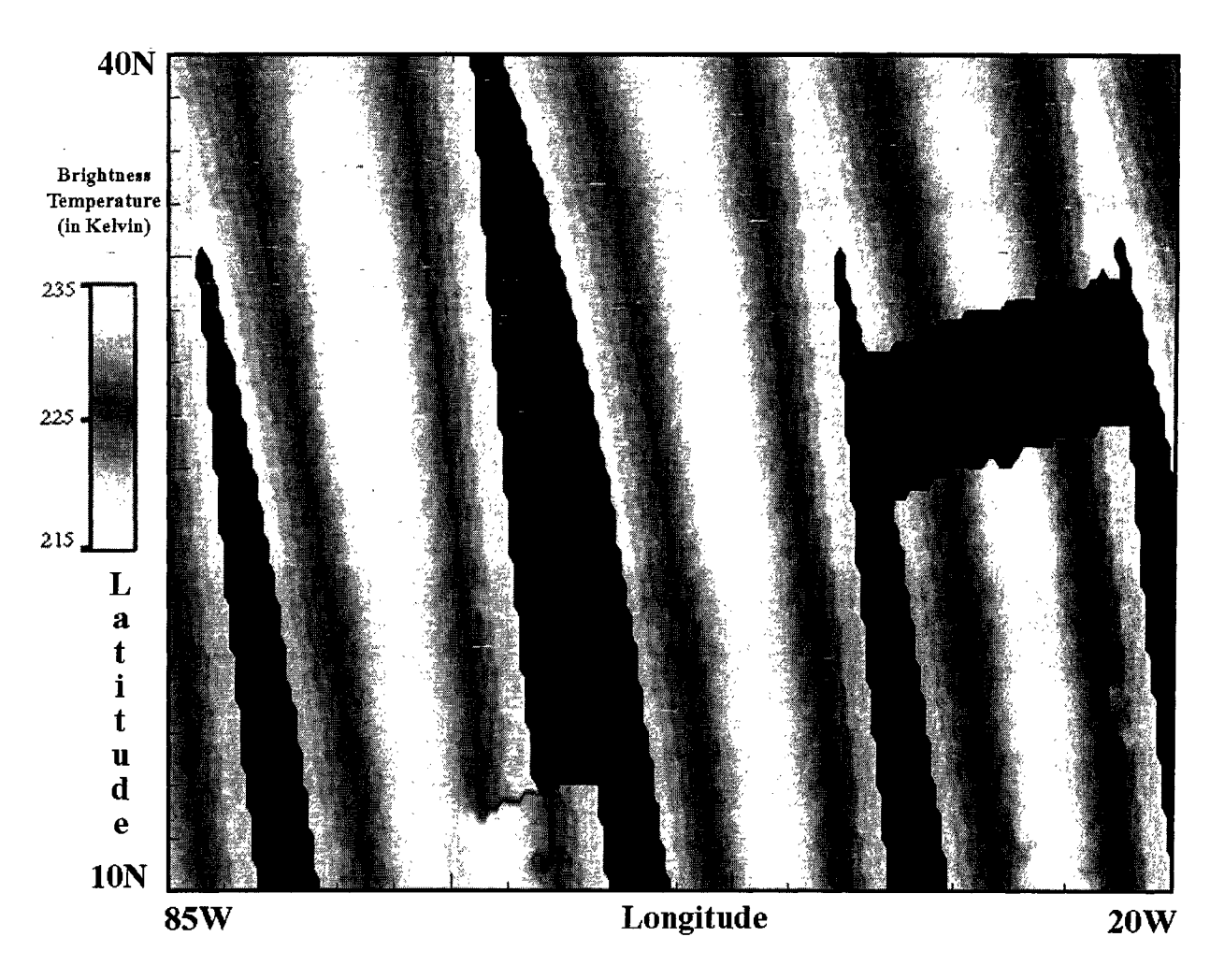


Figure 3-3: AMSU-A Constraints: Limb warming and data-void gaps

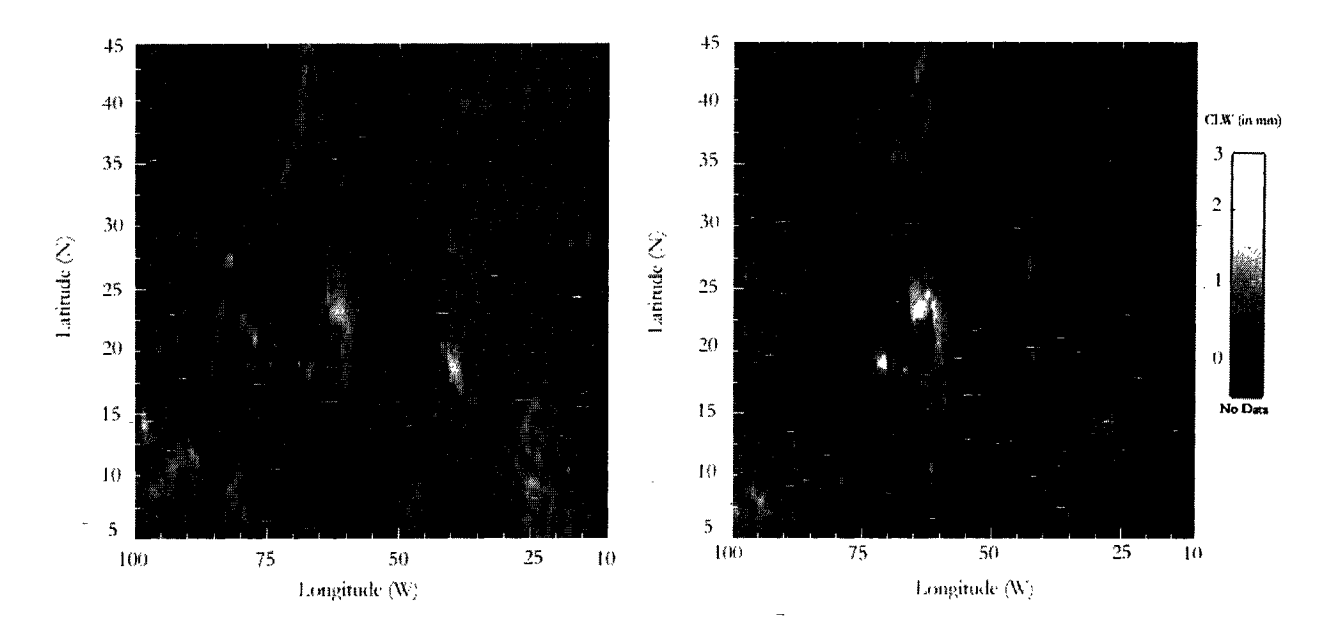


Figure 3-4: Cloud Liquid Water passes, on September 10 12Z (left, descending) and September 11, 1999 00Z (right, ascending)

Figure 3-4 presents the two available passes (ascending and descending) for cloud liquid water (CLW) that were used to find the center of the hurricane (assumed to be near the CLW maximum). The ascending pass proved to be a very good compromise given all the constraints: the hurricane was in the exact middle of the swath (thus less affected by the limb perturbation), the center was scanned at 2300 UTC on September 10 (a close enough approximate to 0000 UTC on September 11) and it happened to be some 36 hours prior to the rapid intensification of hurricane Floyd on September 13 at 1200 UTC (a good opportunity for a proper model spin-up). The retrieval procedure was used on the data from this ascending pass. One can compare the CLW pattern to the water vapour obtained from the GOES-8 satellite in Figure 2-6: even though the two variables are not directly linked, we see a good correlation between very high values of water vapour and CLW both in the hurricane and over the island of Haiti and the Dominican Republic.

3.2 Retrieval Algorithm

The algorithm used in this study was developed by Tong Zhu and Da-lin Zhang at the University of Maryland. It has been successfully applied to the case of hurricane Bonnie (Zhu *et al.* 2002). The algorithm consists of three main steps:

- 1. retrieval of temperatures from AMSU-A brightness temperatures,
- 2. computation of geopotential height using Holland's Maximum Wind Radius (MWR) scheme
- 3. inversion of the gradient balance equation to retrieve the streamfunction to obtain the winds.

Specific humidity retrieval is also investigated.

3.2.1 Temperature retrieval

3.2.1.1 Theoretical background

Grody (in Janssen 1993) proposed an algorithm for retrieving physical temperatures from AMSU brightness temperatures. Temperatures can be retrieved on prescribed pressure levels by performing a weighted, linear combination of the retrieved brightness temperatures. The temperature on a given level, T(p), is then given as:

$$T(p) = C_0(p,\theta) + \sum_{i=1}^n C_i(p,\theta)T_b(v_i,\theta)$$

where θ is the local zenith angle, ν_i is the frequency at channel i and C_i is the weighting coefficient for channel i.

Using rawinsonde soundings collocated and paired with brightness temperature soundings (within 1h and 1° from one another), the coefficients C_i and C₀ were obtained by performing a regression equation. At least 115 rawinsonde soundings were paired with AMSU soundings for each of the 15 scanning angles. Important variations are found, as shown in Table 3-3 for a specific example of temperature retrieval at 850hPa. (Complete description of the coefficient values is given in Appendix B).

Coef	CO	G	C4	C5	C6	C7	(8)	C9	CIO	CII
Angle										
0.3	25.962	0.152	0.440	2,429	1.954	0.983	1.284	0.04	0.683	0.760
3.7	102,552	0.348	1.257	1.146	1.094	1.082	1.679	0.198	0.951	1.033
7 11	214.337	0.096	0.250	2.775	1.083	1.510	1.506	0.529	1.185	0.739
11-15	239,656	0.307	1.280	1.664	1.707	0.852	0.124	0.447	0.185	0.114
15 19	118,205	0.263	0.888	4,757	2.018	0.764	0.714	0.714	0.379	0.033
10.23	142.471	0.016	0.406	1.593	0.203	1.055	0.711	0.588	0.805	0.014
23-26	78,988	0.047	0.506	1.119	0.036	1.270	0.438	0.297	0.186	0.643
26 30	93,384	0.055	0.744	0.685	0.348	0,303	0,092	0.537	0.546	0.562
30 34	148.070	0.192	1.879	0.586	1.351	0.106	0.266	0.139	0.065	0.375
34 38	-215,957	0.364	2.045	- 0.441	1.100	0.385	0.397	0.052	0.327	0.640
38 42	173,519	0.157	1.631	0.347	- 1,003	0.658	0.285	0.177	0.381	0.588
42:46	135,199	0.087	2.001	0.173	1.420	0.806	9.248	0.041	0.274	0,124
46 50	272.788	0.033	2.459	0.492	1.017	0.948	0.342	0.061	0.322	0.382
50 54	99,822	0.110	1.764	0.326	1.436	0.842	2.151	1.254	0.266	0.381
54 - 58	66,107	0.288	1.394	0.463	0.886	1.452	2.112	0.680	0.215	0.103

Table 3-3: Channel weighting coefficients for a temperature retrieval at 850 hPa (adapted from Zhu *et al.* (2002))

Figure 3-5 shows a set of weighting functions for the 12 brightness channels, at nadir, over land.

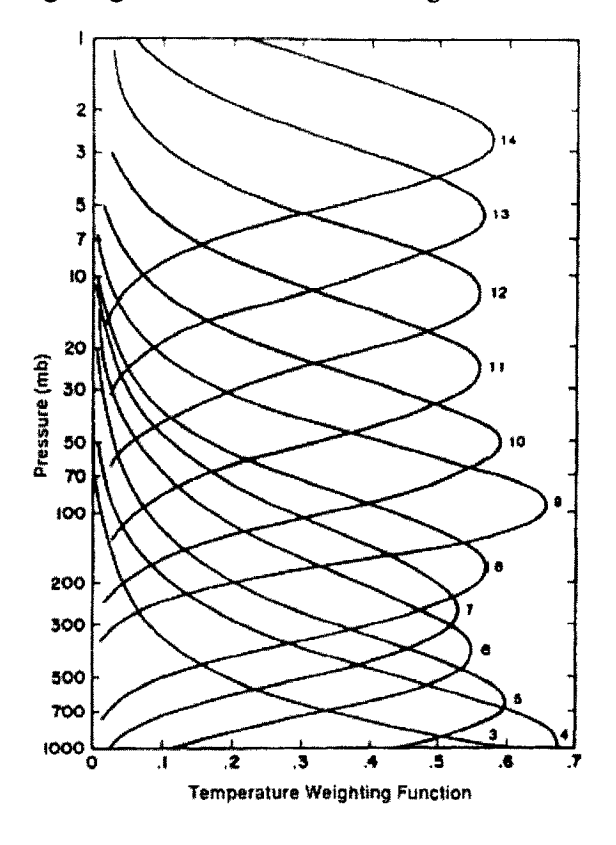


Figure 3-5: AMSU-A Channels 3-14 theoretical weighting functions at nadir over land (adapted from Grody in Janssen, 1993)

Accuracy of the temperature retrieval can be investigated by computing the root-mean square error (RMSE) from the rawinsonde best estimate of temperature. Figure 3-6 presents the RMSE computed from all the rawinsonde observations used in the regression. For the upper and middle troposphere, the error is found to be within 0.8K-1.0K. In the low-levels, higher variability, together with less clearly-defined contributions from the channel weighting (as seen in Figure 3-5), contribute to an increase of the error from 1.0K-1.5K. The same order of magnitude is found for the RMSE in the stratosphere.

For more accurate results, one needs to enquire about the accuracy of rawinsonde temperature measurements. Typically, rawinsonde errors increase as the pressure decreases. In the troposphere (from surface to 200hPa), rawinsonde RMSE lies between 0.2K-0.4K. It increases to 0.5K-1.0K for pressures between 100 and 10hPa.

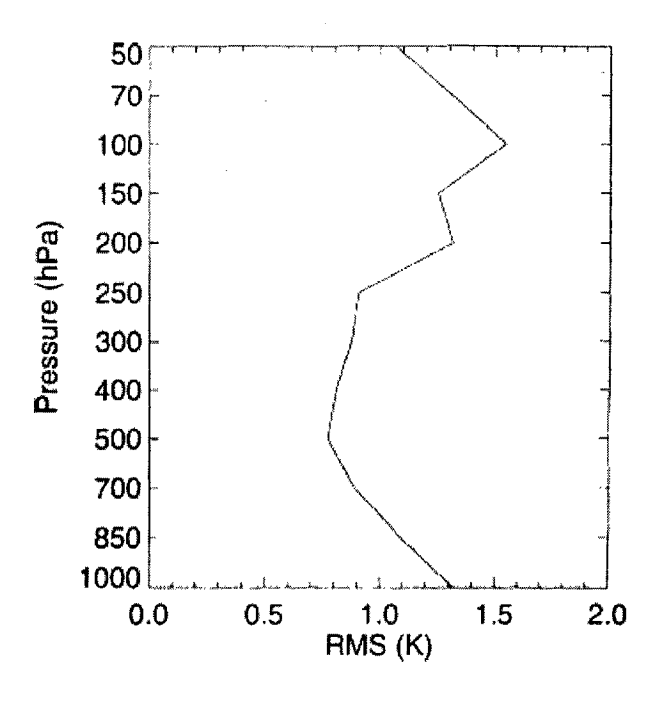


Figure 3-6: Diagnosed RMS error for temperature retrievals compared to rawinsonde observations.

3.2.1.2 Hydrometeor contamination corrections

In most atmospheric conditions, very little perturbation is induced on the brightness temperature retrieval. However, in heavy rainfall conditions, large scattering will induce cold anomalies in the retrieved signal. Two corrections are made at the lower levels when contaminated by heavy rainfall.

In the first correction, we first identify heavy rainfall regions from the integrated Cloud Liquid Water (CLW) retrieved from satellite observations. For regions where CLW is greater than 0.3mm, we discard the 3 lowest-peaking channels (namely channels 3 to 5) in order to limit the hydrometeor contamination. Two sets of coefficients are therefore derived: the first set is for the full 12 AMSU-A sounding channels (3-14) while the second set is used for the last 9 channels (6-14).

In the second correction, we adopted the procedure of Demuth (2001) who performed a hydrometeor correction from 64 cases of tropical cyclones in 1999. Out of 154 AMSU passes, only those 64 were selected for a greater consistency since the tropical cyclones were fully over the oceans. On each pressure level, temperature deviations from the domain mean (12° by 12° domain centered on the storm) is computed and a linear regression is performed, using the CLW values as the independent variable. The slopes obtained on each level are then quadratically fitted to obtain the correction coefficient m, as seen in Figure 3-7. On a pressure level p, the temperature correction can then be applied at each grid point (i,i) as follows:

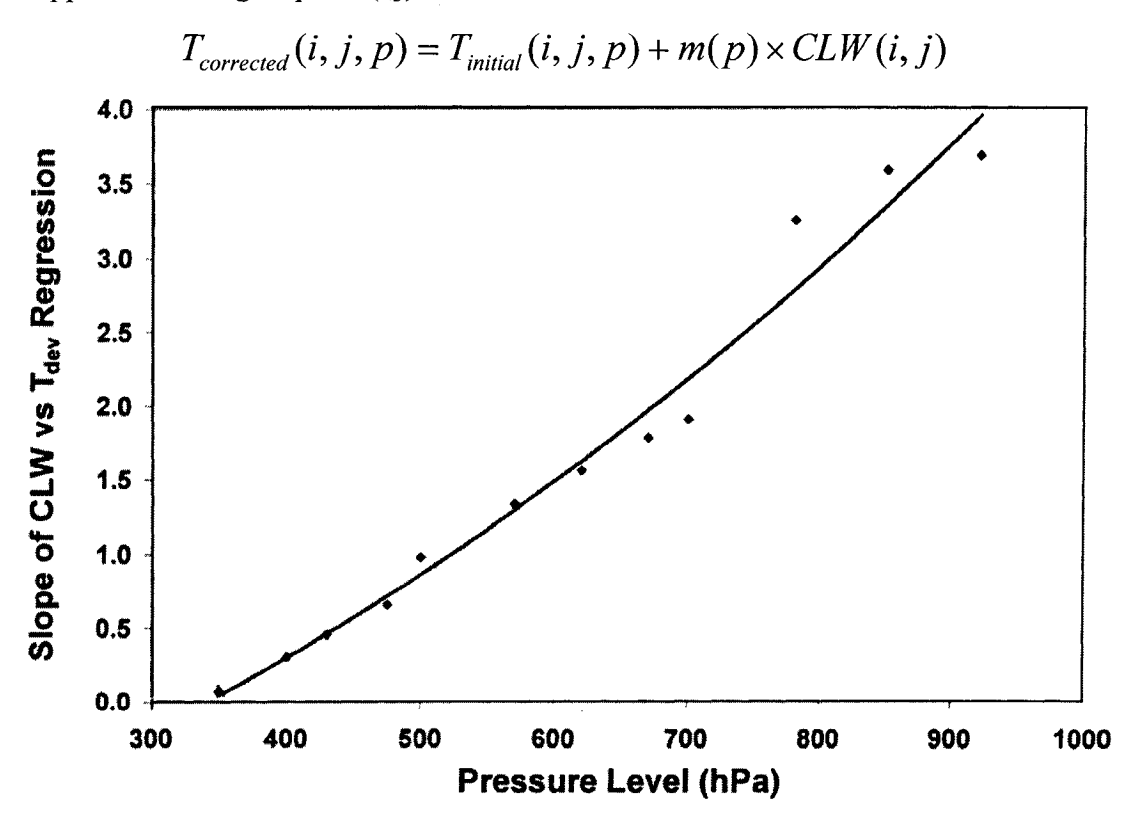


Figure 3-7: Slope m of CLW vs temperature deviation regression, for each pressure level (from Demuth (2001))

The value at 1000 hPa is extrapolated from the quadratic curve and set to a value of 5 K/mm.

Ice correction is also another possible correction to be included for more accurate temperature retrieval. Yet, according to Norman Grody, lead researcher in AMSU physics, "the AMSU measurements are most useful for studying hurricanes since the temperature anomaly occurs way above the freezing level (around 200 to 300 hPa). At these altitudes, few large-ice particles (>1 mm in size) are present so that the effect is lessened on most of the relevant AMSU channels" (Grody, 2002). We thus neglected these effects in this study.

3.2.2 Geopotential-height diagnosis

Upon retrieval of the 3D temperature field, we diagnose the geopotential height field by integrating the hydrostatic equation while specifying an empirical sea level pressure (SLP) distribution according to Holland's Maximum Wind Radius (MWR) scheme.

The rationale here is that, in most available analyses, a weak bogus hurricane vortex is usually inserted in order not to destroy the validity of the analyses. It follows that, for most of the hurricane lifecycle, the analyzed SLP field is usually off by a few tens of hPa in the vicinity of the hurricane, when compared to the best analysis provided by the National Hurricane Center (NHC). Integrating the hydrostatic equation with such a first guess SLP would result in a geopotential height field inconsistent with the retrieved temperatures.

We choose to integrate the hydrostatic equation upward rather than downward to avoid accumulation of the errors in the boundary layer: as seen in Figure 3-6, larger retrieved errors exist in the stratosphere and would thus accumulate down. We therefore use Holland's MWR scheme (Holland, 1980) to specify the initial SLP from which the integration is performed. This scheme necessitates the specification of the maximum wind speed V_{max} , the radius of maximum wind R_{max} and P_c , i.e. the minimum central SLP of the hurricane. Reconnaissance flights from the Hurricane Research Division (HRD) provide us with such data. The surface pressure is then computed radially as follows:

$$P_{sfc}(r) = P_c + (P_{env} - P_c)e^{-\frac{A}{r^B}}$$

where P_{env} is the environmental pressure: we specify it at the boundaries of the retrieval domain as the National Centers for Environment Prediction (NCEP) analysis SLP. This adjustment of the

computed SLP to environmental pressure is made to avoid an axisymmetric pattern in SLP, which would be unrealistic and harder to introduce in the analyses.

A and B are the coefficients derived empirically from several hurricanes wind profiles (Holland, 1980). They are defined as follows:

$$B = \rho e \frac{V_{\text{max}}^2}{(P_{env} - P_c)}$$

$$A = R_{\text{max}}^{B}$$

where ρ is the air density and e the natural logarithm base. According to Holland's study, B should lie between 1 and 2.5.

3.2.3 Gradient Balance Inversion and wind diagnosis

After obtaining the mass field (geopotential height ϕ), we invert the balance equation in order to retrieve the streamfunction ψ . The gradient balance equation has been used in models focusing on tropical studies to give many insights on hurricane dynamics (Emanuel 1986; Shapiro and Willoughby 1982). Also called the non-linear balance equation, it has been used for model initialization as well as bogusing of cyclones in the tropics (Bolin 1956; Baer and Boudra, 1977).

The general form of the equation is:

$$f\nabla_{H}^{2}\psi + 2(\psi_{xx}\psi_{yy} - \psi_{xy}^{2}) + \psi_{x}f_{x} + \psi_{y}f_{y} = \nabla_{H}^{2}\phi$$
(3-3)

where $abla_{
m H}$ is the horizontal 2D gradient operator and f is the Coriolis parameter.

Solving for the geopotential height, given the mass field, is equivalent to seeking solutions to the Poisson equation. However, solving for the streamfunction given the geopotential height is not as straightforward. Shuman (1957) proposed a procedure to invert the balance equation. Solving for the streamfunction then becomes a Monge-Ampere type of problem, for which an ellipticity condition has to be met. It is solved by a successive, over-relaxation method (SOR) since a simple relaxation method would not converge. Lateral boundary conditions also have to be specified to force the convergence of the SOR method: we use the available NCEP streamfunction for that purpose.

Equation (3-3) can be re-written in the following way:

$$\frac{1}{2}(\psi_{xx} + \psi_{yy} + f)^2 - \frac{1}{2}(\psi_{xx} - \psi_{yy})^2 - 2\psi_{xy}^2 + (\psi_x f_x + \psi_y f_y) - (\phi_{xx} + \phi_{yy} + \frac{1}{2}f^2) = 0$$
 (3-4)

We further rewrite it by multiplying by 2 and, while keeping the order of the terms, we regroup the terms between parentheses under a single variable name. It follows:

$$\eta^2 - D_1^2 - D_2^2 + L - Z = 0 \tag{3-5}$$

where η is the absolute vorticity and

$$D_1 = (\psi_{xx} - \psi_{yy})^2, \ D_2 = (2\psi_{xy})^2, \ L = 2(\psi_x f_x + \psi_y f_y) \text{ and } Z = 2(\phi_{xx} + \phi_{yy} + \frac{1}{2}f^2)$$
 (3-6)

From Equation (3-4) we see that the following ellipticity condition has to be met:

$$(D_1^2 + D_2^2 - L + Z) \ge 0 (3-7)$$

Cyclones are associated with low geopotential heights, and usually Z > L, following which the ellipticity condition is more likely to be met. During the SOR, if strong anticyclonic flow is present resulting in the ellipticity condition not being met, we set Z=0 at those points and continue the convergence process. The first guess for ψ is a null field except at the boundaries specified by the NCEP streamfunction. Once the solution has converged to a streamfunction, we easily obtain the non-divergent, horizontal winds V_H by taking the cross-product: $V_H = k \times \nabla \psi$.

3.2.4 Humidity specification

The absence of any vertical sounding for moisture content is definitely a crucial shortcoming in the AMSU retrieval. However, assuming a typical hurricane-like relative humidity profile, we specified a 3D specific humidity field, using the satellite retrieved temperatures and the integrated cloud liquid water (CLW).

An extensive discussion of this subject is given in section 4.1.4.

Chapter 4 Results

4.1 Retrieval

The retrieval algorithm and the subsequent model initialization are carried out at approximately 0000 UTC, September 11 1999. The analyses used at different stages of the algorithm are provided by the Canadian Meteorological Centre (CMC). The AMSU data were kindly provided to us by Ralph Ferraro and Huan Meng from NOAA/NESDIS.

4.1.1 Temperature retrieval

The temperature retrieval is performed on a 10° by 10° domain centred on the hurricane. The brightness temperatures, being on a 0.5° uniform latitude-longitude grid, are interpolated to a grid of 0.25° so as to generate the initial fields with a resolution of about 27km. The two sets of coefficients, for high and low CLW content, are used in the retrieval. Figure 4-1 shows the potential temperature anomalies (PTA) relative to the level mean at the first retrieval level (1000 hPa) when only the set of low-CLW coefficients was used. Figure 4-3 presents the PTA obtained using both sets of coefficients, with the appropriate value chosen depending on the CLW values in the domain. One may note that only the region of high CLW content (> 0.3mm, cf Figure 4-2) is affected by the use of the second set of coefficients. Therefore the overall temperature of the environment around the core is similar between Figure 4-1 and Figure 4-3. However, unrealistic cold anomalies appeared in the core when only the low-CLW coefficients set was used. Given the fact that Floyd was already classified as a hurricane at this time, it is reasonable to assume that strong, deep convection was ongoing and the strong, cold anomalies are caused by the high concentration of CLW (as high as 2.8 mm in the core region as seen in Figure 4-2). The use of the dual set of coefficients yields a strong correction to the anomalies: the warmest correction is of the order of 15K and while the northernmost cold PTA is only partially reduced, the southernmost one is almost completely eliminated. Another possibility to minimize the cold anomalies is to modify the low-CLW coefficients using Demuth's CLW correction (Demuth, 2002). This correction is a simple regression: a quadratic fit to the slope m of CLW versus temperature deviation at various pressure levels using data from 64 cases of tropical cyclones. The values of m for the first 5 pressure levels (i.e. 1000, 850, 700, 500, 400 hPa) are (5.00, 3.51774, 1.72369, 0.31660, 0.03518)

respectively. Using this regression, the maximum observed CLW value of 2.8mm at 1000 hPa would yield a 14K positive correction. Above 400 hPa, all values of *m* are set to zero and no further temperature modifications are made. The corrected temperatures at each (i,j,p) point on a mandatory pressure level p is then given by:

$$T_{corrected}(i, j, p) = T_{original}(i, j, p) + m(p) * CLW(i, j)$$
(4-1)

Although the application of Eq. (4-1) substantially removes part of the cold anomalies (see Figure 4-4), it is less effective than using the dual set of coefficients (see Figure 4-3). Specifically, the coldest temperatures are not reduced by as much, the spiral rain band pattern extending southeastward is not coherent anymore and there is more noise in the overall field. Figure 4-5 presents a comparison of the vertical cross-sections of PTA derived from the single low-CLW set of coefficients, the dual set of coefficients, and the Demuth-corrected PTA (applied only to the lower levels). In all three cases, one can see the notable warm core feature at upper levels: the dual set of coefficients seems to yield a somewhat smoother, less intense anomaly when compared to the single low-CLW set as well as the Demuth-corrected one. The dual-set-retrieved warm core is 6°K colder (but still much warmer than its environment at 10°K) and is located slightly higher (200 hPa rather than 300 hPa) than its single set counterpart. The lower levels are highly unrealistic in the single-set PTA. The application of Demuth's method has pretty well corrected this problem. However the method does not remove completely the cold PTA, which extends upwards all the way to 600 hPa (Figure 4-5 c) around the longitude of 62W. Only in the dual-set PTA is the cold anomaly removed almost entirely. For this reason, as well as for the smoother tropopause transition seen in the dual-set PTA compared to the single-set one, we adopted the dual-set temperatures in this study.

Much of this discussion on temperatures was based on potential temperatures, which were computed from the retrieved temperatures, rather than actual temperatures to remove the effects of gravity. The real temperatures used in the bogus vortex are shown in Figure 4-6 (b, d, f).

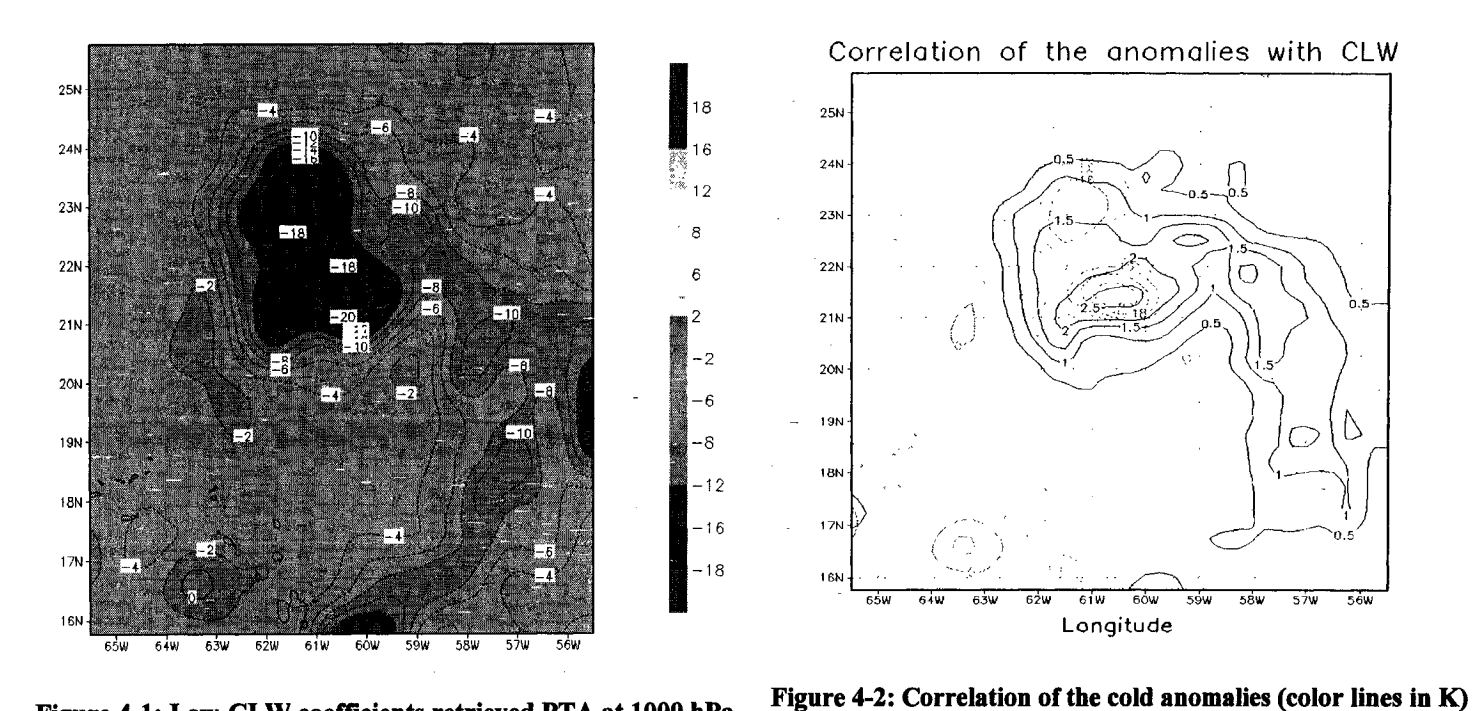


Figure 4-1: Low-CLW coefficients retrieved PTA at 1000 hPa

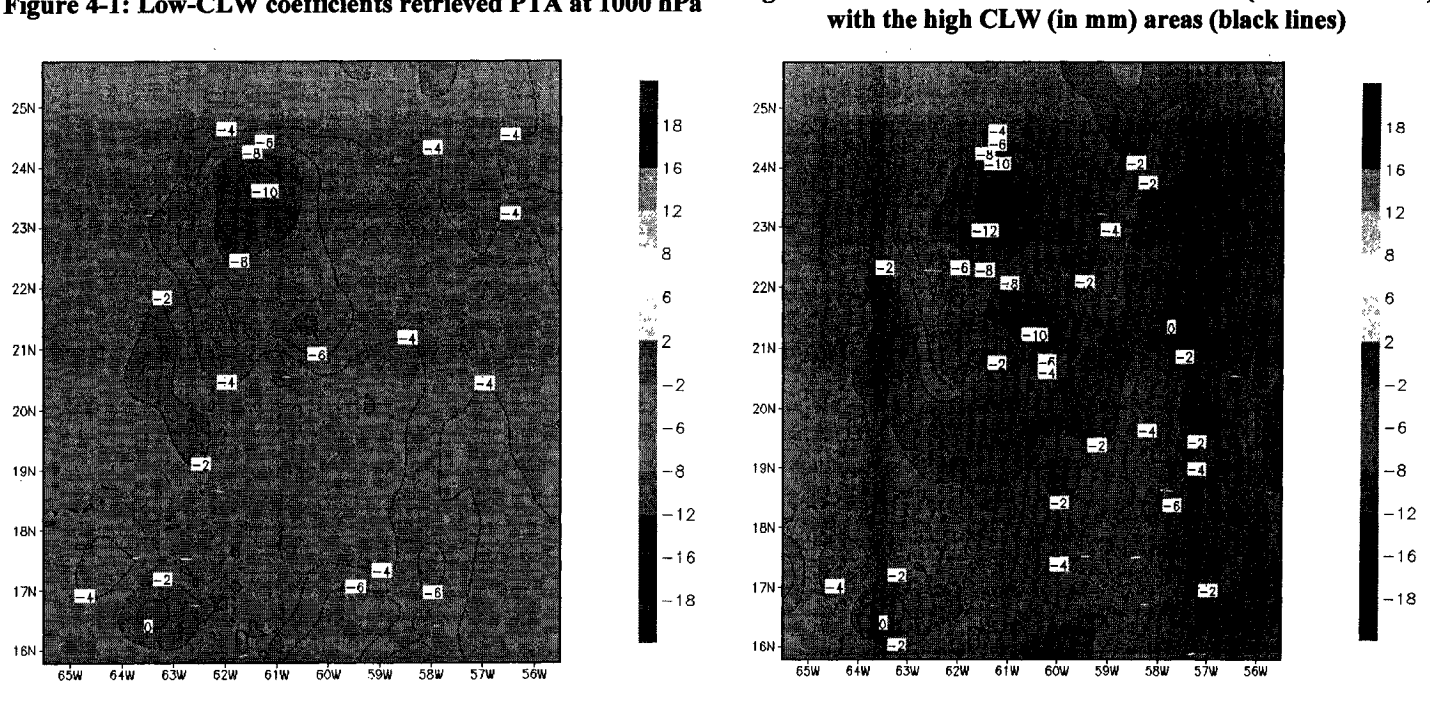
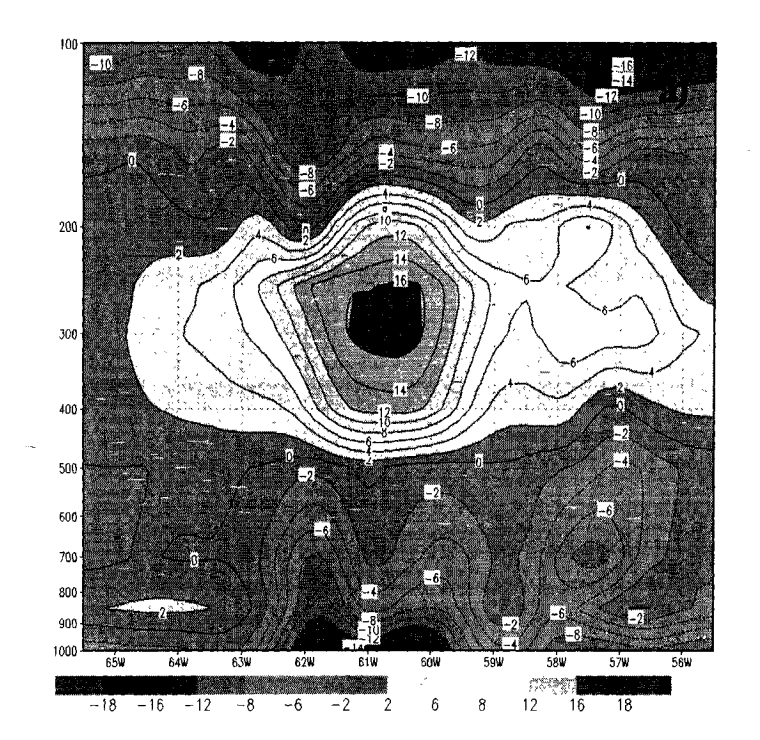
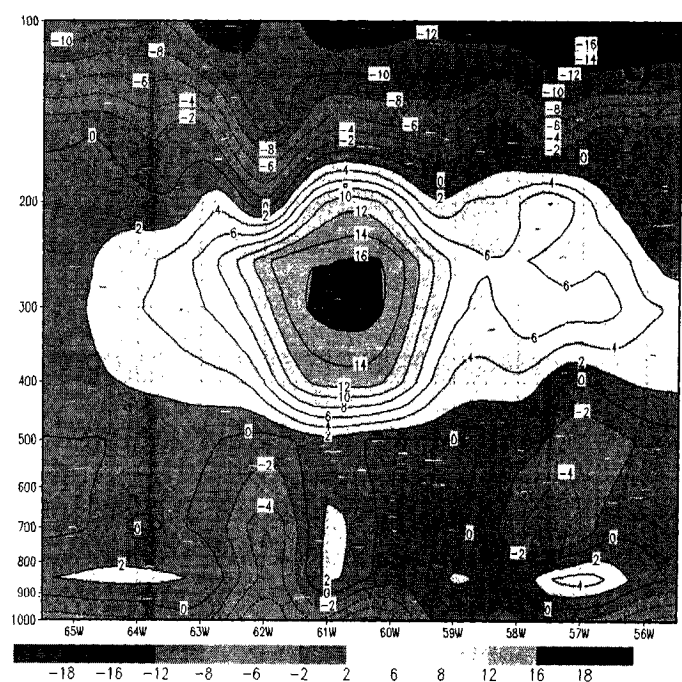


Figure 4-3: Dual coefficients retrieved PTA at 1000 hPa

Figure 4-4: PTA in Fig. 4-1 corrected by Demuth's CLW correction





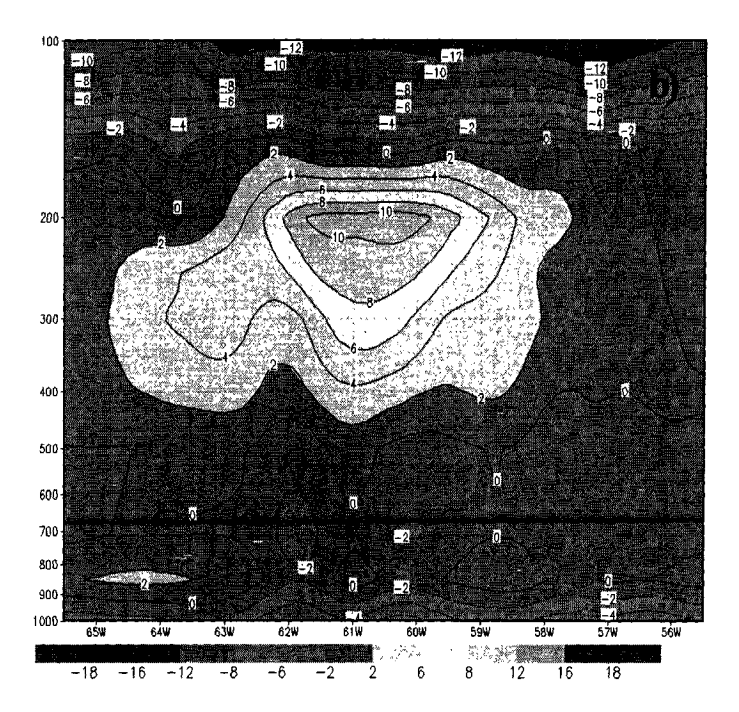


Figure 4-5: Vertical cross-sections of the PTA for
Low-CLW coefficients (a),
dual coefficients (b) and
Demuth's correction (c).

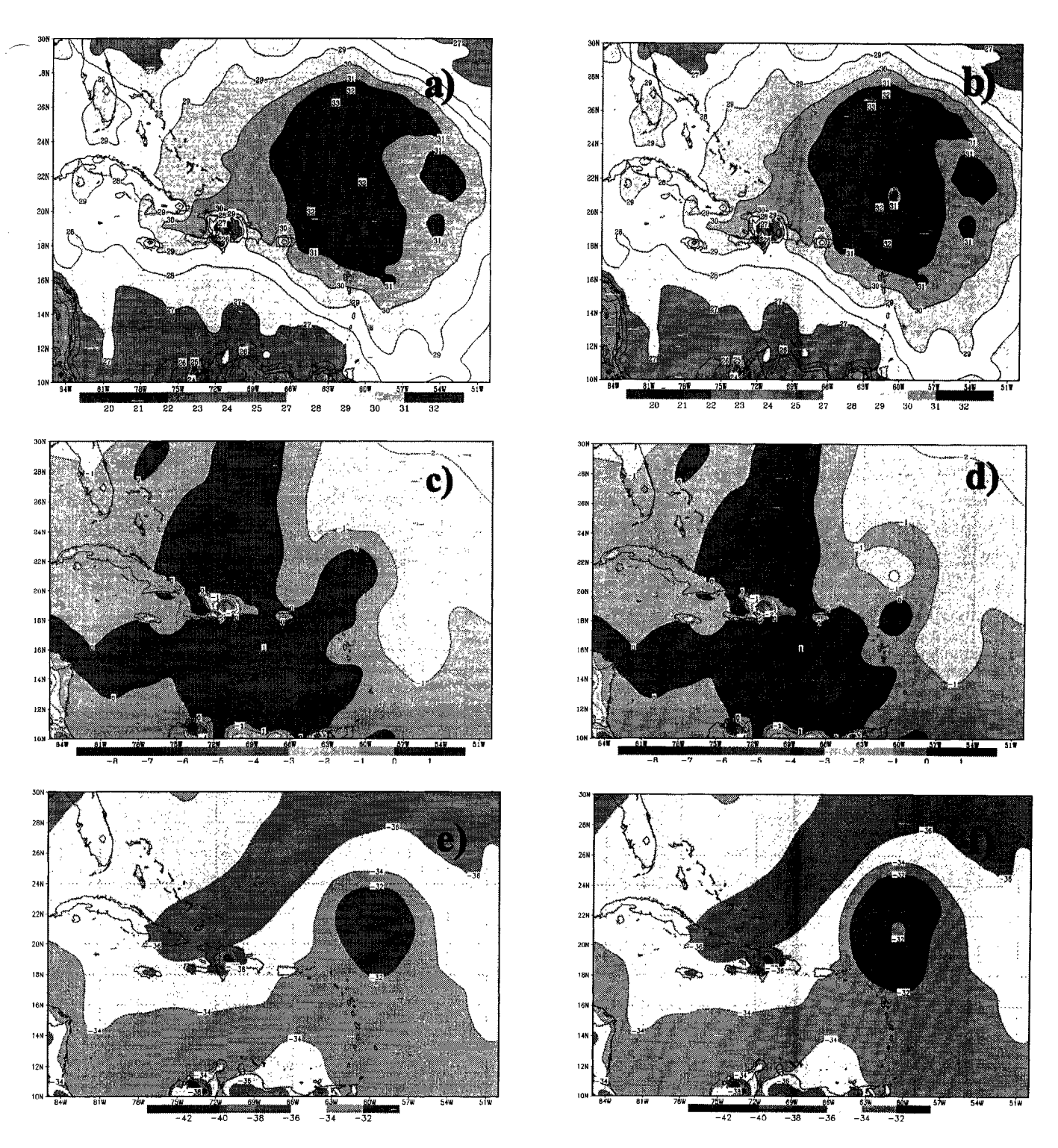


Figure 4-6: Temperatures from CMC analyses (left panels) and temperatures modified by the bogus vortex (right panels) at the surface (a,b), 5km (c,d) and 10km (e,f) at 0000 UTC September 11.

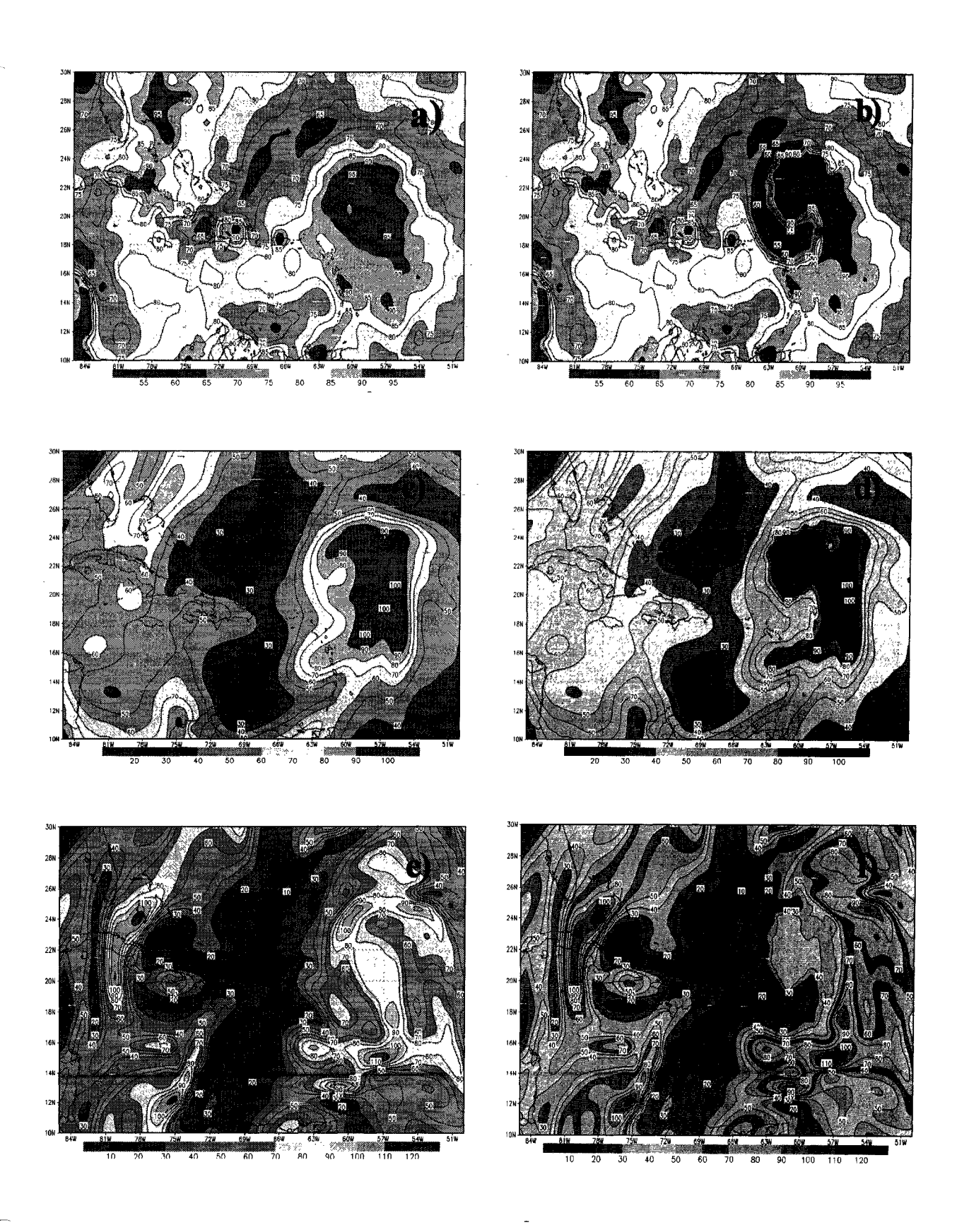


Figure 4-7: Same as in Figure 4-6, except for relative humidity

For modeling purposes only, the obtained data were further modified slightly at the lower levels to allow for conditional instability since the coarse vertical resolution does not allow us to resolve the planetary boundary layer (PBL). We therefore removed the small, remaining cold anomalies in the three first levels (namely 1000, 850, 700) by setting them to zero and applied smoothing to yield a smooth geopotential height field.

4.1.2 Geopotential height diagnosis

Figure 4-9 presents the SLP distribution as diagnosed by Holland's scheme. The values of V_{max} , R_{max} and P_c used in the calculation are 75 knots (37.5 m/s), 65km and 971 hPa respectively. These values are appropriate for 0000 UTC September 11 in accordance of Figure 2.7.

Since we integrate the hydrostatic equation upwards, the initial disturbance in the geopotential induced by the circular SLP is present throughout the whole column in the vertical. As a result, even levels located above the tropical tropopause exhibit the features of the anomalous low. However, given the length scales in the tropics, consideration of geostrophic adjustment indicates that the mass field will tend to adjust to the wind field. The wind field is therefore the keystone of the retrieval.

The obtained geopotential heights are further corrected to account for the errors accumulated throughout the integration. Those errors come directly from errors in the retrieved temperatures and in the accuracy of the algorithm. We compute the accumulated error at the top by taking the difference between the CMC geopotential height at 50 hPa minus the retrieved geopotential height at that level. We assume that the storm introduces little if any perturbation in the upper stratospheric levels and redistribute this error downwards using a linear weighting function that peaks at 50 hPa but vanishes at the surface. The redistribution of the error is normalized. The temperatures are modified accordingly to account for the changes in the geopotential heights. The correction to the temperature is however negligible (the maximum temperature change being less than 0.5 degrees)

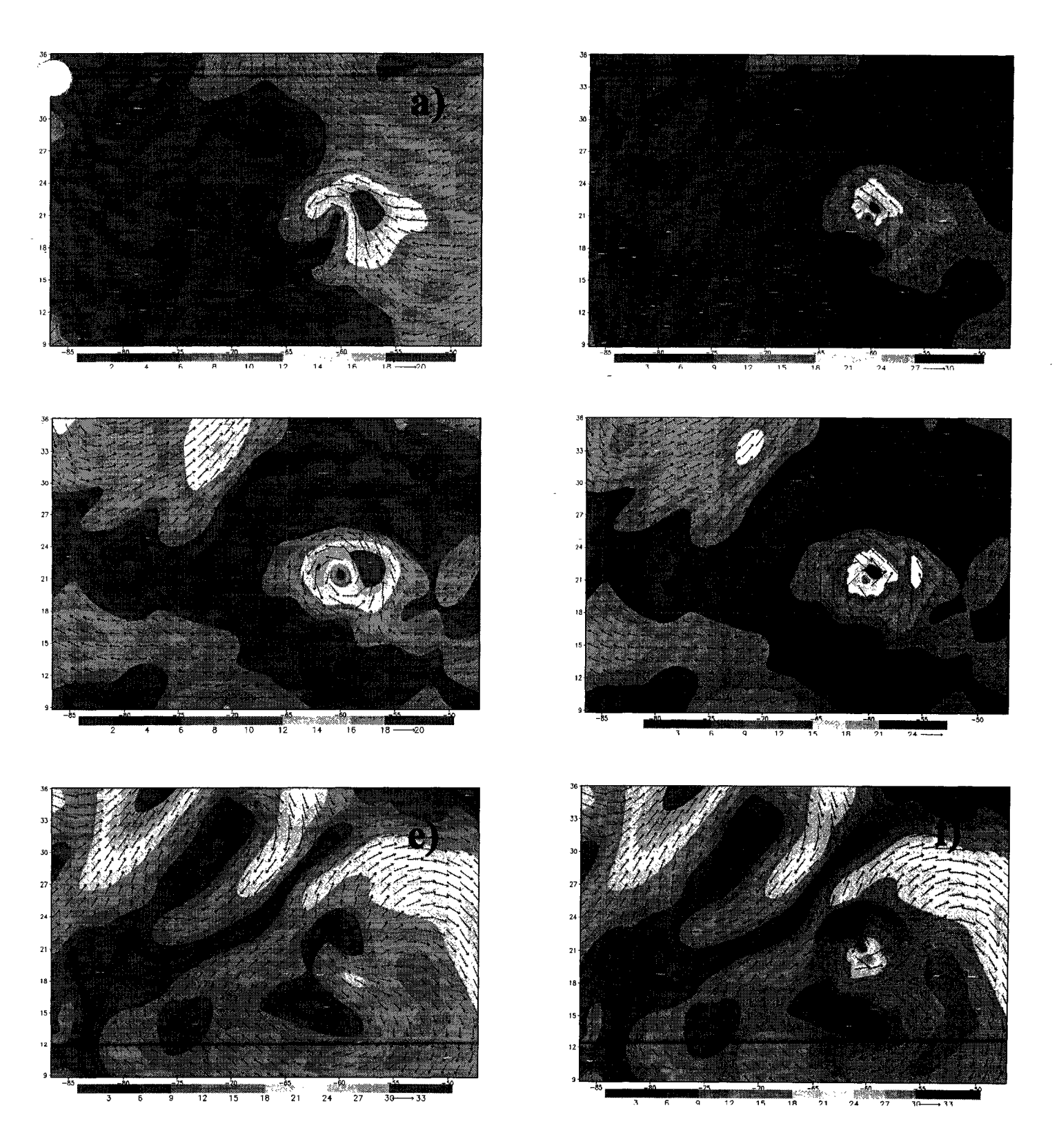


Figure 4-8: Same as Figure 4-6, except for horizontal winds in m/s.

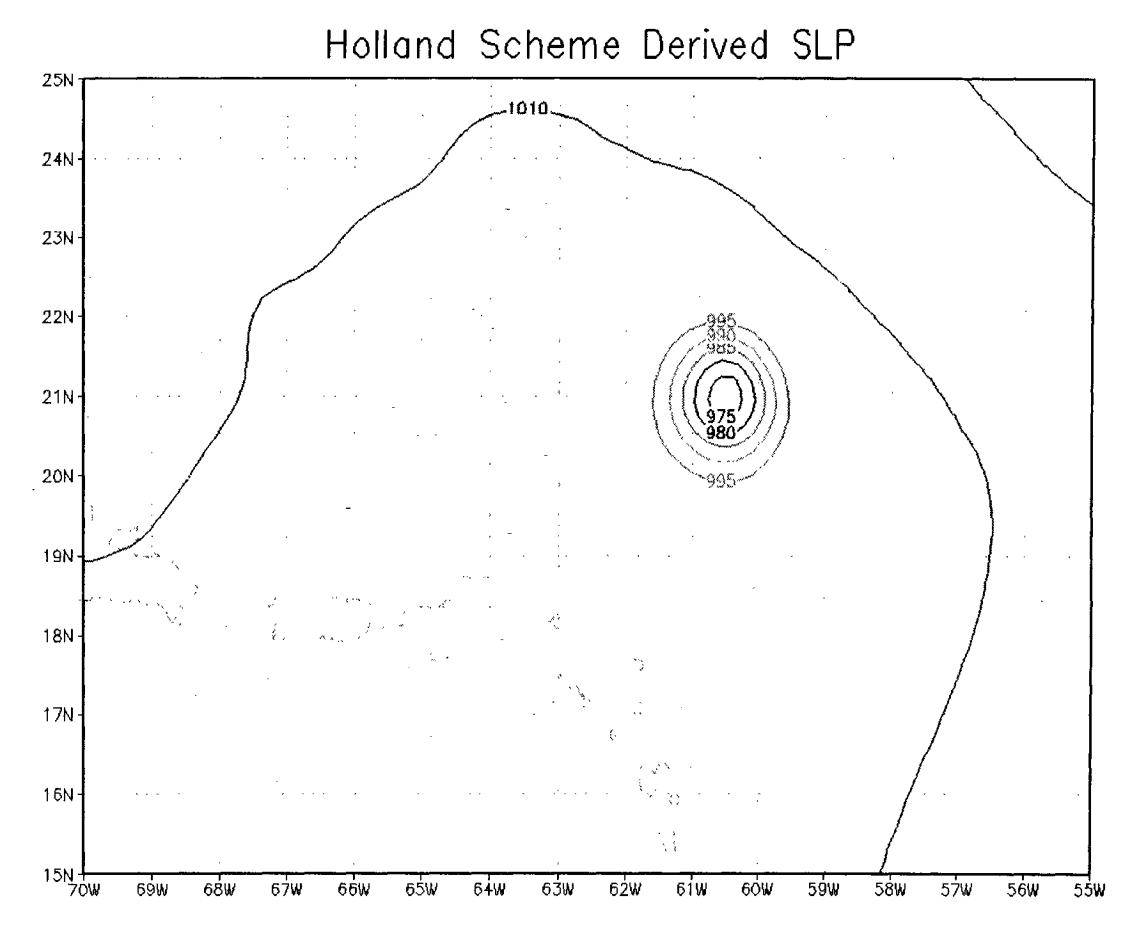


Figure 4-9: Holland scheme derived sea level pressure (hPa) at 0000 UTC, September 11.

4.1.3 Wind retrieval

As explained in section 3.2.3, the wind retrieval is solved through successive overrelaxations as given in Shuman (1957). His final equation for the stream function computation is as follows:

$$\psi^{n+1} - \psi^n = (1+w) \left\{ \eta^n - \left[(D_1^n)^2 + (D_2^n)^2 - L^n + Z \right]^{1/2} \right\}$$
 (4-2)

where all the terms are defined in 3.2.3, with the exception of w, which is the over-relaxation factor. The subscript n denotes the n-th iteration of a quantity. From Equation (4-2), it is clear that the residual must be added back to the previous step's guess. The weight with which it is added depends on the w factor. Consequently, it was found in this study that the magnitude of w could

influence not only the convergence rate but also the solution that the iteration would converge to. The values of the stream function at the boundary were assumed constant and equal to those given by the CMC analysis. The algorithm was nonetheless able to reproduce the overall pattern of the best-analyzed winds (compare Figure 4-8 b with Figure 2-7). The vertical structure of winds was found to be very much dependent on the value on w. Ellipticity problems as well as the magnitude of the first guess might be the main causes for such sensitivity.

Figure 4-8 displays the horizontal winds at three significant heights: surface, 5km (mid troposphere) and 10km (upper troposphere). One can clearly see that the bogus vortex is much smaller and stronger than its CMC counterpart. With a maximum wind speed of 32 m/s as opposed to 22 m/s for the CMC, it does a better job at capturing the real intensity of the hurricane yet not fully resolving the 38m/s estimated by the AOML at the time. The weaker retrieved winds may result partly from the quality of the data and partly from the assumption made to satisfy the ellipticity condition in the relaxation algorithm by setting the negative values in the Laplacian of the geopotential height to zero. Better convergence methods exist other than the successive over-relaxation method but they were not implemented in this study.

4.1.4 Relative Humidity Specification

No AMSU-B data were used in this study because of antenna contamination problems that were solved only after 1999. Nonetheless, model initialization required specification of a consistent specific humidity field. Zhu *et al.* (2002) proposed a simple mechanism using the available total precipitable water (TPW) product. Specifically, by using a typical hurricane relative humidity profile, one could compute the specific humidity at all points using the available temperatures. Each column is then integrated to calculate the TPW that such relative humidity profile would yield. The difference between the satellite retrieved TPW and the typical hurricane profile's TPW would then be redistributed linearly to generate a specific humidity profile so that these 2 TPW values agree. In our study, we adopted the above method using the relative humidity profile from the hurricane Andrew simulation of Liu *et al.* (1997). However, in regions of high CLW (i.e. with values larger than 0.3mm) we limit the maximum relative humidity to 95 %. This resulted in near-saturated conditions in the lower to mid-levels of the vortex (95% relative humidity in those regions of high CLW).

Figure 4-7 presents the relative humidity results in the bogus vortex as well as the corresponding CMC relative humidity fields at three significant heights: surface, 5km and 10km. It is clear that the CMC analyses display dubious, supersaturated moisture content especially in the mid and upper levels: regions of supersaturation as high as 110% are found with local peaks at 120% in the upper levels. In the region of the bogus vortex, it is clear that we remove much of this supersaturation at mid and upper levels and the effect at the surface is very significant: the dry environmental air entrained cyclonically from the west and southwest to the south is captured by our method in reasonable agreement with the satellite imagery at that time (compare Figure 4-7 b with Figure 2-5 and Figure 2-6)

Using a fairly crude estimate for relative humidity, we nonetheless manage to describe more accurately the moisture content of the atmosphere at the initial time of our numerical simulations. This will prove to be critical to simulate realistically the evolution of the hurricane.

4.2 Bogusing

The lack of observational data over the oceans makes the task of tropical cyclone forecasting a complex issue. The accuracy of numerical modeling is very dependent on the data used for model initialization. The vortices present in analyses are usually too weak, poorly defined and possibly misplaced to obtain a proper simulation. The usual standpoint in operational centers is that tampering with the analyses to introduce a realistic vortex might end up destroying their validity if done carelessly. As a result, operation centers such as the one at CMC alter little the initial fields obtained by the global models (in the case of CMC, GEM is the global model used to obtain the analyses (CRM 1998)).

In order to improve the numerical modeling and forecasting of tropical cyclones, it can however prove necessary to implant a synthetic vortex into the large-scale analyses. This initialization technique is called vortex bogusing.

The bogus vortex is specified accordingly to the observed overall structure, the intensity, the position, the radius of maximum winds (RMW) as well as the maximum wind speed of the real vortex. Of the various bogusing techniques, we follow the work of Zhu *et al.* (2002) in which various analysis products are used to derive the bogus vortex. Since the streamfunction is forced to be that given by the CMC analysis at the boundaries of the retrieval domain and the retrieved winds are balanced according to the balance equation, the disruption to the initial fields is minimized. We

implanted the retrieved vortex into the analyses fields over a 400km radius (Zou and Xiao (2000) used a 300km radius for their BDA scheme) and used a circular buffer zone with a width of about 100km to linearly adjust the vortex fields to the large-scale counterparts. The two-dimensional field involved in the bogusing procedure is sea level pressure while the three dimensional fields are temperature, geopotential height, horizontal non-divergent winds and specific humidity (later converted to relative humidity).

4.3 Numerical Simulations

Once the obtained vortex is introduced in the CMC analyses fields, the modified fields are used to initiate the model simulation.

4.3.1 Model Design

The present study uses the fifth version of the state-of-the-art PSU-NCAR non-hydrostatic 3D limited area mesoscale model (MM5, see Dudhia 1993 and Grell 1995 for a more detailed description). The exact model version is 2.1.2, which was the final version of MM5V2 prior to the recent upgrade to version MM5V3 (not used here). The vertical coordinate used is the terrain-following σ coordinate, similarly defined as in the previous, hydrostatic version of the model (MM4, see Anthes 1987), explicitly: $\sigma = (p - p_{top})/(p_{sfc} - p_{top})$, where p is pressure, and p_{sfc} and p_{top} are respectively the pressure at the surface and top of the model. There are 24 vertical σ -levels distributed as follows [0.00 0.03 0.08 0.13 0.18 0.22 0.28 0.32 0.38 0.43 0.47 0.52 0.58 0.63 0.67 0.73 0.77 0.83 0.87 0.91 0.94 0.97 0.99 1.00], which gives a highest resolution of 6 levels in the planetary boundary layer (PBL) defined as the 1km height. The MM5 is used to simulate hurricane Floyd over a 72h period (from 0000 UTC September 11 until 0000 UTC September 14, 1999), with a 60 second timestep. The integration domain covers 163 by 124 grid points with a 27km grid spacing on a Mercator map projection, defined such that its latitude is true at 0 N (see Figure 4-10). The domain thus covers an area of 4374km (zonally) by 3321km (meridionally).

Moist processes are predicted using the cloud-resolving Goddard microphysics scheme (Tao-Simpson 1993), which includes prognostic equations for explicit simulation of cloud water, ice, snow, rainwater and graupel. The radiation scheme is a cloud-resolving scheme that accounts

for both long-wave and short wave interactions with both explicit clouds and clear air (Dhudia 1993; Grell et al. 1995).

The Betts-Miller (BM) cumulus parameterization scheme (Betts and Miller 1986; 1993) is used to remove any conditional instability. The triggering condition for convection depends on three main criteria: there must be Convective Available Potential Energy (CAPE), the convective cloud depth must be over a certain threshold value and the sounding must be moist. Amongst the drawback of using the BM scheme is the lack of downdrafts: at the mature stage it has been shown that downdrafts exist within the convective cells and the inner sides of the eyewall (Liu *et al.*, 1999).

The model is initialized at 0000 UTC September 11, 1999 using the Canadian Meteorological Centre (CMC) global analyses on pressure surfaces interpolated horizontally from their original 0.9° uniform resolution to a 0.25° resolution latitude-longitude grid (for the sake of bogusing the vortex at the resolution at which it is retrieved). As far as the vertical resolution is concern, the dataset comprises the same 12 mandatory levels used in the retrieval, namely 1000 hPa, 850 hPa, 700 hPa, 500 hPa, 400 hPa, 300 hPa, 250 hPa, 200 hPa, 150 hPa, 100 hPa, 70 hPa, 50 hPa; no vertical interpolation is made on that dataset once the bogus vortex is introduced. The boundary conditions are provided throughout the integration by the similarly modified CMC analyses.

Of significant interest is the sea surface temperature (SST), which is kept constant throughout the simulation. It is obtained as part of the CMC analyses and features the warm SST anomaly around 68°N, 23°N as observed in the AVHRR imagery (see Figure 2-8). The magnitude of the SST warm anomaly is however different in the CMC analyses (30°C, see Figure 4-10) as opposed to the one retrieved by the AVHRR (32°C) and is found to be closer to the real SST at that time obtained in various other SST analyses (MCSST, Reynolds SST (not shown)). In the sensitivity test, the SST is kept constant in time and uniform in space at 28°C to investigate the effect of the warm SST anomaly on the track and intensity, as well as the development and evolution of the hurricane.

4.3.2 Simulation results

Three simulations are made: one with full interpolated CMC analyses without the bogus vortex (hereafter referred to as ANA), one with the modified CMC analyses in which the bogus vortex was introduced (referred to as BVX) and the SST sensitivity test, similar in all points to BVX but with a constant SST field of 28°C (referred to as SSS). The simulation results will be compared to the National Hurricane Center Best Analysis (referred to as BA), considered the best depiction of the evolution of the real hurricane. Of first interest is the track prediction by the MM5 for each experiment. The track is defined as the smoothed line connecting the various positions of the central SLP low center for a given simulation. Figure 4-10 presents the respective tracks for BA, ANA, BVX and SSS. The CMC analyses SST warm anomaly is also shown (note that it is irrelevant for experiment SSS which has a constant SST field) and it lies along the tracks of BA, ANA and BVX. Figure 4-11 depicts the distance from the BA track in each of the simulations. One can see that a spin up lag, as well as a southward deviation in all three simulations, lead to a sharp increase of the distance to the BA track. However, for both ANA and BVX, once the spin up period (roughly 24h) is over, the track seems to converge back to the BA track. After 36h, ANA and BVX perform somewhat similarly: they are always at about 70-100km (3-4 grid points) north of the BA track. At the end of the 72h run however, the ANA track has departed even further north (170km) while the BVX has kept a steadier 100km maximum distance to the BA track. In experiment SSS however, the initial development is identical to BVX with a southward deviation but it eventually starts to evolve differently after 18h. The SSS track then departs to the north and keeps increasing further north through the rest of the simulation. The maximum deviation from the BA track occurred at the end of 72h and is 245km to the north.

Of second interest is the intensity prediction of hurricane Floyd. The two standard quantities to examine are the minimum central sea level pressure (MSLP) as well as the maximum winds (UVMAX). For a hurricane in its mature stage, Emanuel (1988) showed that there is a direct inverse correlation between the two: a strong drop in MSLP will correlate with a strong increase of UVMAX. The destructive power of the hurricane lies mostly in the intensity of the wind gusts and the stress they can exert on structures. Emphasis is usually placed on the maximum winds. Figure 4-12 shows the maximum wind magnitude evolution for BA, ANA, BVX and SSS. Figure 4-13 presents the corresponding evolution of MSLP. As explained at length in section 2.1, the BA indicates that Floyd, initially a category-2 hurricane, intensified slightly during the first 12 hours on September 11, and weakened in the next 12 hours to about 85 knots. It then proceeded to intensify

continuously all through September 12 (reaching category-4 status by the end of the day) until 1200 UTC on September 13 when it reached its UVMAX of 135 knots (and an MSLP of 921 hPa). Finally, in the last 12 hours, it started losing of its peak intensity, but still retained enough intensity to remain a category-4 hurricane at 115 knots.

In experiment BVX, we initialize the model with our more realistic bogus vortex (having the right MSLP of 971 hPa as in BA, with a UVMAX of 57 knots, off by 23 knots from BA's UVMAX, due to imperfections in the wind retrieval algorithm). There is some adjustment taking place in the first 6h leading to a filling in MSLP of 16 hPa (from 971 hPa initial to 987 hPa). After the readjustment, the MSLP starts to drop over the next 18h, reaching an almost identical value as BA's MSLP after 24h. Over the next 12h, the UVMAX intensifies faster than the BA but a key transition in its evolution seems to occur between 36h and 42h into the simulation; the previously steadily intensifying winds (10 knots per 6h, similar to the BA) start losing a few knots during that period, leading to a cessation in the pressure drop of the MSLP yet yielding a "bang-on" MSLP at 42h. (We shall discuss this transition in detail later) From then on, the UVMAX evolution is almost similar to the BA, with a 10-knots negative bias introduced from that destabilization period. Without that bias, it appears clearly that BVX would have resolved the peak intensity and overall evolution of the hurricane winds. The MSLP performs slightly less well from 24h to 72h, deepening too fast from 24h to 42h, being almost exact from 42h to 54h and filling too fast from 54h to 72h. It does however capture closely the absolute MSLP of the lifecycle of Floyd at 925 hPa (as compared to the BA's absolute minimum of 921 hPa) and never departs by much more than 10 hPa from the BA MSLP.

In the ANA run, there are several problems, the cause of which is not fully understood. Starting off with a weak vortex (initially 999 hPa and 39 knots, off by 28 hPa from the BA's MSLP of 971 hPa and by 41 knots from BA's UVMAX of 80 knots) but with a lot of available moisture, the vortex intensifies continuously to a stronger hurricane than obtained in BVX, initialized with the stronger and more realistic bogus vortex. In terms of MSLP, there is a drastic deepening within the first 24h, dropping from 999 hPa to 943 hPa. Such intensification, together with the final MSLP of 890 hPa and the weak initial vortex, seems quite unrealistic. Further study is required to pinpoint the reason behind this explosive deepening with a weak initial vortex. One possibility is the extremely moist atmosphere in the CMC analyses which may allow the spin-up of the hurricane from a weak vortex initial state. In that sense the moisture adjustment in the region of the bogus

vortex may impact positively to yield a more correct evolution of the hurricane. The moisture adjustment technique remains nonetheless a crude one in this study and further improvements should definitely be attempted in the future.

Finally, in the sensitivity run SSS, the effects of a constant 28°C SST are felt quite obviously on both the evolution of the track and the intensity. Although the track remains identical to BVX for the first 18 hours, the intensity deviates from BVX starting at 6h into the simulation. The UVMAX and MSLP do not intensify as much and from there on, the vortex never spins up to the same extent. It also fails to capture the overall evolution of the intensity, reaching a weaker MSLP of 955 hPa and weaker UVMAX of 93 knots at the end of the 72 hours, not resolving the hurricane's maximum intensity around 1200 UTC on September 13. After 42h, it also misses the westnorthwestward turn from its northwestward propagation (as resolved in BVX) and is thus found to deviate quite extensively to the north of the BA track, thereby missing the warm SST anomaly region known as the "warm blob" in the BVX and ANA SST field. It can be seen from Figure 4-10 that most of the region where spin up occurs has 29°C to 29.5°C SST in BVX and ANA. Thus a 1°C to 1.5°C colder SST in SSS can account for the lack of further intensification and organization, the lack of a west-northwestward turn and subsequent warm blob-induced intensification. Obviously the warm blob (>2°C difference) is not present in SSS but it is clear that missing such a heating potential would induce a weaker intensification of the hurricane. This stresses the importance of an adequate, realistic SST field given that 1-2°C difference can affect tremendously the hurricane evolution to the extent where the main features of the hurricane at not reproduced.

We come back here on the slight weakening occurring between 36h and 42h in the BVX run. It is of notable importance since, without its occurrence, our simulation would have captured the maximum wind speed as described in the BA. Figure 4-10 shows clearly that after 36h, the northwestward-propagating BVX track takes on a west-northwestward direction. It is also obvious that the SSS track starts to deviate further north after this moment. Given that the only difference between the SSS and the BVX is the constant SST, one could infer that the positive difference in latent heat release subsequent to a warmer SST (in the case of BVX) could affect the hurricane's thermodynamics so as to induce this change in propagation. However, resolution of this issue is outside the scope of this work.

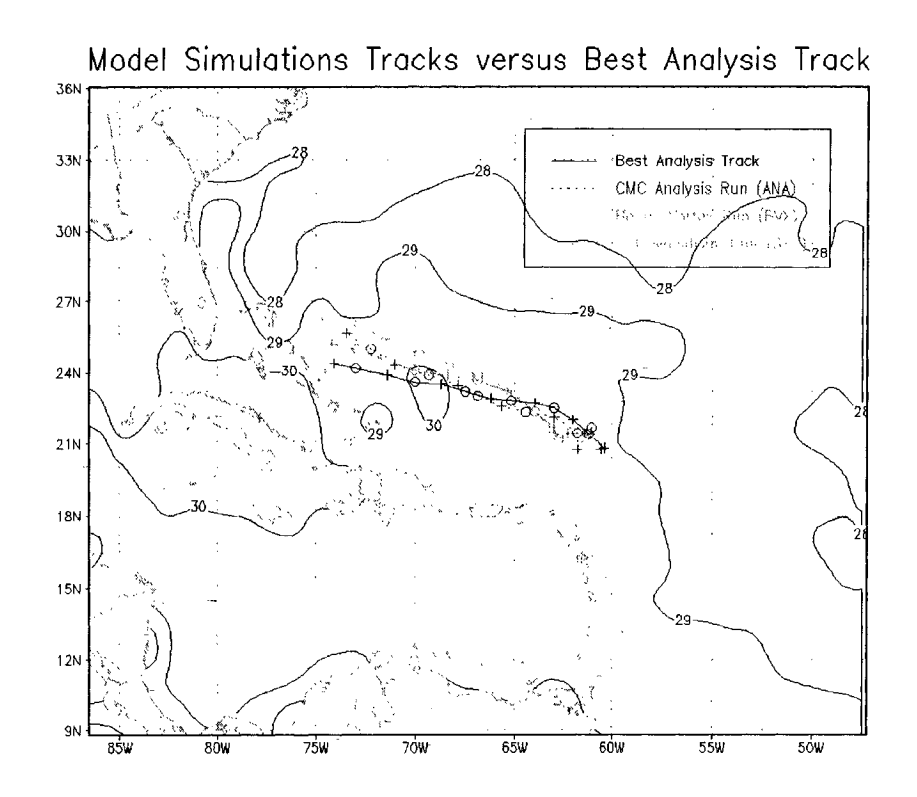


Figure 4-10: MM5 simulated tracks compared to the NHC Best Analysis Track, with SST contours superimposed

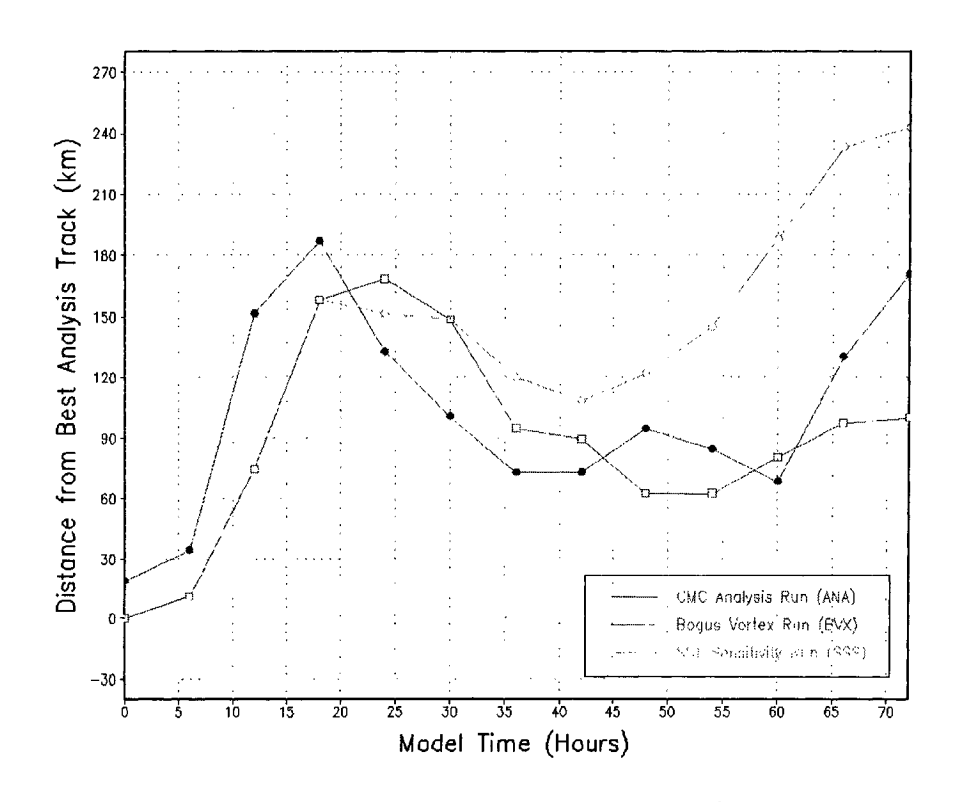


Figure 4-11: Evolution of the distance of each simulated track from the Best Analysis Track

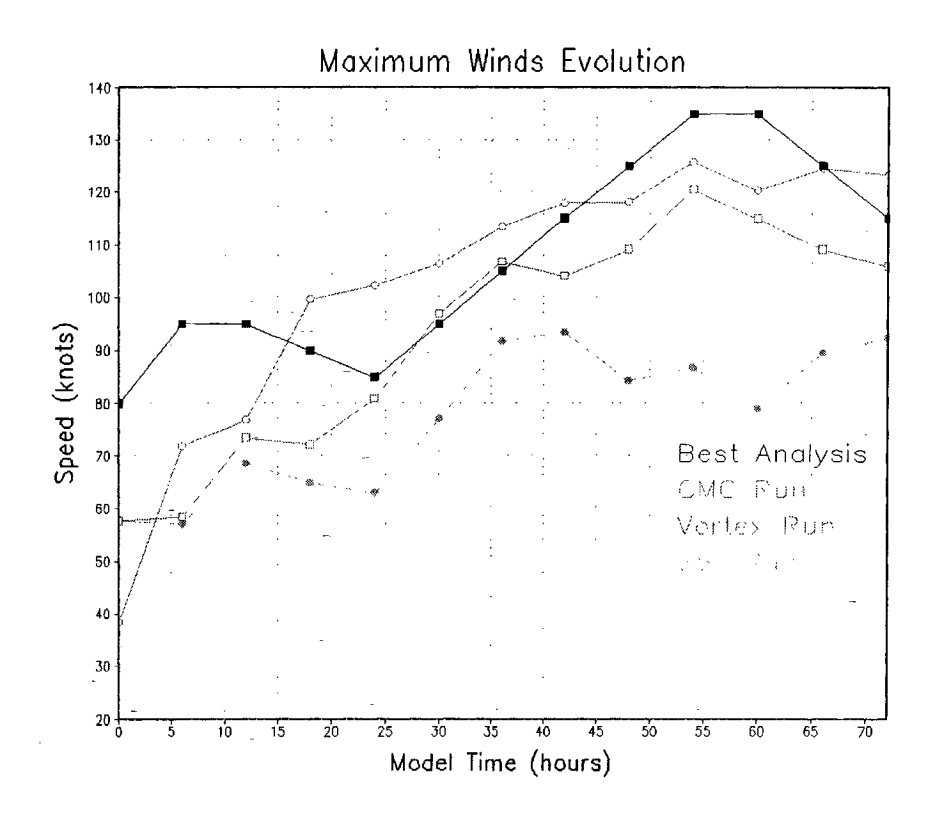


Figure 4-12: Evolution of the maximum surface winds for the different runs

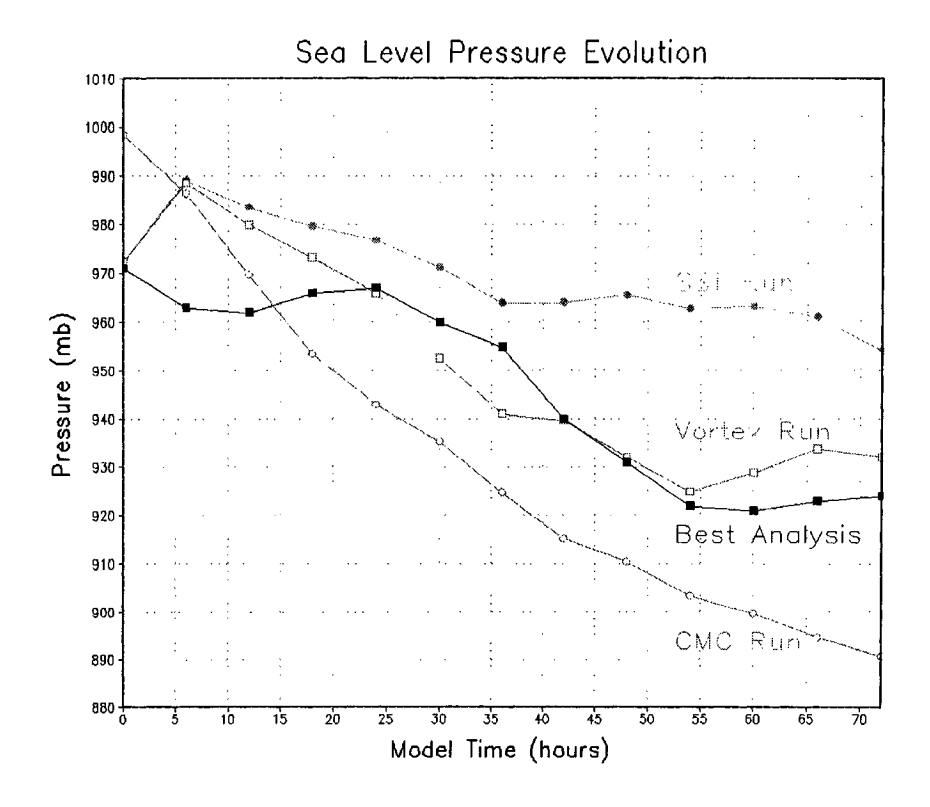


Figure 4-13: Same as in Fig. 4-12 except for minimum Sea Level Pressure

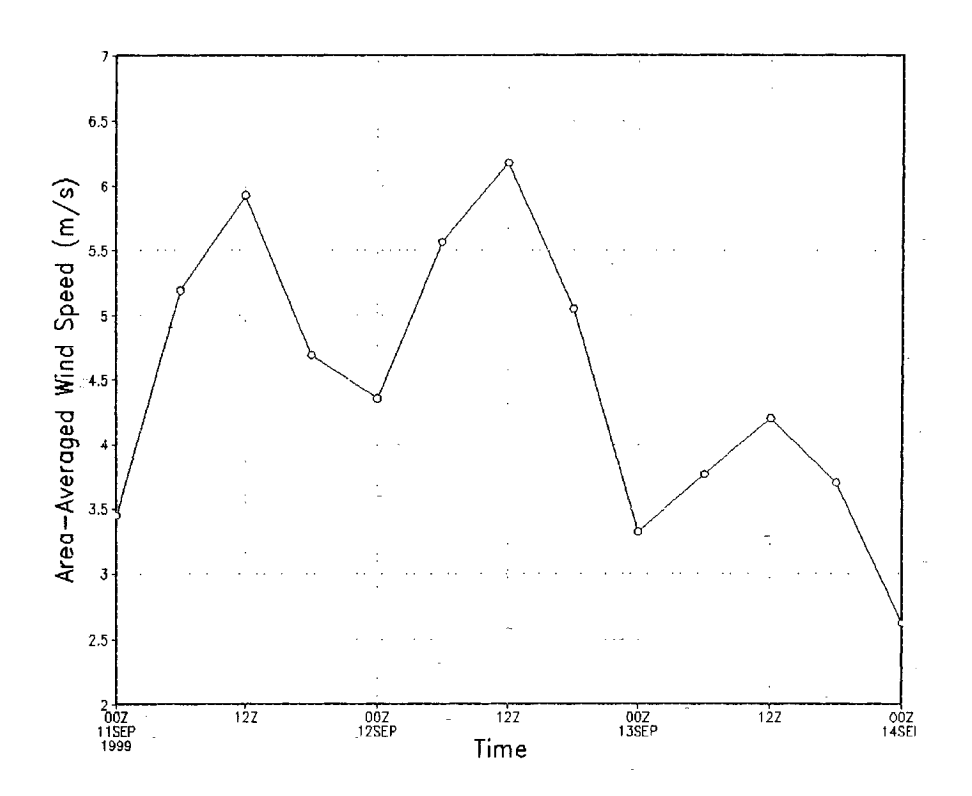


Figure 4-14: Evolution of the area-averaged environmental wind shear speed over a 600km x 600km area

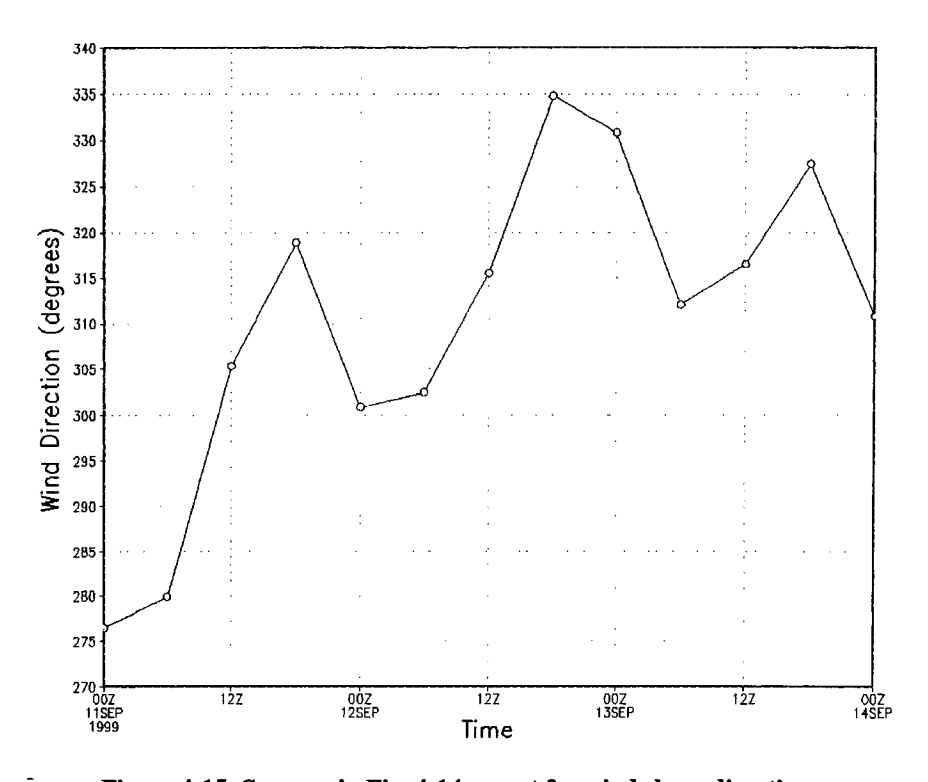


Figure 4-15: Same as in Fig. 4-14 except for wind shear direction

Another potential explanation for this sudden shift in direction may lie in the variations of the vertical wind shear. We can compute the wind shear between two typical heights, one just above the PBL and the other one in the upper troposphere. The evolution of the wind shear averaged over a 600x600km² area between the altitudes of 8km and 1km is plotted in Figure 4-14. It can be seen that at 36h into the simulation (i.e. 1200 UTC on September 12) the wind shear reached a maximum value of 6.2 m/s before weakening thereafter, while its direction shifted from northwest to north-northwest. That increase in shear may explain in part the temporary weakening of hurricane Floyd in BVX from 36h to 42h.

A final result concerning the thermodynamics structure and evolution of hurricane Floyd is hereafter investigated. Zhang *et al.* (2002) showed that the equivalent potential temperature (θ_e) could be considered as a near-conservative variable above the maritime boundary layer (MBL). Yet deposition/sublimation as well as freezing/melting processes do not allow for total conservation of θ_e . They also showed that the net positive θ_e tendency at the inner edge of the eyewall was directly linked to the central θ_e increases and, indirectly, to the increases in its radial gradient. Furthermore, the use of θ_e allows us to obtain an estimate of the hurricane intensity through its minimum central pressure. Malkus and Riehl (1960) derived the following empirical relation between the central maximum equivalent potential temperature $\theta_{e \text{ max}}$ and the minimum SLP,

$$SLP_{\min} = 1000 - 2.5(\theta_{e_{\max}} - 350)$$
 (4-3)

From Figure 4-16 f, we can see that at the surface θ_{emax} is on the order of 380K. This would yield a value of 925 hPa for the SLP, which is exactly what is observed at that time. The minimum SLP in BVX at that time is however on the order of 932 hPa, suggesting that some inconsistency may exist either in the empirical formulation of Equation (4-3) or in the way that the SLP is computed. The latter possibility is probable and is supported by the notable imbalance in the ANA run: at 72h, when the winds are barely 125 knots yet the MSLP is on the order of 890 hPa. Such MSLP is usually accompanied by much stronger winds (eg. Hurricane Gilbert in 1988 reached an absolute MSLP of 888 hPa with gusts as high as 150knots). It may suggest that the computation of MSLP may need to be improved in MM5. From Equation (4-3) it would seem that 350K is a reference value for θ_e . Figure 4-16 (a to e) presents the evolution of that isosurface throughout the simulation. Two separate results arise: the formation of a closed θ_e "tube" seems to denote ongoing deep convection and the radial expansion of the isosurface denotes overall intensification of the

hurricane through increases in θ_e in the inner core. From panel a), one can clearly see that at the initial time our specification of the bogus vortex does not allow for any deep convection: the upper dip in the isosurface indicates the presence of the warm core but, with no vertical motion initially bogused in, there is no connection between the lower and upper surfaces. In panel b), 12 hours into the simulation, the hurricane is still in the spin-up stage. However, convection is starting to get organized and the downward dip and the upward bulge are on the verge of connecting. Note that the spiral rain bands are starting to appear at the lower surface in motion around the hurricane. The near-conservation of θ_e in the vertical direction in the eyewall is quite evident by the almost vertical orientation of the "tube" above the MBL. The intensification then continues at 48h and 72h, as is indicated in panels d) and e) where the θ_e "tube" widens as the upper level high θ_e air is entrained down into the center. One can also see that the upper level surface funnel is widening considerably, accounting for the intense warming of the upper center and consequent downward dips of θ_e .

The evolution of the isosurface of θ_e at a constant value of 350K is very useful to depict the advection and transport of static energy in an air parcel between the lower and upper atmosphere in a hurricane. It also offers a nice visual tool to gain insight on the dynamics which are taking place as the hurricane develops!

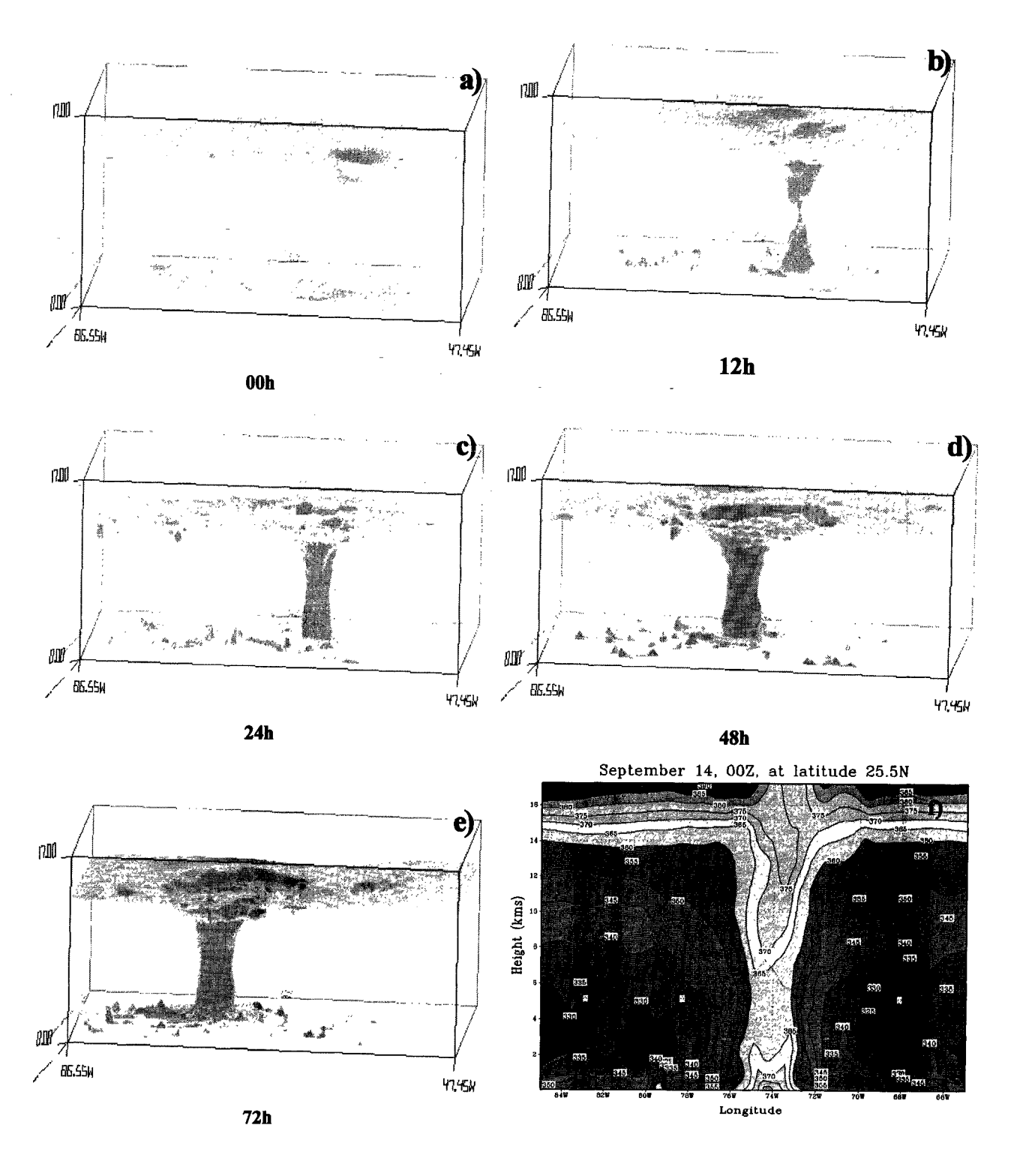


Figure 4-16: Evolution of Equivalent Potential Temperature (θe).

The first 5 panels (a to e) represent the time evolution of the 350k θe isosurface while panel (f) presents a cross-section of θe through the center of the hurricane at 72h.

Chapter 5 Summary, future work and conclusions

5.1 Summary

The AMSU-A data have been used to retrieve a realistic vortex of hurricane Floyd, using Zhu *et al.* (2002) 's retrieval algorithm. Temperatures are derived from the microwave brightness temperatures and a significant warm core (10-16K) is found to be located at the typical pressure level of 250 hPa. Using the algorithm, an adequate SLP is derived and integrated hydrostatically using the retrieved temperatures to obtain the 3D geopotential heights, which are in turn used to invert the balance equation in order to compute the 3D streamfunction and finally the 3D winds. Problematic lower-level cold anomalies are investigated and a satisfactory solution is found through removal of the 3 lowest-peaking channels of the AMSU. Moisture content is specified using typical relative humidity profiles in a hurricane.

The complete vortex (temperature, moisture, winds, and geopotential heights) is inserted into the CMC analyses in order to estimate the impact of vortex bogusing on the hurricane simulation. Three runs are performed in MM5 and compared to the NHC's Best Analysis: one run using the unmodified CMC analyses (ANA), one run using the bogus-vortex modified analyses (BVX) and one sensitivity run to estimate SST effects on the development of the hurricane (SSS).

It is found that the ANA simulation deepens extensively if not unrealistically even though it is initialized with a weak vortex, though warm and moist. The reasons behind this unrealistic intensification could not be resolved within this study.

The BVX simulation initially undergoes re-adjustment during spin up indicating that there is some imbalance or model-inconsistent fields present in the initial conditions. However, after spin up, the evolution of the hurricane's minimum sea level pressure (MSLP), the maximum winds and the track are reproduced reasonably accurately - with a 925 hPa absolute MSLP almost capturing the observed absolute MSLP of 921 hPa - and could have been almost perfect if it were not for a slight weakening as the hurricane shifts west-northwestward around 36h into the simulation, resulting in a negative 10-15 knots difference between the simulated maximum winds and the Best Analysis winds. At the end of the 72h of the simulation, the deviation from the Best Analysis track is on the order of 100km, which is comparable to the average forecast error of track deviation using

GFDL's bogus vortex initialization technique (Bender, 1997) and to the error obtained during the simulation of hurricane Felix using the BDA scheme (Zou, 2000).

The SSS simulation starts with the exact same fields as the BVX, except for a uniform SST set at 28 degrees Celsius. The impact of this colder SST on the simulation is quite drastic: the details of the MSLP evolution are not captured, the absolute MSLP attained is lower by 30 hPa compared to BVX and the track fails to capture the west-northwestward turn around 36h and therefore deviates as far as 250km north after 72h. Simulations are thus found to be extremely sensitive to variations of 1 to 2 degrees in the specified SST. Extreme caution must therefore be exercised with the specification of the SST field, which is thought to be one of the key factors that influence the hurricane evolution (Emanuel, 1986).

5.2 Future work

As quoted in the introduction from Kurihara *et al.* (1993), specification of a bogus vortex is a difficult issue when one needs to account for realistic features and yet achieve model consistency. The moisture field is thought to affect significantly the evolution of the storm. As we could see in the ANA simulation, it is very possible that the unrealistic intensification of the vortex was due to an over-moist analysis. Further study is needed to fully assess the effect of the moisture specification in the CMC analyses.

The initial imbalance or model-inconsistent fields present in the initial condition should also be investigated: in this study, the use of CMC analysis fields (SLP, streamfunction) at the boundaries was believed to help minimize the shocks that could arise from the insertion of the vortex into the large-scale analysis since the derived fields would blend in. A possible attempt could be to use the technique described in Kurihara *et al.* (1993) in order to filter out the analyzed vortex and to replace it with the bogus vortex.

Furthermore, hurricane Floyd occurred in September 1999. At that time, the data from AMSU-B was contaminated due to antenna interference problems but the problem has since been fixed (Weng *et al.*, 2000; Grody *et al.*, 2001). The author believes that, using the operational AMSU-B products, more accurate moisture content could be estimated. The increased temporal resolution provided by the use of three AMSU satellites (namely, NOAA 15, NOAA 16 and NOAA 17) could also prove very fruitful in new simulations of hurricanes occurring in and after 2002. The

new algorithms developed for wind and SLP retrieval could also very well be incorporated in order to minimize the impact of parameterization, specification and computation of these parameters.

Refined techniques based on the Carr and Elsberry (1992) suggestions could be devised to compute the complete winds from the axisymmetrical winds calculated using AMSU (e.g. using the technique of Demuth (2001) or Spencer (2001)), the retrieved environmental steering winds through analyses or satellite water vapour imagery (Zou, 2000), and the asymmetrical wind component. This method avoids the problem of having to invert the balance equation: the ellipticity condition cannot be met at all points and sensitivity of the solution when the stability of the convergence method is altered.

5.3 Conclusion

Hurricane Floyd was a large and monstrous category-4 hurricane at its peak intensity. It caused massive floods (as high as 21 inches of accumulated rain over North Carolina and Virginia, see Fig.2-4), claimed the lives of 57 people and caused extensive destruction along its path. Total damage was estimated to be on the order of 4.5 billion dollars, making it the third costliest hurricane ever.

Accurate forecasts still remain the best way to protect the population against such hazardous catastrophes. Improvements in forecasts can be made through various techniques (ensemble forecasts, data assimilation, etc...) and it has been shown in the present study that specifying a more realistic hurricane vortex through vortex bogusing using AMSU data can significantly improve the track and intensity forecasts. Refinements of the technique should be implemented and more cases should be studied in order to fully assess the potential of this technique, bearing in mind that the ultimate goal is to make it a reliable, operational feature of data assimilation.

Appendix A: The Saffir-Simpson Scale

The Saffir-Simpson Hurricane Scale is a 1-5 rating based on the hurricane's present intensity. This is used to give an estimate of the potential property damage and flooding expected along the coast from a hurricane landfall. Wind speed, determined using the U.S. 1-minute average, is the determining factor in the scale, as storm surge values are highly dependent on the slope of the continental shelf in the landfall region. Note that all winds are using the U.S. 1-minute average. Herbert Saffir, a consulting engineer specialist in wind damage to buildings, and Robert Simpson, who was then director of the National Hurricane-Center, invented the scale in the early 1970s.

CATEGORY	1
Wind speed range	64-82 kt (119-153km/hr)
Central SLP Range	> 980 mb
Storm Surge (above normal)	4-5 feet (about 1-2 m)
Potential damage	No real damage to building structures. Damage primarily to unanchored mobile homes, shrubbery, and trees. Some damage to poorly constructed signs. Also, some coastal road flooding and minor pier damage.

CATEGORY	2
Wind speed range	83-95 kt (154-177km/hr)
Central SLP Range	965 – 979 mb
Storm Surge (above normal)	6-8 feet (about 2-3 m)
Potential damage	Some roofing material, door, and window damage of buildings. Considerable damage to shrubbery and trees with some trees blown down. Considerable damage to mobile homes, poorly constructed signs, and piers. Coastal and low-lying escape routes flood 2-4 hours before arrival of the hurricane centre. Small craft in unprotected anchorages break moorings.

CATEGORY	3
Wind speed range	96-113 kt (178-209km/hr)
Central SLP Range	945 - 964 mb
Storm Surge (above normal)	9-12 feet (about 3-4 m)
Potential damage	Some structural damage to small residences and utility buildings with a minor amount of curtain wall failures. Damage to shrubbery and trees with foliage blown off trees and large trees blown down. Mobile homes and poorly constructed signs are destroyed. Low-lying escape routes are cut by rising water 3-5 hours before arrival of the centre of the hurricane. Flooding near the coast destroys smaller structures with larger structures damaged by battering from floating debris. Terrain continuously lower than 5 ft above mean sea level may be flooded inland 8 miles (13km) or more. Evacuation of low-lying residences with several blocks of the shoreline may be required.

CATEGORY	4
Wind speed range	114-135 kt (210-249km/hr)
Central SLP Range	920 – 944 mb
Storm Surge (above normal)	13-18 feet (about 4-6 m)
Potential damage	More extensive curtain wall failures with some complete roof structure failures on small residences. Shrubs, trees, and all signs are blown down. Complete destruction of mobile homes. Extensive damage to doors and windows. Low-lying escape routes may be cut by rising water 3-5 hours before arrival of the centre of the hurricane. Major damage to lower floors of structures near the shore. Terrain lower than 10 ft above sea level may be flooded requiring massive evacuation of residential areas as far inland as 6 miles (10km).

CATEGORY	5
Wind speed range	> 135 kt (> 249km/hr)
Central SLP Range	< 919 mb
Storm Surge (above normal)	> 18 feet (> 6 m)
Potential damage	Complete roof failure on many residences and industrial buildings. Some complete building failures with small utility buildings blown over or away. All shrubs, trees, and signs blown down. Complete destruction of mobile homes. Severe and extensive window and door damage. Low-lying escape routes are cut by rising water 3-5 hours before arrival of the centre of the hurricane. Major damage to lower floors of all structures located less than 15 ft above sea level and within 500 yards of the shoreline. Massive evacuation of residential areas on low ground within 5-10 miles (8-16km) of the shoreline may be required.

Appendix B: Temperature retrieval coefficients

The coefficients used for the temperature retrieval are reproduced here for reference. These coefficients were obtained through a regression equation by matching the observed temperatures, obtained by many various rawinsonde soundings at islands over the global tropical oceans, to the AMSU-A satellite-obtained brightness temperatures. As explained in Chapter 3, there are two sets of coefficients that need to be derived since cloud liquid water (CLW) contaminates the lower-peaking brightness temperatures by scattering the microwave signal, effectively making the received signal colder than real. For the low-CLW coefficients, at each of the 15 scanning angles, 115 rawinsonde soundings were used together with 1800 collocated AMSU brightness temperature soundings (channels 3-11) in the regression. For the high-CLW case (i.e. high precipitation regions), 2000 observations of rawinsonde soundings at islands over the global tropical oceans were collocated with the brightness temperatures from channels 6 to 11.

In the following Appendix, the top table displays the coefficients used for retrieval in a low CLW column whereas the bottom table displays those used in a high CLW column.

Coeff	C0	C3	C4	C5	C6	C7	C8	C9	C10	C11
Angle							-			
00-03	-153,548	-0,5344	2,1899	1,6776	-1,6414	-3,1102	3,3756	-1,8332	1,587	-0,0813
03-07	-118,191	-0,1286	0,5515	3,3232	-3,7385	0,3315	1,5524	-0,76	-0,0332	0,4376
07-11	-84,6059	-0,2519	1,2117	2,6208	-3,5678	0,8934	0,9978	-0,4249	0,3861	-0,4826
11-15	-135,948	-0,3359	1,6625	0,9809	-0,779	-0,5561	0,5605	-0,0437	0,2159	-0,0987
15-19	-53,7516	-0,4719	3,0126	-0,4189	-3,1525	2,6299	0,0249	-0,6387	0,1541	0,1559
19-23	111,5979	-0,2744	2,5211	-0,208	-2,74	1,1213	0,7041	-0,5075	-0,5228	0,4985
23-26	191,1944	-0,3459	2,8873	-1,0393	-1,732	-0,4614	1,0657	-1,1104	0,1651	0,8145
26-30	64,1235	-0,3074	3,4646	-2,3836	-0,5709	0,7466	-0,4429	0,159	-0,582	0,7213
30-34	-78,0031	-0,4555	3,3344	-0,3126	-2,4656	0,0091	1,9315	-0,1249	-1,5281	0,9332
34-38	-71,7699	-0,252	3,4672	-0,9718	-1,8056	-0,6763	2,3249	-0,8381	-0,4115	0,4785
38-42	-54,627	-0,2103	3,4686	-0,8896	-2,9807	1,6984	1,0503 ⁻	-0,789	-0,2013	0,0972
42-46	94,0634	-0,1496	2,9567	-1,4316	-1,6114	1,4563	0,1991	-1,17	1,2032	-0,7975
46-50	93,4068	-0,1201	3,6181	-2,9213	-0,0629	0,1395	0,5949	-0,6702	0,2391	-0,1657
50-54	100,965	-0,1091	4,1522	-3,4356	-0,9659	0,3098	0,5428	-0,7923	-0,1576	1,0253
54-58	-129,987	0,0541	3,5192	-3,3041	0,3665	1,2779	-0,0325	-0,9412	-0,2848	0,9577

LEVEL 1000

Coeff	CO	C3	C4	C5	C6	C7	C8	C9	C10	C11
Angle										
00-03	-129,765	0	0	0	5,8524	-8,7431	5,4755	-1,3652	-0,9819	1,3937
03-07	-64,1841	0	0	0	2,8988	-2,6588	1,5562	0,408	-2,8647	2,0478
07-11	-45,6327	0	0	0	2,3418	-1,4252	0,5653	-1,1026	0,4911	0,4684
11-15	-43,4915	0	0	0	3,6636	-2,2822	-0,7352	1,2188	-1,5565	0,9706
15-19	162,6759	0	0	0	1,0899	-0,3922	-0,0844	-0,5591	-0,9517	1,352
19-23	222,1033	0	0	0	1,5257	-1,3621	0,1871	-0,1392	-1,6006	1,5703
23-26	250,8558	0	0	0	1,6194	-1,7703	-0,1648	-0,4924	-0,7454	1,6082
26-30	168,971	0	0	0	2,3344	-2,3364	0,219	-0,116	-1,1394	1,4357
30-34	-35,8147	0	0	0	2,6893	-3,1708	3,2227	-0,3266	-3,7173	2,5919
34-38	99,0684	0	0	0	0,6406	-0,299	1,724	-0,3517	-4,0384	3,062
38-42	29,7241	0	0	0	1,3098	1,1746	-1,1057	-0,15	-1,4518	1,2416
42-46	270,1008	0	0	0	0,5852	0,3002	-0,6833	-1,9162	1,9808	-0,2475
46-50	205,4806	0	0	0	-0,005	0,854	-0,3388	-1,4555	-0,01	1,2646
50-54	76,7494	0	0	0	1,3632	-1,3995	0,9661	-1,712	-0,5764	2,1872
54-58	-177,385	0	0	0	2,79	-0,9839	0,5019	-1,3481	-0,7874	1,7774

Coeff	C0	С3	C4	C5	C6	C7	C8	C9	C10	C11
Angle										
00-03	-25,9617	-0,1524	0,4402	2,4294	-1,9537	-0,9826	1,2845	0,0039	-0,6825	0,7595
03-07	-102,552	-0,3179	1,2566	1,1464	-1,0937	-1,0821	1,6786	-0,198	-0,9507	1,033
07-11	-214,337	-0,0958	0,2497	2,7746	-1,0827	-1,5098	1,5055	0,5292	-1,1853	0,739
11-15	-239,656	-0,3072	1,2801	1,6641	-1,7072	0,852	-0,1236	0,4475	-0,1851	0,1144
15-19	-118,205	-0,263	0,8881	1,7575	-2,0183	0,7642	0,7142	-0,7136	0,379	0,0329
19-23	-142,471	-0,0158	0,406	1,5933	-0,203	-1,0547	0,7112	-0,5878	0,8047	0,0144
23-26	-78,9881	0,0474	0,5058	1,119	0,0359	-1,27	0,4381	-0,2967	0,1858	0,6433
26-30	-93,3839	0,0547	0,7443	0,6848	-0,3485	-0,3028	0,0916	-0,5367	0,5456	0,5622
30-34	-148,07	-0,1922	1,8786	0,5862	-1,3508	-0,1059	0,2657	0,1386	0,065	0,3747
34-38	-215,957	-0,3935	2,0447	0,4406	-1,1992	0,3847	0,3972	-0,0523	-0,3267	0,6399
38-42	-173,519	-0,1569	1,6313	0,347	-1,0028	0,6581	0,2846	-0,1775	-0,3814	0,588
42-46	-135,199	-0,0873	2,0014	0,1729	-1,4203	0,8063	0,2481	0,041	-0,2737	0,1241
46-50	-272,788	-0,0331	2,4592	-0,4916	-1,0166	0,9476	0,3419	-0,0607	-0,3219	0,3824
50-54	-99,8216	0,1102	1,7644	0,3259	-1,4365	-0,842	2,1509	-1,2536	0,2663	0,3814
54-58	-66,1065	0,2879	1,3941	0,4626	-0,8863	-1,4518	2,1124	-0,6803	0,2151	-0,1034

LEVEL

Coeff	C0	C3	C4	C5	C6	C7	C8	C9	C10	C11
Angle										
00-03	-2,4648	0	0	0	3,3627	-4,4485	2,4587	0,2424	-2,3022	1,7991
03-07	-60,5235	0	0	0	3,068	-3,2969	1,6839	0,7436	-2,9116	2,0712
07-11	-194,08	0	0	0	3,5484	-2,999	0,9459	0,1573	-1,1303	1,4064
11-15	-149,742	0	0	0	3,158	-0,9217	-1,4718	1,6735	-1,8517	1,142
15-19	26,2818	0	0	. 0	2,0348	-1,2473	0,2192	-0,6299	-0,0208	0,6542
19-23	-86,0974	0	0	0	3,2212	-2,5198	0,3195	-0,414	0,2145	0,6509
23-26	-58,0237	0	0	0	2,5771	-1,5361	-0,4371	-0,1637	-0,2772	1,1958
26-30	-45,9162	0	0	0	2,5699	-1,9611	0,1833	-0,5911	-0,0249	1,1383
30-34	-119,43	0	0	0	2,7355	-2,2893	1,2427	-0,183	-1,5505	1,6864
34-38	-104,751	0	0	0	1,8463	-0,575	0,2303	0,1128	-2,0319	2,0115
38-42	-100,313	0	0	0	1,8257	0,241	-0,7914	-0,1474	-0,8432	1,2882
42-46	51,8195	0	0	0	1,5317	-0,4938	-0,5169	-0,883	0,6112	0,6817
46-50	-121,08	0	0	0	1,1237	0,492	-0,34	-1,0421	-0,2994	1,7655
50-54	-87,9488	0	0	0	2,5404	-2,4452	2,0421	-1,9287	-0,2123	1,5423
54-58	-8,912	0	0	0	2,8034	-2,938	1,4922	-1,1504	0,3412	0,6701

Coeff	CO	C3	C4	C5	C6	C7	C8	C9	C10	C11
Angle			•							
00-03	52,2085	0,0651	-0,3578	1,5778	0,2039	-1,1384	-0,0268	-0,7569	0,9088	0,3605
03-07	15,5615	-0,0776	0,0547	1,4968	-0,19	-0,495	-0,4784	-0,3059	0,3503	0,6058
07-11	-60,4868	0,0106	-0,4431	2,3335	0,0501	-1,6314	0,2997	-0,3122	0,2701	0,6967
11-15	-88,1024	-0,1417	0,4214	1,115	0,91	-1,4214	-0,4933	0,3298	0,0763	0,5877
15-19	13,9708	-0,0176	-0,1587	2,0583	-0,2538	-1,4167	0,3839	-0,2757	0,4474	0,1996
19-23	38,9415	-0,1767	0,6048	0,9277	-0,3259	-0,5283	0,2183	-0,2742	0,1047	0,3236
23-26	28,2815	-0,1287	0,3203	. 1,9785	-1,149	-0,7792	0,718	0,278	-0,7055	0,3605
26-30	41,6466	-0,0194	0,423	0,5023	0,5125	-0,3674	-0,5832	0,3903	-0,1694	0,2059
30-34	64,1396	0,0567	-0,2506	1,6135	0,2373	-0,9027	-0,348	0,2317	0,38	-0,2286
34-38	38,0791	-0,1205	-0,0158	2,0317	-1,2842	0,6176	-0,4533	-0,1413	0,4417	-0,1921
38-42	64,5105	-0,0121	0,0746	1,4316	-0,3732	-1,1215	0,8613	-0,732	0,3834	0,2764
42-46	45,5253	-0,1439	0,8028	0,8136	-0,0943	-1,2045	0,6748	-0,0001	-0,4731	0,4582
46-50	4,9864	-0,0168	0,1646	1,6416	-0,8235	-0,1924	0,2191	-0,2175	0,0727	0,1961
50-54	42,6969	0,0037	0,1965	1,2306	0,4536	-1,3799	0,5402	0,4084	-0,4832	-0,0708
54-58	26,9378	-0,0852	0,7382	1,5308	-0,3534	-1,1141	0,337	1,1774	-0,8848	-0,4182

LEVEL 700

Coeff	C0	C3	C4	C5	C6	C7	C8	C9	C10	C11
Angle										
00-03	65,5108	0	0	0	2,3827	-2,3305	0,356	-0,7247	0,3192	0,7977
03-07	31,1893	0	0	0	2,3238	-1,4104	-0,7553	0,1377	-0,5002	1,1389
07-11	-56,5171	0	0	0	2,8889	-2,2257	-0,2906	-0,3417	0,2323	1,0469
11-15	-47,2232	0	0	0	3,3899	-2,2778	-1,1405	0,8751	-0,6342	1,04
15-19	107,8219	0	0	0	2,6736	-2,5989	-0,0262	-0,3332	0,4275	0,4731
19-23	96,8567	. 0	0	0	1,9565	-1,4692	-0,2422	-0,0929	-0,2692	0,7994
23-26	113,2234	0	0	0	1,8619	-1,0779	-0,6151	0,6136	-1,1759	1,0035
26-30	76,938	0	0	0	2,2542	-1,3292	-0,6304	0,4513	-0,5107	0,5297
30-34	84,9383	0	0	0	2,2083	-1,5019	-0,1763	0,0347	-0,1095	0,2847
34-38	87,8178	0	0	0	1,4616	-0,1349	-0,7396	-0,1273	0,0254	0,2605
38-42	115,3754	0	0	0	1,6133	-1,4128	0,3516	-0,9098	0,3377	0,6436
42-46	159,8876	0	0	0	1,9914	-2,4758	0,7782	-0,8045	0,1778	0,7552
46-50	95,2108	0	0	0	1,7674	-1,6032	0,3498	-0,773	0,3479	0,6326
50-54	75,3873	0	0	0	2,7901	-2,5526	0,7227	0,1162	-0,6711	0,405
54-58	122,6291	0	0	0	3,2082	-3,3739	0,5849	0,5375	-0,4322	0,0841

Coeff	C0	C3	C4	C5	C6	C7	C8	C9	C10	C11
Angle										
00-03	145,1755	0,0115	-0,1649	0,0987	1,4619	-0,8176	-0,5764	-0,9705	0,9866	0,391
03-07	114,1269	0,1454	-0,9263	1,5197	0,7154	-0,1935	-1,3505	-0,1402	0,7123	0,0492
07-11	72,5158	0,1351	-0,8482	1,0868	2,0807	-1,0075	-1,5331	0,7457	-0,0537	0,0938
11-15	29,735	0,1029	-0,7323	0,9464	2,1371	-0,8554	-1,2674	0,7075	-0,1009	-0,0486
15-19	31,6778	0,1088	-0,8636	1,4112	1,8144	-1,0799	-0,8576	0,9337	-0,4998	-0,0954
19-23	80,1189	0,0966	-0,6914	1,0531	1,3463	-0,7302	-0,4623	0,5386	-0,6397	0,1839
23-26	48,837	-0,0659	-0,0748	0,8594	-0,0013	1,1929	-1,176	0,6039	-0,7211	0,2019
26-30	17,5627	-0,0036	-0,5776	1,2595	1,3974	-0,669	-0,5842	0,7434	-0,7918	0,1646
30-34	122,0054	-0,0029	-0,2393	0,5632	1,026	0,1234	-1,1668	0,566	-0,4686	0,1163
34-38	95,1896	-0,0579	-0,6499	1,7869	-0,066	-0,2737	0,0386	-0,0936	-0,5158	0,4481
38-42	89,8472	0,0538	-0,6403	1,9339	0,2678	-1,6633	0,482	-0,0752	-0,1063	0,3797
42-46	75,9755	0,0492	-0,4999	1,7656	0,5147	-2,1166	0,5384	-0,39	0,8264	0,0101
46-50	131,0387	-0,0372	-0,5056	1,4906	0,5591	-1,077	-0,4936	0,3652	-0,1386	0,3107
50-54	57,5806	-0,0765	-0,1173	1,8977	-0,407	-0,8628	0,0149	0,6259	-0,8641	0,5441
54-58	-71,5089	0,0445	-0,751	2,3313	_1,782	-3,6489	2,0278	-0,0393	-0,7733	0,3775

LEVEL 500

Coeff	CO	C3	C4	C5	C6	C7	C8	C9	C10	C11
Angle									-	
00-03	144,542	0	0	0	1,2652	-0,5805	-0,7354	-0,9645	1,1067	0,3318
03-07	106,6783	0	0	0	1,4901	0,0525	-1,7457	-0,1796	0,8527	0,1044
07-11	61,0236	0	0	0	2,4337	-0,7534	-1,7919	0,8542	-0,0369	0,0411
11-15	18,4503	0	0	0	2,4359	-0,7828	-1,2718	0,5844	0,147	-0,172
15-19	36,4653	0	0	0	2,5967	-1,0646	-1,0897	0,8764	-0,2321	-0,2248
19-23	73,1906	0	0	0	1,8644	-0,7106	-0,5047	0,507	-0,6036	0,176
23-26	87,5109	0	0	0	0,8865	1,1517	-1,6397	0,7276	-0,8268	0,3857
26-30	31,7071	0	0	0	2,259	-0,7012	-0,9477	1,0018	-0,9648	0,2501
30-34	132,4649	0	0	0	1,4169	0,0583	-1,2655	0,594	-0,4785	0,1567
34-38	102,4387	0	0	0	1,6687	-0,9775	-0,0616	-0,1782	-0,1474	0,313
38-42	130,6557	0	0	0	1,8714	-1,8981	0,2327	-0,3505	0,0401	0,5948
42-46	136,9665	0	0	0	2,1004	-2,5932	0,4408	-0,8158	1,1708	0,1665
46-50	164,1749	0	0	0	2,1934	-2,2795	-0,101	0,1661	0,111	0,2579
50-54	115,2803	0	0	0	2,3213	-2,5529	0,5242	0,309	-1,0163	0,9753
54-58	12,848	0	0	0	3,6072	-4,1646	1,6659	-0,3089	-0,3021	0,5127

Coeff	C0	C3	C4	C5	C6	C7	C8	C9	C10	C11
Angle										
00-03	156,2772	0,2533	-0,5356	-1,0792	1,9622	1,716	-2,6751	-1,4077	1,7756	0,4103
03-07	89,2945	0,3508	-1,3864	1,1457	0,7849	1,499	-2,6301	-0,8235	1,731	-0,0216
07-11	-6,5237	0,1362	-0,5948	0,102	2,6523	0,268	-2,368	0,1539	0,8731	-0,202
11-15	-27,7083	0,1681	-0,8649	0,4619	3,0876	-0,5526	-1,7424	0,1382	0,9403	-0,5314
15-19	-64,6714	0,2224	-1,0991	1,3142	2,5532	-0,6476	-1,5469	0,4302	0,8301	-0,8133
19-23	-43,0258	0,1495	-0,7567	0,6082	2,05	0,3005	-1,435	0,2196	0,1565	-0,1044
23-26	-54,3931	-0,0339	0,1335	0,3276	1,0244	0,0127	0,0033	-0,4355	0,1021	0,0832
26-30	-73,5547	0,0619	-0,3599	0,3173	2,0456	-0,0947	-0,8268	0,1981	-0,3067	0,2851
30-34	36,9924	0,17	-1,0194	0,7872	2,0166	0,5651	-2,1129	0,5896	0,1342	-0,2608
34-38	-8,1335	0,0485	-1,1135	1,7063	₋ 1,5147	-0,395	-1,1121	0,1594	0,2261	-0,0091
38-42	1,8547	-0,0058	-0,4326	0,8994	1,886	-1,069	-1,0607	0,2491	0,3646	0,1444
42-46	17,0191	0,0829	-0,9783	1,5916	2,3292	-2,3257	-0,3399	0,288	0,4067	-0,1322
46-50	43,8769	0,1287	-1,055	2,035	0,7288	-1,2376	-0,1719	-0,1511	0,4207	0,1261
50-54	-33,7681	0,0912	-0,9597	2,6475	0,369	-2,0814	1,0056	-0,963	1,1572	-0,132
54-58	-3,45	0,0179	-0,0982	1,0468	0,7575	-0,7536	-0,8115	0,3553	0,6378	-0,1263

LEVEL 400

Coeff	C0	СЗ	C4	C5	C6	C7	C8	_C9	C10	C11
Angle										
00-03	148,3505	0	0	0	-0,899	3,5508	-3,0587	-1,6861	2,5538	-0,062
03-07	72,7351	0	0	0	0,2873	2,2462	-2,6716	-1,2152	2,2425	-0,194
07-11	-18,5415	0	0	0	1,9397	0,6632	-2,3162	0,1886	0,9572	-0,3841
11-15	-54,1187	0	0	0	2,4245	-0,1515	-1,5123	-0,1712	1,4206	-0,8092
15-19	-69,0581	0	0	0	2,8975	-0,4139	-1,6754	0,2744	1,191	-1,021
19-23	-66,9423	0	0	- 0	1,8617	0,5558	-1,3155	0,1369	0,2789	-0,2432
23-26	-37,1778	0	0	0	1,6498	-0,0761	-0,2692	-0,3574	-0,0057	0,2189
26-30	-85,2085	0	0	0	1,927	0,1398	-0,8635	0,1932	-0,2845	0,2516
30-34	31,9113	0	0	0	1,4867	1,1765	-2,3435	0,5174	0,4925	-0,4627
34-38	-24,1455	0	0	0	2,5627	-0,8078	-1,2104	0,0505	0,912	-0,4124
38-42	21,9391	0	0	0	2,2829	-1,1678	-0,9494	-0,0222	0,5807	0,1782
42-46	26,0212	0	0	0	3,0456	-2,3808	-0,2988	0,1515	0,4902	-0,1247
46-50	74,6541	0	0	0	2,3013	-1,9307	-0,1207	-0,286	0,5979	0,1279
50-54	8,924	0	0	0	2,8423	-2,9435	0,9383	-1,0685	0,9987	0,207
54-58	41,7644	0	0	0	2,0533	-1,3094	-0,9348	0,1522	0,8701	0,0256

Coeff	C0	C3	C4	C5	C6	C7	C8	C9	C10	C11
Angle										
00-03	-45,0347	0,1439	0,1573	-1,822	1,3669	3,2955	-2,3204	-1,6452	1,6789	0,4019
03-07	-103,023	0,2762	-0,8094	0,2719	1,1529	1,9786	-1,6197	-0,8373	1,3299	-0,2947
07-11	-112,727	0,1607	-0,2817	-0,4458	2,3544	1,2651	-1,5917	0,5208	-0,3164	-0,21
11-15	-95,1623	0,1126	-0,202	-0,9029	3,0062	0,6619	-0,9833	-0,4	0,7164	-0,6124
15-19	-84,5788	0,076	-0,0652	-0,3651	1,2664	1,8655	-0,9485	-0,8024	0,9102	-0,5919
19-23	-119,975	0,1268	-0,087	-0,8202	1,8468	1,9666	-1,1756	-0,3529	-0,0738	0,0867
23-26	-50,4787	-0,036	0,6707	-1,8026	1,4042	1,5483	0,2258	-1,6236	-0,005	0,8567
26-30	-38,256	0,099	0,0899	-1,6071	3,0318	0,5173	-0,871	-0,7038	0,1757	0,4516
30-34	-0,5195	0,205	-0,8035	0,0207	2,7797	0,1619	-1,6514	0,7087	-0,4206	-0,0053
34-38	-72,1226	0,1425	-1,3871	1,5482	1,6476	0,3125	-1,3059	0,0419	-0,0947	0,3647
38-42	-44,0546	0,0072	-0,4282	0,3542	2,0287	0,0822	-0,8669	-0,0948	0,0966	-0,023
42-46	-124,973	0,1253	-1,1913	2,0664	2,2115	-1,9643	0,3336	0,3545	-0,4027	-0,0563
46-50	-38,5479	0,0858	-0,8242	1,2923	1,7224	-1,096	-0,3385	-0,4249	0,7747	-0,0626
50-54	-56,4296	0,1389	-1,2207	2,8971	0,556	-2,2213	1,1942	-1,0626	1,2291	-0,3328
54-58	89,4708	0,0076	-0,6663	0,7004	1,28	-0,5749	-0,7884	-0,6343	0,9622	0,3233

LEVEL 300

Coeff	CO	C3	C4	C5	C6	C7	C8	C9	C10	C11
Angle										
00-03	-55,6697	0	0	0	-1,3858	4,6822	-2,3866	-1,8985	2,2551	-0,0184
03-07	-113,012	0	0	0	0,3277	2,4713	-1,352	-1,1884	1,6473	-0,448
07-11	-122,193	0	0	0	1,4086	1,4285	-1,1779	0,2553	-0,0346	-0,4184
11-15	-121,427	0	0	0	1,2889	1,2409	-0,5693	-0,7223	1,1135	-0,8787
15-19	-97,2675	0	0	0	0,6694	2,0967	-0,8162	-0,8695	0,9503	-0,6511
19-23	-151,851	0	0	0	0,7047	2,2908	-0,8458	-0,4479	0,0352	-0,1239
23-26	-89,6635	0	0	0	0,1709	1,3503	0,8207	-1,6595	0,0691	0,6178
26-30	-93,0515	0	0	0	0,7137	1,4052	-0,3869	-1,1047	0,6346	0,1092
30-34	-23,3971	_ 0	0	0	1,5482	0,9749	-1,7555	0,5743	0,0072	-0,2996
34-38	-102,654	0	0	0	2,11	0,2197	-1,4315	-0,0649	0,7158	-0,1712
38-42	-43,7381	0	0	0	1,7573	0,0921	-0,6198	-0,2607	0,2917	-0,1125
42-46	-105,439	0	0	0	3,2587	-2,0098	0,2644	0,1722	-0,2727	-0,0172
46-50	-29,8934	0	0	0	2,5397	-1,4744	-0,2719	-0,4403	0,8793	-0,1517
50-54	-17,3298	0	0	0	2,9739	-2,856	0,9651	-1,1068	1,0691	-0,021
54-58	101,504	0	0	0	0,9422	-0,1558	-0,9427	-0,5676	1,0687	0,1907

Coeff	C0	C3	C4	C5	C6	C7	C8	C9	C10	C11
Angle							2002			
00-03	-36,0257	0,0852	0,226	-1,5655	0,666	2,3665	0,0845	-2,3179	1,2025	0,4472
03-07	-54,2372	0,1503	-0,4304	-0,3903	0,1312	2,4908	0,3514	-1,9872	0,882	0,0585
07-11	-31,5714	0,1252	-0,2034	-0,8269	1,1903	1,7844	0,0886	-0,5258	-0,8055	0,3069
11-15	-23,9455	0,1632	-0,4177	-0,7753	0,8602	2,6622	-0,524	-0,8961	-0,172	0,225
15-19	-127,482	-0,042	0,7286	-1,4993	0,9681	2,1407	-0,0109	-1,4066	0,6765	-0,0254
19-23	-189 , 842	0,0077	0,5581	-1,4761	1,9001	1,9016	-0,7402	-0,6688	0,313	-0,0137
23-26	-130,49	-0,0957	0,8971	-1,9801	1,6541	1,5825	0,3707	-1,6838	0,546	0,2533
26-30	-46,8006	0,1024	0,0154	-1,2589	2,2336	1,1779	-0,7803	-0,578	0,0442	0,2359
30-34	-50,4304	0,1153	-0,5501	- 0,1132	1,9682	0,8502	-1,1544	-0,0801	0,5881	-0,674
34-38	-112,763	0,0392	-0,9469	1,3867	1,4983	0,0505	-0,4754	-0,6928	1,0781	-0,5378
38-42	31,7467	-0,0439	0,0956	-0,6621	1,0764	1,0329	0,7793	-1,7641	0,5021	-0,1642
42-46	-69,8321	0,1076	-1,0248	1,1948	1,7713	-1,0172	1,6022	-1,2369	-0,2054	0,0717
46-50	31,1534	0,0849	-0,6168	0,5389	1,5092	-0,6466	0,9418	-1,7215	1,029	-0,2827
50-54	-87,4195	0,1337	-0,7686	1,1973	2,5508	-2,3485	1,3894	-1,0194	0,8322	-0,6398
54-58	50,6195	-0,1072	-0,3161	0,0521	1,6095	0,1015	-0,9593	-0,7691	0,9865	0,1609

LEVEL 250

Coeff	CO	C3	C4	C5	C6	C7	C8	C9	C10	C11
Angle										
00-03	-45,4369	0	0	0	-1,5462	3,4494	0,0288	-2,5017	1,6611	0,1018
03-07	-65,9366	0	0	0	-1,2096	3,1187	0,5153	-2,3183	1,4054	-0,2339
07-11	-41,1575	0	0	0	-0,2653	2,133	0,4913	-0,6621	-0,6118	0,0501
11-15	-56,1918	0	0	0	-0,9818	3,3307	-0,0711	-1,2768	0,3167	-0,0955
15-19	-138,982	0	0	0	-0,1144	2,2711	0,2878	-1,4067	0,4642	0,054
19-23	-205,287	0	0	0	0,72	2,0734	-0,4739	-0,7046	0,3408	-0,1399
23-26	-160,042	0	0	0	0,4922	1,2759	0,905	-1,6516	0,5821	0,0358
26-30	-94,4681	0	0	0	0,3504	1,9253	-0,3737	-0,9228	0,417	-0,0402
30-34	-61,3261	0	0	0	1,2467	1,3497	-1,2687	-0,1328	0,8742	-0,8709
34-38	-128,463	0	0	0	2,3092	-0,3028	-0,5391	-0,7901	1,6961	-0,9079
38-42	18,3894	0	0	0	0,2172	1,1242	1,0635	-1,7925	0,5806	-0,2976
42-46	-87,3696	0	0	0	1,9275	-0,7682	1,598	-1,1706	-0,2802	0,0135
46-50	18,2755	0	0	0	1,4721	-0,4968	0,8901	-1,6105	1,0227	-0,4086
50-54	-85,3646	0	0	0	3,1176	-2,0762	1,0002	-0,9234	0,7776	-0,5886
54-58	45,943	0	0	0	0,9579	0,2275	-0,713	-0,7152	1,0094	-0,0102

Coeff	C0	СЗ	C4	C5	C6	C7	C8	C9	C10	C11
Angle							•			
00-03	-25,6976	0,0571	-0,2804	0,6303	-1,2866	0,6935	3,7789	-2,8755	1,339	-0,9667
03-07	-10,6819	-0,2183	0,7964	-0,5525	-2,3621	2,5643	3,4187	-3,3563	1,3276	-0,5764
07-11	-4,7693	-0,3853	1,4287	-0,5129	-3,1573	1,2847	5,0167	-4,7522	2,6491	-0,5662
11-15	13,149	0,0585	-0,2527	1,561	-4,3157	2,3021	3,564	-2,6682	-0,0956	0,7851
15-19	156,9613	0,1307	-0,9713	0,6091	-0,4721	-1,0852	4,378	-2,1103	-1,4918	1,3452
19-23	179,8731	0,2382	-1,4058	1,0481	-0,5692	-0,0321	2,6649	-2,0361	0,1496	0,1919
23-26	14,8007	0,1595	-0,6184	-0,1509	1,35	0,8468	0,5877	-0,4426	0,2491	-1,053
26-30	24,3828	0,0443	-0,1631	-0,2956	0,3582	1,2664	1,2321	-1,1635	0,1878	-0,5887
30-34	80,7755	-0,1093	0,6573	-1,2536	-0,5354	1,8525	2,2661	-2,13	0,1944	-0,2767
34-38	75,509	-0,1668	1,2796	-2,6681	0,2155	1,3331	3,3216	-3,095	0,1514	0,3506
38-42	64,8395	-0,111	0,7511	-1,1846	-1,8293	3,9673	1,1905	-2,8953	0,8215	0,0185
42-46	143,8281	-0,0559	1,1152	-1,3447	-1,6094	1,4083	3,9407	-3,8089	0,3642	0,3487
46-50	135,5132	~ -0,0888	0,5947	-0,7068	-1,195	1,9782	2,5881	-3,4689	0,9256	-0,2377
50-54	96,7376	0,246	-1,8364	1,7181	0,8889	-1,6162	3,9366	-2,9553	-0,0358	0,2702
54-58	25,3065	-0,0913	-1,0094	1,7828	-1,1479	1,7486	1,438	-2,3596	0,0876	0,4387

LEVEL 200

Coeff	CO	C3	C4	C5	C6	C7	C8	C9	C10	C11
Angle										
00-03	-20,935	0	0	0	-0,6952	0,4539	3,8372	-2,8846	1,2096	-0,8475
03-07	-0,9307	0	0	0	-1,9294	2,1129	3,374	-3,0993	1,0207	-0,46
07-11	23,468	0	0	0	-1,9621	0,6354	4,7424	-4,5648	2,2611	-0,1723
11-15	38,0166	0	0	0	-2,049	1,6809	2,9522	-2,2182	-0,652	1,1374
15-19	109,4126	0	0	0	-1,1212	-0,4066	4,3053	-2,1332	-1,1538	1,0321
19-23	135,9312	0	. 0	0	-1,1718	0,5839	2,8573	-2,188	0,4383	-0,1073
23-26	-28,0581	0	0	0	0,2941	1,1791	1,1001	-0,6822	0,4787	-1,293
26-30	4,1167	0	0	0	-0,407	1,6652	1,3266	-1,2569	0,3385	-0,7165
30-34	71,4444	0	0	0	-1,2898	1,8535	2,3131	-2,0055	0,2568	-0,4317
34-38	63,9298	0	0	0	-1,7634	1,3968	3,8121	-3,0838	0,0562	0,3318
38-42	59,6046	0	0	0	-2,4428	4,0158	1,2793	-2,848	0,7422	0,0076
42-46	162,8334	0	0	0	-1,8086	1,3726	3,681	-3,7813	0,3994	0,4297
46-50	138,3958	0	0	0	-1,421	1,9477	2,6466	-3,5193	0,908	-0,1691
50-54	83,5786	0	0	0	0,3567	-0,3092	3,1006	-2,5378	0,0106	-0,0111
54-58	79,4996	0	0	0	-0,7305	1,6309	1,4441	-2,4667	0,4552	0,3063

Coeff	C0	C3	C4	C5	C6	C7	C8	C9	C10	C11
Angle										
00-03	6,628	-0,0054	-0,1593	1,3759	-0,516	-1,3031	0,7798	3,2126	-3,2353	0,7316
03-07	71,0613	-0,1624	0,5217	0,3093	-1,0012	-1,8127	2,9128	1,0363	-2,3248	1,1709
07-11	25,588	-0,2839	0,7881	0,1825	-2,1281	-0,3332	2,9601	0,0552	-1,3871	1,0137
11-15	29,9751	-0,3114	0,8808	0,5932	-3,6353	1,0612	2,5402	-0,5282	-0,4487	0,6985
15-19	151,9277	-0,0699	0,631	-0,7856	-1,2764	-0,4448	2,7222	-0,5539	-0,562	0,7336
19-23	149,0337	-0,144	0,2958	0,4639	-2,1851	-0,6132	3,0564	-0,6856	-0,321	0,4903
23-26	46,6104	0,1169	-1,1646	2,0102	-0,6457	-1,6496	2,2684	0,3406	-0,1947	-0,3067
26-30	57,9371	0,0558	-0,297	1,7844	-4,0904	0,923	3,4213	-1,1641	-0,1178	0,2488
30-34	-23,8597	-0,0395	0,3957	0,3643	-2,6101	-0,1992	4,1824	-1,5346	-0,8358	1,3817
34-38	41,0001	-0,1289	0,1937	0,4888	-3,792	2,7778	3,0309	-0,7303	-2,6887	1,6909
38-42	-92,7416	-0,1153	0,5256	0,6761	-1,9762	0,0409	3,6622	-0,2283	-1,488	0,2663
42-46	82,3152	-0,0967	0,7933	-0,5652	-2,0799	1,7515	1,8674	-0,7543	-0,1039	-0,1586
46-50	5,0537	0,0119	0,3091	-0,6931	-0,2917	0,3365	2,2102	-0,6394	-0,5928	0,3559
50-54	-72,647	-0,2205	1,5016	-1,4637	-1,1048	3,0071	0,9733	-0,1407	-1,2039	-0,0506
54-58	-114,379	-0,1395	1,4642	-0,641	-1,9008	2,4522	2,3644	-0,9675	-1,4464	0,2491

LEVEL 150

Coeff	CO	СЗ	C4	C5	C6	C7	C8	C9	C10	C11
Angle										
00-03	17,8641	0	0	0	1,6457	-2,5318	1,124	3,2954	-3,816	1,1424
03-07	84,4918	0	0	0	0,3843	-2,5201	2,7957	1,3893	-2,917	1,4889
07-11	44,4737	0	0	0	-0,8632	-0,7233	2,5048	0,3503	-1,7738	1,3421
11-15	75,6424	0	0	0	-1,4586	0,172	2,0216	-0,0544	-1,0736	1,1102
15-19	163,9892	0	0	0	-1,449	-0,6387	2,8556	-0,5372	-0,7673	0,8763
19-23	181,2858	0	0	0	-1,2254	-0,9475	2,7615	-0,5859	-0,4449	0,6985
23-26	71,3428	0	0	0	0,0961	-1,2217	1,8789	0,2547	-0,1287	-0,1859
26-30	94,3936	0	0	0	-1,5919	0,0296	3,0994	-0,9427	-0,6114	0,6541
30-34	-13,8723	0_	0	0	-1,3946	-0,7863	4,4233	-1,6296	-1,2724	1,7516
34-38	57,4722	0	0	0	-2,8165	2,2373	3,0682	-0,7569	-2,7167	1,7879
38-42	-41,2882	0	0	0	-0,5441	-0,2286	3,344	-0,4871	-1,4881	0,6038
42-46	116,5341	0	0	0	-1,7474	1,3335	1,8962	-0,9619	0,0765	-0,0623
46-50	-5,346	0	0	0	-0,9602	0,85	2,0227	-0,58	-0,7021	0,4179
50-54	-60,5508	0	0	0	-0,781	1,916	1,7152	-0,4763	-1,2234	0,145
54-58	-96,1603	0	0	0	0,0022	0,6066	2,9882	-1,3707	-1,4257	0,6288

Coeff	CO	C3	C4	C5	C6	C7	C8	C9	C10	C11
Angle	-									
00-03	-12,4232	-0,0045	-0,2841	-0,5123	1,3081	-0,0889	-1,2003	3,2945	-1,4038	-0,0158
03-07	-19,3195	0,0662	-0,3984	-0,0203	0,72	-0,4519	-0,9337	3,109	-1,3026	0,3349
07-11	54,18	-0,0112	0,1538	-0,3126	0,6035	-0,9114	-0,2599	3,5375	-2,0872	0,0685
11-15	106,4851	0,1855	-1,2734	2,3495	-1,7767	-0,4971	0,3137	2,6372	-1,0751	-0,3126
15-19	83,8704	0,04	-0,4719	0,3249	1,214	-2,2036	-0,1281	3,6382	-2,2141	0,4389
19-23	35,3021	0,0114	-0,0607	0,3578	0,1087	0,1922	-2,2981	4,4338	-1,7777	-0,1378
23-26	-121,546	-0,0276	0,8	0,3085	0,3634	-2,3597	0,5397	2,5603	0,859	-1,572
26-30	-22,6312	-0,1212	1,1189	0,1224	-1,4555	-0,9596	0,8467	2,3791	-0,2992	-0,5665
30-34	-89,4351	-0,179	0,2614	0,0374	1,2339	-2,1304	0,1402	2,9817	-0,9982	0,0015
34-38	-61,879	-0,1435	-0,9042	1,5623	-0,4584	0,4188	-1,3088	3,8344	-2,5513	0,8015
38-42	73,3349	0,027	-0,4544	-0,2691	0,7278	0,0009	-1,3536	3,5159	-2,1739	0,7084
42-46	144,7889	0,1152	-0,452	0,236	-1,0429	0,6698	-0,5068	3,413	-3,1289	1,1144
46-50	125,9211	0,0389	0,5913	-0,9738	0,1413	-1,9236	1,7787	1,9186	-1,4151	0,3116
50-54	113,56	-0,1357	0,6601	-0,9509	-0,2875	-0,7908	1,2203	1,9995	-2,0041	0,7994
54-58	192,2916	-0,2133	1,986	<u>-</u> 1,5657	-3,6014	1,4304	2,4491	-0,8071	0,4398	0,0017

LEVEL 100

Coeff	CO	C3	C4	C5	C6	C7	C8	C9	C10	C11
Angle										
00-03	-21,0128	0	0	0	-0,3412	1,1845	-1,8531	3,3009	-0,765	-0,4052
03-07	-30,6438	0	0	0	-0,0842	0,1167	-1,079	2,9103	-0,7935	0,0922
07-11	55,472	0	0	0	0,3814	-0,9349	-0,1543	3,4885	-2,0609	0,0514
11-15	103,0852	0	0	0	-0,0387	-0,7368	-0,0311	2,692	-0,9918	-0,3112
15-19	57,813	0	0	0	0,9147	-1,8623	-0,1895	3,6559	-2,0524	0,2807
19-23	41,0899	0	0	0	0,5954	0,0231	-2,3528	4,4478	-1,838	-0,0645
23-26	-104,598	0	0	0	2,2236	-2,7322	-0,0943	2,7265	0,4597	-1,155
26-30	40,5975	0	0	0	0,951	-2,5625	0,852	2,459	-0,7696	-0,0992
30-34	-67,3262	0	0	0	1,5921	-2,4393	-0,0727	3,2433	-1,0121	-0,0346
34-38	-84,2937	0	0	0	0,8432	-0,7374	-1,1029	3,6256	-1,4231	0,1548
38-42	49,6082	0	0	0	-0,3463	0,1424	-0,9393	3,4753	-1,9986	0,4664
42-46	122,7003	0	0	0	-1,3152	1,1614	-0,7806	3,6466	-3,2909	1,0701
46-50	124,1358	0	0	0	-0,6485	-1,1409	1,3931	1,926	-1,5829	0,5351
50-54	116,7688	0	0	0	-0,6698	-1,1627	1,6368	1,8987	-1,9546	0,7603
54-58	185,2276	0	0	0	-2,0237	-0,6452	3,4014	-1,2014	0,312	0,3837

Coeff	CO	C3	C4	C5	C6	C7	C8	C9	C10	C11
Angle						, ,				
00-03	9,9526	0,0447	-0,2761	0,2648	1,2578	-1,188	-0,9967	2,8721	-1,0951	0,037
03-07	13,758	-0,0738	0,4046	-0,6499	0,7898	-0,3117	-1,2549	1,5341	0,6767	-0,1809
07-11	115,1586	0,1783	-1,1305	1,4054	-0,7658	0,1277	-0,783	1,107	0,8271	-0,4463
11-15	92,7016	0,1191	-1,2543	1,6384	-0,6519	-0,3164	-0,5349	1,0448	0,5826	-0,0266
15-19	239,7848	-0,0769	-0,9142	-0,2497	1,8337	-1,2196	-0,8233	1,5262	-0,9342	0,8302
19-23	65,0956	0,106	-1,759	1,0284	2,235	-1,468	-1,1872	2,0807	-0,7123	0,3837
23-26	62,0853	0,0244	-0,9302	-0,1968	1,8889	-0,3484	-1,5101	0,457	1,9434	-0,5606
26-30	262,326	0,1156	-1,41	0,985	-0,9958	0,3299	-0,329	0,1248	0,4153	0,693
30-34	30,813	-0,2887	-0,0656	0,4991	-0,4251	-0,5572	0,7289	0,2623	0,306	0,3733
34-38	94,3953	-0,1428	0,6853	0,8686	-0,2327	0,2277	-0,8623	1,3334	0,2471	0,1981
38-42	154,1343	-0,0009	-0,0396	-0,2325	-1,5662	2,0378	-1,1723	1,4953	-0,7256	0,581
42-46	57,971	0,084	-0,2287	0,4284	-1,3271	0,6766	0,0207	1,2513	-0,5422	0,4027
46-50	94,8539	-0,0139	-0,2087	0,0617	-0,0669	-0,2558	-0,5137	1,7973	-0,4834	0,2782
50-54	107,0166	-0,1585	0,8088	-1,0428	0,3073	-0,6397	-0,3043	2,1741	-0,8359	0,1971
54-58	32,7399	-0,089	0,536	0,3253	-1,6768	0,7475	0,1483	2,0677	-1,7326	0,4738

LEVEL

Coeff	CO	СЗ	C4	C5	C6	C7	C8	C9	C10	C11
Angle				•	•					
00-03	10,761	0	0	0	1,1586	-0,9756	-1,1332	2,8599	-0,9993	0,0057
03-07	16,5123	0	0	0	0,4548	-0,3967	-1,1238	1,5574	0,6424	-0,2149
07-11	99,6014	0	0	0	-0,3662	0,496	-1,13	1,2675	0,8405	-0,5251
11-15	71,6645	0	0	0	-0,2404	-0,1742	-0,4633	0,7445	1,1492	-0,3087
15-19	110,0755	0 .	0	0	-0,3279	0,2649	-0,925	1,8069	-0,5891	0,2918
19-23	15,4173	0	0	0	0,4412	-0,0819	-1,1124	1,9042	-0,0793	-0,1599
23-26	48,528	0	0	0	-0,0715	0,0729	-0,8659	0,2849	2,3799	-1,0031
26-30	221,0187	0	0	0	-2,1734	1,5856	-0,6158	0,253	0,641	0,3999
30-34	75,0866	0	0	0	-0,0862	-0,8116	0,1008	0,804	0,5346	0,134
34-38	100,5746	0	0	0	-0,5064	-0,0327	-0,6436	1,3298	0,1466	0,2749
38-42	145,6363	0	0	0	-1,9479	2,0885	-1,0546	1,5056	-0,6964	0,5089
42-46	66,0579	0	0	0	-1,0583	0,8617	-0,2597	1,286	-0,5388	0,4394
46-50	81,8652	0	0	0	-0,1974	-0,3112	-0,3989	1,8775	-0,4678	0,137
50-54	112,924	0	0	0	0,0401	-1,1654	0,1962	2,0299	-0,7936	0,1922
54-58	66,3359	0	0	0	-0,2231	-0,4107	0,4483	1,775	-1,5797	0,6885

Coeff	CO	C3	C4	C5	C6	C7	C8	C9	C10	C11
Angle										
00-03	48,1906	-0,2953	0,7814	-0,9974	-0,4525	2,061	-1,1316	0,3377	0,564	-0,0918
03-07	2,9469	-0,2586	0,7522	-0,648	0,079	0,9203	-1,1462	0,8407	0,7912	-0,3832
07-11	27,7587	-0,2812	0,7983	-0,3152	-0,1146	-0,1428	-0,1969	0,323	1,2711	-0,5167
11-15	31,0147	-0,1049	-0,0865	1,0692	-1,1094	0,1369	-0,2575	0,567	0,8307	-0,2326
15-19	120,4477	-0,0179	0,0889	-0,4983	0,392	-0,2875	-0,3037	-0,1367	1,4194	-0,1654
19-23	45,7926	-0,1049	-0,0809	0,1333	0,0633	0,5317	-1,2224	0,5737	0,9368	-0,0605
23-26	82,1861	0,1632	-1,0018	1,1335	0,4381	-1,0837	-0,7916	-0,1986	2,6081	-0,6376
26-30	154,543	0,2013	-0,8965	1,623	-2,6132	1,9607	-1,6939	-0,196	2,1927	-0,2349
30-34	13,2307	0,0565	-0,5212	1,406	-1,3714	-0,3404	0,6617	-0,8972	2,3974	-0,4664
34-38	59,3421	-0,0956	0,8082	-0,172	-1,4329	-0,0378	0,3003	-0,6733	2,1712	-0,1617
38-42	139,3441	-0,0191	0,0891	0,5309	-1,7317	0,2672	0,2412	0,0059	0,8994	0,0919
42-46	114,0764	-0,0291	0,2357	-0,0397	-0,628	-0,8011	0,7994	-0,059	0,8809	0,1292
46-50	75,7637	0,0595	-0,5683	1,3669	-1,0404	-0,9767	0,4202	0,3083	1,3499	-0,272
50-54	-70,3679	0,0027	0,0593	1,168	-1,1523	-0,6966	1,549	-0,8251	2,2868	-1,1322
54-58	62,6961	0,0461	-0,2573	0,2421	-0,4295	0,376	-1,0775	1,7734	-0,0585	0,1184

LEVEL

Coeff	CO	C3	C4	C5	C6	C7	C8	C9	C10	C11
Angle										
00-03	37,4287	0	0	0	-0,9287	2,202	-1,4313	0,5453	0,7498	-0,2942
03-07	7,2184	0	0	0	0,1707	0,7465	-1,3966	1,0613	0,7737	-0,4031
07-11	44,1994	0	0	0	0,397	-0,3022	-0,5637	0,687	0,8622	-0,2889
11-15	46,9401	0	0	0	0,2979	-0,2917	-0,5273	0,7102	0,7143	-0,1194
15-19	98,9539	0	0	0	-0,2527	-0,037	-0,2206	-0,1032	1,4047	-0,2172
19-23	52,6807	0	0	0	-0,21	0,7955	-1,3665	0,5921	1,062	-0,1135
23-26	72,5926	0	0	0	0,3961	-0,659	-0,7673	-0,3799	2,7527	-0,6759
26-30	146,4333	0	0	0	-1,3926	1,8965	-1,8763	-0,151	1,9496	-0,0502
30-34	31,3104	0	0	0	-0,1965	-0,565	0,6129	-0,9795	2,2242	-0,226
34-38	97,832	0	0	0	-0,7475	-0,1174	0,2131	-0,5833	1,4328	0,3828
38-42	161,7697	0	0	0	-0,9362	0,1422	0,0454	-0,0847	0,8873	0,2483
42-46	131,7775	0	0	0	-0,3655	-0,9903	0,7977	-0,1702	0,9757	0,1778
46-50	104,8155	0	0	0	0,2121	-1,6082	0,5009	0,1576	1,4964	-0,2283
50-54	-40,6485	0	0	0	0,8225	-1,6872	1,7088	-1,0564	2,1361	-0,751
54-58	64,9813	0	0	0	-0,5626	0,6622	-1,2535	1,8223	-0,0389	0,0856

References

Anthes, R.A, 1972: The development of asymmetries in a three-dimensional numerical model of tropical cyclone. *Monthly Weather Review*, **100**, 461-476.

Anthes, R.A., E.-Y. Hsie, and Y.-H. Kuo, 1987: Description of the Penn State/NCAR mesoscale model version 4 (MM4). NCAR Tech. Note NCAR/TN-282, 66pp. [Available from NCAR Publications Office, P.O. Box 3000, Boulder, CO 80307-3000]

Arakawa, A., and W. H. Schubert, 1974: Interaction of a cumulus cloud ensemble with the large-scale environment, Part I. *Journal of the Atmospheric Sciences*, **31**, 674-70

Avila, L.A., 1995: Preliminary report, Hurricane Roxanne, 7-21 October 1995. [Available online at http://www.nhc.noaa.gov/1995roxanne.html]

Baer, F., and D. Boudra, 1977: Numerical Prediction and Modification of Cyclone-Scale Precipitation. *Monthly Weather Review*, **105**, 603–617.

Beer, T., and L. Giannini, 1980: Tropical Cyclone Cloudbands. *Journal of the Atmospheric Sciences*, **37**, 1511–1520.

Bender, M.A., R. Ross, R.E. Tuleya and Y. Kurihara, 1993: Improvements in tropical cyclone track and intensity forecast using the GFDL initialization system. *Monthly Weather Review*, **121**, 2046-2061.

Bender, Morris A., 1997: The Effect of Relative Flow on the Asymmetric Structure in the Interior of Hurricanes. *Journal of the Atmospheric Sciences*, **54**, No. 6, pp. 703–724.

Betts, A.K., 1986: A new convective adjustment scheme. Part I: Observational and Theoretical Basis. *Quarterly Journal of the Royal Meteorological Society*, **112**, 677-692.

Betts, A.K., and M.J. Miller, 1986: A new convective adjustment scheme. Part II: Single Column tests using GATE wave, BOMEX, ATEX and Arctic air-mass data sets. *Quarterly Journal of the Royal Meteorological Society*, **112**, 693-709.

Betts, A.K., and M.J. Miller, 1993: The Betts-Miller scheme. *The representation of cumulus convection in numerical models*, K.A. Emanuel and D.J. Raymond, Eds. Amer. Meteor. Soc., 246pp.

Bolin, B., 1956: An improved barotropic model and some aspects of using the balance equation for three-dimensionnal flow. *Tellus*, **8**, 61-75.

Braun, S.A., 2002: A Cloud-Resolving Simulation of Hurricane Bob (1991): Storm Structure and Eyewall Buoyancy. *Monthly Weather Review*, **130**, 1573–1592.

Brueske, K.F., and C.S. Velden, 2003: Satellite-Based Tropical Cyclone Intensity Estimation Using the NOAA-KLM Series Advanced Microwave Sounding Unit (AMSU). *Monthly Weather Review*, **131**, 687-697.

Carr, L.E., and R.L. Elsberry, 1992: Analytical tropical cyclone asymmetric circulation for barotropic model initial conditions. *Monthly Weather Review*, **120**, 644-652.

Charney, J.G., 1963: Notes and Correspondence: A Note on Large-Scale Motions in the Tropics. *Journal of the Atmospheric Sciences*, **20**, 607-609.

Chen, Y., and M.K. Yau, 2001: Spiral bands in a simulated hurricane. Part I: Vortex Rossby wave verification. *Journal of the Atmospheric Sciences*, **58**, 2128-2145.

Cione, J.J., P. Black, and S.Houston, 2000: Surface Observations in the Hurricane Environment, *Monthly Weather Review*, **128**, 1550-156.

CRth J., Desmarais, JG, Gravel, S., Mhhot, A., Patoine, A., Roch, M., and Staniforth, A. 1998: The Operational CMC-MRB Global Environmental Multiscale (GEM) Model. Part II: Results. *Monthly Weather Review*: 126, No. 6, pp. 1397–1418.

Corbosiero, K.L., and J. Molinari, 2002: The Effects of Vertical Wind Shear on the Distribution of Convection in Tropical Cyclones. *Monthly Weather Review*, **130**, 2110–2123.

DeMaria, M., J.A. Knaff, S.Q. Kidder, and M.D. Goldberg, 2000: Tropical Cyclone Wind Retrievals Using AMSU-A Data from NOAA-15. 10th Conference on Satellite Meteorology and Oceanography, Long Beach, CA, 149-152.

Demuth, J.L., 2001: Objectively estimating tropical cyclone intensity and wind structure using the Advanced Microwave Sounding Unit. Masters Thesis, Colorado State University, Department of Atmospheric Science, 132pp.

Dudhia, J. 1993: A nonhydrostatic version of the Penn State-NCAR mesoscale model: Validation tests and simulation of an Atlantic cyclone and cold front. *Monthly Weather Review*, **121**, 1493-1513.

Dvorak, V.F., 1975: Tropical cyclone intensity analysis and forecasting from satellite imagery. *Monthly Weather Review*, **103**, 420-430.

, 1984: Tropical cyclone intensity analysis using satellite data. NOAA Technical Report NESDIS 11, 47 pp.

Emanuel, K.A. 1986: An air-sea interaction theory for tropical cyclones. Part I. *Journal of the Atmospheric Sciences*, **42**, 1062-1071.

, 1988: The Maximum Intensity of Hurricanes. *Journal of the Atmospheric Sciences*: **45**, 1143–1155.

, 1999: Thermodynamic control of hurricane intensity. *Nature*, **401**, 665-669.

Frank, W.M. 1977: The Structure and Energetics of the Tropical Cyclone I. Storm Structure. *Monthly Weather Review*, **105**, 1119-1135.

Fujita, T., 1952: Pressure distribution within a typhoon. Geophysical Magazine. 23, 437-451.

Garratt, J.R., 1977: Review of Drag Coefficients over Oceans and Continents, *Monthly Weather Review*, **105**, 915-929.

Gray, W.M., 1979: Hurricanes: Their formation, structure, and likely role in the tropical circulation. Meteorology over the Tropical Oceans, D.B. Shaw, Ed., Royal Meteorological Society, 155-199.

Grell, G. A., J. Dudhia, and D.R. Stauffer, 1995: A description of the fifth generation Penn State/NCAR mesoscale model (MM5). NCAR Tech Note NCAR/TN-398+STR, 138pp. [Available from NCAR Publications Office, P.O. Box 3000, Boulder, CO 80307-3000]

Grody, N.C., F.Weng, and R.Ferraro, 1999: Application of AMSU for obtaining water vapor, cloud liquid water, precipitation, snow cover, and sea ice concentration. 10th Int. ATOVS Study Conf., Boulder, CO, 230-240.

_______, 2000: Application of AMSU for obtaining hydrological parameters, *Microwave Radiometry and Remote Sensing of the Earth's Surface and Atmosphere*, P. Pampaloni and S. Paloscia, Eds., VSP, 339-351.

Grody, N.C., 1993: Remote sensing of the atmosphere from satellites using microwave radiometry, *Atmospheric Remote Sensing By Microwave Radiometry*, M.A. Janssen, Ed., John Wiley & Sons, Inc., 259-334.

Grody, N.C., 2002: Personal communication.

Guiney, J.L, and M.B. Lawrence, 1998: Preliminary report, Hurricane Mitch, 22 October-5 November 1998. [Available online at http://www.nhc.noaa.gov/1998mitch.html

Holland, G.J., 1980: An analytic model of the wind and pressure profiles in hurricanes. *Monthly Weather Review*, **108**, 1212-1218.

Kain, J. S., and J. M. Fritsch, 1990: A One-Dimensional Entraining/Detraining Plume Model and its Application in Convective Parameterization. *Journal of the Atmospheric Sciences*, **47**, 2784-2802.

Kasahara, A., 1961: A numerical experiment on the development of tropical cyclone. *Journal of Meteorology*, **18**, 259-282.

Kidder, S.Q., W.M. Gray, and T.H. Vonder Haar, 1978: Estimating tropical cyclone central pressure and outer winds from satellite microwave sounder data. *Monthly Weather Review*, **108**, 1458-1464.

Kidder, S.Q., M. D. Goldberg, R. M. Zehr, M. DeMaria, J. F. W. Purdom, C. S. Velden, N. C. Grody, and S. J. Kusselson, 2000: Satellite analysis of tropical cyclones using the Advanced Microwave Sounding Unit (AMSU). *Bulletin of the American Meteorological Society*, **81**, 1241-1259.

Kraus, E.B., 1972: Atmosphere-Ocean Interaction. Clarendon Press, 275 pp.

Krishnamurti, T.N., D. Oosterhof, and N. Dignon, 1989: Hurricane prediction with a high resolution global model. *Monthly Weather Review*, **117**, 631-669.

_____, J. Xue, H.S. Bedi, K. Ingles, and D. Oosterhof, 1991: Physical initialization for numerical weather prediction over tropics. *Tellus*, **43AB**, 53-81.

_____, S.K. Roy Bhowmik, D. Oosterhof, and G.Rohaly, 1995: Mesoscale signatures within the Tropics generated by physical initialization. *Monthly Weather Review*, **123**, 2771-2790.

Kuo, H.L. 1965: On formulation and intensification of tropical cyclones through latent heat release by cumulus convection. *Journal of the Atmospheric Sciences*, **22**, 40-63

______, 1974: Further studies of the parameterization of the influence of cumulus convection on large-scale flow. *Journal of the Atmospheric Sciences*, **31**, 1232-1240.

Kurihara, Y., 1980: On the Transformation of a Tropical Easterly Wave into a Tropical Depression - A Simple Numerical Study. *Journal of the Atmospheric Sciences*, **42**, 68-77.

M.A. Bender and R. J. Ross, 1993: An Initialization Scheme of Hurricane Models by Vortex Specification. *Monthly Weather Review*, **121**, 2030–2045.

Liu, Y., D.L. Zhang and M.K. Yau, 1997: A Multiscale Numerical Study of Hurricane Andrew (1992). Part I: Explicit Simulation and Verification. *Monthly Weather Review*, **125**, 3073-3093.

Liu, Y., D.L. Zhang and M.K. Yau, 1999: A Multiscale Numerical Study of Hurricane Andrew (1992). Part II: Kinematics and Inner-Core Structures. *Monthly Weather Review*, **127**, No. 11, pp. 2597–2616.

Malkus, J.S., and H. Riehl, 1960: On the dynamics and energy transformations in steady-state hurricanes. *Tellus*, **12**, 1-20.

Marks, F.D., R.A. Houze Jr., and J.F. Gamache, 1992: Dual-aircraft inverstigation of the inner core of the Hurricane Norbert. Part I: Kinematic structure. *Journal of the Atmospheric Sciences*, **49**, 919-942.

Mathur, M.B., 1991: The National Meteorological Center's Quasi-Lagrangian Model for hurricane prediction. *Monthly Weather Review*, **119**, 1419-1447.

Moorthi, S., and M. J. Suarez, 1992: Relaxed Arakawa Schubert: A parameterization of moist convection for general circulation models. *Monthly Weather Review*, **120**, 978-1002.

NESDIS website, 2003: History of the Polar Orbiting Environmental Satellites [Available online at http://orbit36i.nesdis.noaa.gov/atovs/info/history.html]

NOAA KLM User Guide, 2000 [Available online at http://www2.ncdc.noaa.gov/docs/klm]

Ooyama, K.V., 1969: Numerical simulation of the life cycle of tropical cyclones. *Journal of the Atmospheric Sciences*, **26**, 4-40.

Orlanski, I., 1975: A rational subdivision of scales for atmospheric processes. *Bulletin of the American Meteorological Society*, **56**, 527-530.

MM5 V2-12, 1999 [Available online at http://www.mmm.ucar.edu/mm5/mm5sysv2.html]

Pasch, R.J, T.B. Kimberlain and S.R. Stewart, 1999: Preliminary report, Hurricane Floyd, 7-17 September 1999. [Available online at http://www.nhc.noaa.gov/1999floyd.html]

Rappaport, E., 1993: Preliminary report, Hurricane Andrew, 16-28 August 1992. [Available online at http://www.nhc.noaa.gov/1992andrew.html]

Rosenkrantz, P. W., D.H. Staelin, and N.C. Grody, 1978: Typhoon June (1975) viewed by a scanning microwave spectrometer. *Journal of Geophysical Research*, **83**, 1857-1868.

Rosenthal, S.L., 1970: A circularly-symmetric primitive equation model of tropical cyclone development containing an explicit water-vapour cycle. *Monthly Weather Review*, **98**, 106-120.

Ross, R.J., and Y. Kurihara, 1992: A simplified scheme to simulate asymmetries due to the beta effect in barotropic vortices. *Journal of the Atmospheric Sciences*, **49**, 1620-1628.

Shapiro, L.J., and H.E. Willoughby, 1982: The Response of Balanced Hurricanes to Local Sources of Heat and Momentum. *Journal of the Atmospheric Sciences*, **39**, 378–394.

Shea, D.J., and W.M.Gray, 1973: The Hurricane's Inner Core Region. I. Symmetric and Asymmetric Structure. *Journal of the Atmospheric Sciences*, **30**, 1544-1564.

Shuman, F., 1957: Numerical Methods in Weather Prediction: I. The Balance Equation. *Monthly Weather Review*, **85**, 329-332.

Spencer, R.W., and W.D. Braswell, 2001: Atlantic tropical cyclone monitoring with AMSU-A: Estimation of maximum sustained wind speeds. *Monthly Weather Review*, **129**, 1518-1532.

Sundqvist,H., 1970: Numerical simulations of the development of tropical cyclones with a ten-level model. Part I. *Tellus*, **22**, 359-390.

Tao, W.K., and J. Simpson, 1993: The Goddard cumulus ensemble model. Part I: Model description. *Terrestrial, Atmospheric and Oceanic Science*, **4**, 35-72.

Velden, C.S., and W.L. Smith, 1983: Monitoring Tropical Cyclone Evolution with NOAA Satellite Microwave Observations. *Journal of Climate and Applied Meteorology*, **22**, 714-724.

Velden, C.S, 1989: Observational analyses of North Atlantic tropical cyclones from NOAA polar-orbiting satellite microwave data. *Journal of Applied Meteorology*, **28**, 59-70.

Velden, C.S., T.L. Olander, and R.M. Zehr, 1998: Development of an objective scheme to estimate tropical cyclone intensity from digital geostationary satellite infrared imagery. *Weather and Forecasting*, **13**, 172-186.

Weng, F., and N.C. Grody, 2000: Retrieval of ice cloud parameters using a microwave imaging radiometer. *Journal of the Atmospheric Sciences*, **57**, 1069-1081.

Yamasaki, M., 1968: Detailed analysis of a tropical-cyclone simulated with a 13-layer model. *Papers in Meteorology and Geophysics*, **20**, 559-585.

Zhang, D.L., Y. Liu, and M.K. Yau, 2002: A Multiscale Numerical Study of Hurricane Andrew (1992). Part V: Inner-Core Thermodynamics. *Monthly Weather Review*, **130**, 2745-2763.

Zhu, T., D.L. Zhang, and F. Weng: 2002. Impact of the Advanced Microwave Sounding Unit Measurements on Hurricane Prediction. *Monthly Weather Review*, **130**, 2416-2432.

Zou, X., and Q. Xiao, 2000: Studies on the initialization and simulation of a mature hurricane using a variational bogus data assimilation scheme. *Journal of the Atmospheric Sciences*, **57**, 836-860.